

# **Dissertation**

## **Nanoparticle and Macromolecular Transfer across the Human Placental Barrier**

submitted by

**Michael Gruber MSc. BSc.**

for the Academic Degree of  
**Doctor of Philosophy (PhD)**

at the  
**Medical University of Graz**

**Department of Obstetrics and Gynaecology**

under the Supervision of  
**Assoc. Prof. Dr. Christian WADSACK**

**2021**

## Declaration

I hereby declare that this thesis is my own original work and that I have fully acknowledged by name all of those individuals and organizations that have contributed to the research for this thesis. Acknowledgement has been made in the text and appendix to all other materials used. Throughout this thesis and in all related publications I followed the “Standards of Good Scientific Practice and Ombuds Committee at the Medical University of Graz“.

Graz, 20.07.2021

Michael Gruber

## Disclosures

Parts of this thesis was published in a peer-reviewed journal and permission to reprint the figures and content parts was granted under the open access publication agreement of the publisher and the authors under the open access licence CC BY 4.0 (<https://creativecommons.org/licenses/by/4.0/legalcode>).

The thesis includes results published in: *Gruber M.M., Hirschmugl B., Berger N., Holter M., Radulović S., Leitinger G., Liesinger L., Berghold A., Roblegg E., Birner-Gruenberger R., Bjelic-Radisic V., Wadsack C., Plasma proteins facilitates placental transfer of polystyrene particles. J Nanobiotechnology [Internet]. 2020 Dec 9;18(1):128.*

The co-authors of the publication contributed within the frame of preparing the data for publishing. All co-authors agreed to the use of data within this thesis.

The following researchers contributed actively to the results used in this thesis:

Birgit Hirschmugl trained and consulted the candidate in the usage of the *ex vivo* placental perfusion model. Birgit performed around the half of the perfusion experiments with the IgG2- anti-RANKL antibody, assisted and consulted in the laboratory analysis and data analysis of these generated samples. Birgit prepared some of the antipyrene samples for analysis. This work took place at the Department of Obstetrics and Gynaecology at the Medical University of Graz

Natascha Berger assisted with the generation of some of the electron microscopic pictures during her enrolment at the department of obstetrics and gynaecology at the Medical University of Graz. The work was performed at the Cell Biology, Histology and Embryology Department of the Gottfried Schatz Research Center Medical University of Graz.

Magdalene Holter performed the biostatistics calculation in SAS for the polystyrene nanoparticle concentration in the four different perfusion media at the department of Biostatistics at the Medical University of Graz.

Snježana Radulović prepared parts of the embedded tissue samples for electron microscopy at the Cell Biology, Histology and Embryology Department of the Gottfried Schatz Research Center Medical University of Graz.

Gerd Leitinger supervised Luca Schmid and Snježana Radulović and assisted in the interpretation of the electron microscopic pictures at the Cell Biology, Histology and Embryology Department of the Gottfried Schatz Research Center Medical University of Graz. Andrea Berghold supervised Magdalena Holter and consulted in biostatistics questions for the nanoparticle part of the thesis at the department of Biostatistics at the Medical University of Graz.

Eva Roblegg enabled the DLS measurements and consulted in nanoparticle characterization methods at the Department of Pharmaceutical Technology & Biopharmacy at the Karl Franzens University Graz. Ruth Birner-Gruenbnerger supervised Laura Liesinger, consulted in the sample preparation, the storage for the proteomics analysis and consulted in the proteomics data analysis at the research unit of functional proteomics at the Medical University of Graz.

Vesna Bjelic-Radusic generated the idea to investigate the IgG 1-anti-HER2 antibody at the placental barrier and consulted in clinical relevant questions during her time at the department of obstetrics and gynaecology of the Medical University of Graz.

Christian Wadsack supervised and consulted the candidate at the Department of Obstetrics and Gynaecology at the Medical University of Graz.

Laura Liesinger performed the protein digest and the proteomic measurement of the protein biocorona on the polystyrene nanoparticles and the measurement of the IgG 2-anti-RANKL specific peptide at the research unit of functional proteomics at the Medical University of Graz under the supervision of Prof. Ruth Birner-Grünberger.

Following technicians assisted with sample preparation during the thesis:

Susanne Kopp helped in the sample preparation of antipyrine *ex vivo* perfusion samples for QC and parts of the sample preparation for immunohistological and immunofluorescence microscopical examination.

Luca Schmid embedded the perfusion fixed placental tissue sections, generated ultra-thin sections and stained the samples at the Cell Biology, Histology and Embryology Department of the Gottfried Schatz Research Center Medical University of Graz under the supervision of Prof. Gerd Leitinger.

## **Acknowledgements**

The doctoral candidate Michael Gruber received funding from the “Austrian Research Promotion Agency (FFG, PlaZentaTox, 844741)” and “PhD Program in Molecular Medicine” at the Medical University of Graz through the PhD Program “Molecular Medicine (MolMed)”.

Here I am pleased to thank the people who accompanied and supported me to achieve my academic goals.

In the beginning, I want to thank my supervisor **Christian Wadsack** that he allowed me to develop and conduct the research tasks linked to these studies. His guidance and mentoring participated to a high degree in my development within the last years.

I want to thank my thesis committee members, **Udo Markert** and **Christian Windpassinger**, for the open and constructive comments during my PhD time. A big part of which I am very grateful for is the personal and scientific interaction with everybody at the European Placenta Perfusion workshops. This remarkably fruitful open-minded scientific exchange setting and the connected discussion helped me develop my ideas immensely.

My warmest thanks go to my colleagues during this time at the obstetrics and gynaecology department at the Medical University of Graz. You all contributed so much in many ways to make this time so memorable, unforgettable, joyful and lovely. We shared so many experiences during working hours and even more in our spare time. Especially thanks to **Alejandro, Ate, Birgit, Bettina, Moni, Jimmy and Susi** for joining even my wedding in Greece and so much more.

Last but not least, I would like to thank my dear and wise wife, **Niki**. Not only did you stand by me from the beginning of the dissertation to the end, but you also became the warm and caring mother of our two little girls, **Anastasia and Artemis**, who were born during this time. Infinite thanks for all your support during these years. And now to you, my little ones, if you ever read this, I want to tell you how much you sweetened my life during this time.

## **Zusammenfassung**

Der Transfer von Makromolekülen und der Transfer von Nanopartikeln (NP) über die Plazenta gewinnen aufgrund der zunehmenden Exposition an Bedeutung. Diese Bedeutung beruht einerseits auf der therapeutischen Seite durch den Einsatz von NP-basierten Medikamenten und Biopharmazeutika wie Immunglobuline gamma (IgG). Andererseits erhöht sich durch den vermehrten Einsatz von Nanopartikeln und Biopharmazeutika im täglichen Leben das unbekannte Risiko für den Fötus während der Schwangerschaft. Das eine geringe Anzahl an untersuchten NPs die Plazenta passieren kann, wurde bereits gezeigt. Ob dieser Transfer in Gegenwart physiologisch relevanter Makromoleküle erfolgt, ist jedoch noch nicht untersucht und verstanden. Anders sieht die Datenlage für den Transfer von IgG über die Plazenta aus. Es ist bekannt, dass diese Proteine, vermittelt durch den neonatalen Fc-Rezeptor (FcRn), die Plazentaschranke passieren können. Ob und inwieweit spezifische therapeutische IgG die Plazenta passieren oder die Plazenta beeinflussen, wurde bisher in wenigen Fällen untersucht. Im ersten Teil der Dissertation konnte der plazentare Transfer von 80 nm Polystyrol (PS) und 100 nm Poly(lactid-co-glycolid) (PLGA) NP in einem humanen *ex-vivo* Perfusionsmodell gezeigt werden. Die Daten zeigten weiters das in Anwesenheit von Antipyrin (AP) 500 nm PS NP in der mütterlichen Zirkulation an Konzentration abnehmen. Bei den 80 nm PS NP wurde ein Einfluss von Plasmaproteinen auf den NP Transfer nachgewiesen. Albumin konnte als Transfervermittler der 80 nm PS NP über die Plazenta nachgewiesen werden.

Im zweiten Teil der Dissertation wurde der plazentare Transfer von zwei therapeutischen Antikörpern, einem anti-HER2 IgG1 und einem anti-RANKL IgG2 mit dem Perfusionsmodell untersucht. Es konnte die Expression von HER2 und RANKL in der Term Plazenta bestätigt bzw. erstmals gezeigt werden. Ein plazentarer Transfer des IgG1 konnte mittels ELISA nicht nachgewiesen werden, dafür ein Naheverhältnis des IgG mit FcRn und dem Lysosomen assoziiertem Membran Protein 1 (LAMP1) nach Perfusion.

Spezifische Peptide des IgG2 wurden mit Proteomics in fetaler Zirkulation nachgewiesen wobei therapeutisch intakte Antikörper nicht eindeutig nachgewiesen wurden. Mit einem funktionellen Ansatz, bei welchem freies RANKL nachgewiesen wurde konnte gezeigt werden, dass die Term Plazenta RANKL in die fetale Zirkulation abgibt.

Die generierten Daten legen einen Einfluss AP auf die Eigenschaften und die Plazentare Aufnahme von PS NP an der Plazentaschranke nahe. Die Relevanz einer Biocorona an PS NP

während der Perfusion und die Eigenschaft der Biocorona die Plazentagängigkeit der NP zu erhöhen war ersichtlich. Eine Hypothesen generierende Abschätzung wie PS NP an der Plazenta prozessiert werden konnte erstellt werden, welche aber in Zukunft im Detail überprüft werden sollte. PLGA als biodegradierbares Material zeigte die potentielle Möglichkeit Medikamente über die Plazenta zu schleusen.

Da der anti-HER2 IgG1 die Plazenta nicht passieren konnte aber zusammen mit FcRn und LAMP 1 gezeigt wurde lässt annehmen das Antikörper deren Epitop auf oder in der Plazenta vorhanden sind nicht zwingen das Gewebe überqueren. Beschriebene negative folgen für den Feten könnten somit direkt mit einer IgG Plazenta Interaktion in Zusammenhang stehen. Bei den anti-RANKL IgG2 kann ein negativer Effekt auf die Plazenta bei kurzer Exposition und therapeutischen Konzentrationen weder bestätigt noch widerlegt werden. Weitere Studien um die Relevanz von RANKL in der Plazenta zu untersuchen sind angezeigt.

## **Abstract**

Macromolecular transfer and transfer of nanoparticles (NP) across the placenta are gaining importance due to increasing exposure of NP to humans. On the one hand, this importance is based on the targeted therapeutic application of NP-based drugs and biopharmaceuticals such as immunoglobulins gamma (IgG). On the other hand, the increased general use of nanoparticles and biopharmaceuticals poses unknown hazards to the foetus during pregnancy. The ability of NPs to cross the placenta was shown for a limited number of investigated NPs. However, whether this transfer occurs in the presence of physiologically relevant macromolecules has not yet been investigated. Knowledge on placental IgG transfer is better established than for NPs. It is known that IgG, mediated by the neonatal Fc receptor (FcRn), can cross the placental barrier. Whether and to what extent specific therapeutic IgGs cross the placenta or act directly on the placenta was only investigated for few antibodies.

In the first part of the thesis, the placental transfer of 80 nm polystyrene (PS) and 100 nm polylactide-co-glycolide (PLGA) NP was demonstrated in a human ex-vivo perfusion model. Perfusion data showed that antipyrine (AP) decreased 500 nm PS NP concentration in the maternal circulation. For 80 nm PS NP, an influence of plasma proteins on NP transfer was demonstrated. Albumin was found to mediate transfer of 80 nm PS NP across the placenta.

The second part of the thesis used the perfusion model to investigate the placental transfer of two therapeutic antibodies, anti-HER2 IgG1 and anti-RANKL IgG2. The expression of HER2 was confirmed, and expression of RANKL was shown in the term placenta. ELISA could not detect a placental transfer of IgG1, but a close relationship of IgG with FcRn and lysosome-associated membrane protein 1 (LAMP1) after perfusion could be detected.

Specific peptides of IgG2 were detected by proteomics in foetal circulation, whereas intact therapeutic antibody was not detected. A functional approach detecting free RANKL showed that the term placenta releases RANKL into the foetal circulation.

Generated data suggest an influence of AP on properties and placental uptake of PS NP at the placental barrier. The relevance of a biocorona on PS NP during perfusion and its ability to increase the placental transfer of NP was evident. A hypothesis-generating estimate of how the placenta processes PS NP was made, but this should be examined in detail in the future. PLGA as a biodegradable material showed potential to deliver drugs across the placenta.

Since the anti-HER2 IgG1 could not cross the placenta but was detected together with FcRn and LAMP 1, it is assumable that antibodies whose epitope are present on or in the placenta

do not cross the tissue. The negative consequences described for the foetus could be directly related to an IgG placenta interaction. For anti-RANKL IgG2, a negative effect on the placenta after short exposures with therapeutic concentrations can neither be confirmed nor denied. Data suggests further studies to investigate the relevance of RANKL in the placenta.

## Table of Contents

Abbreviations .....	1
1. Introduction.....	3
1.1. The human <i>ex vivo</i> placental perfusion model .....	4
1.2. Definitions of nanoparticles .....	7
1.3. Biocorona definition and overview .....	8
1.4. Role of immunoglobulin $\gamma$ during pregnancy.....	9
1.4.1. Immunoglobulin $\gamma$ .....	11
1.4.2. The neonatal Fc-receptor facilitator of placental IgG transfer .....	12
1.4.3. Immunoglobulin based biopharmaceutics.....	13
2. Hypothesis and Objectives.....	16
3. Material and Methods .....	17
3.1. Ethical approval.....	17
3.2. Dual <i>ex vivo</i> placental perfusion.....	17
3.2.1. Subjects, tissue collection and handling.....	17
3.2.2. Applied perfusion media .....	19
3.2.3. Dual <i>ex vivo</i> placental perfusion setting.....	20
3.2.4. Applied compounds.....	26
3.3. Characterization of Nanoparticles .....	29
3.3.1. Biocorona formation .....	29
3.3.2. Nanoparticle tracing analysis (NTA) .....	29
3.3.3. Dynamic light scattering (DLS) and Zeta potential .....	29
3.3.4. Transmission electron microscopy.....	30
3.3.5. Fluorochrome analysis .....	31
3.4. Quantification of IgG2-anti-RANKL antibody and IgG1-anti HER2 antibody.....	32

3.4.1.	ELISA.....	32
3.5.	Proteomics .....	34
3.5.1.	Sample processing and LC-MS/MS analysis of nanoparticles .....	34
3.5.2.	Sample processing and LC-MS/MS analysis of IgG2-anti-RANKL antibody ..	37
3.5.3.	LC-MS/MS data analysis .....	39
3.6.	Microscopy .....	40
3.6.1.	Fluorescence Microscopy of 500 nm PS particles .....	40
3.6.2.	Microscopy of IgG2-anti-RANKL antibody & IgG1-anti HER2 antibody .....	41
3.7.	Cell Culture Experiments .....	43
3.7.1.	BeWo transwell cell experiments.....	43
3.7.2.	Endothelial cell culture assays .....	44
3.8.	Statistical analysis.....	45
4.	Results .....	45
4.1.	Placental perfusion of nanoparticles.....	45
4.1.1.	Characteristics of polystyrene nanoparticles .....	45
4.1.2.	Characteristics of PLGA nanoparticles .....	52
4.1.3.	Perfusion settings influence perfusion outcome for NPs .....	54
4.1.4.	PLGA particles cross the placenta.....	59
4.1.5.	Biocorona on 80 nm polystyrene nanoparticles changes depending on circulation and time .....	60
4.1.6.	80 nm polystyrene nanoparticles were detectable in placental syncytium.....	68
4.1.7.	Albumin mediates placental transport of 80 nm polystyrene nanoparticles .....	70
4.2.	Therapeutic and non-therapeutic IgGs at the placental barrier.....	77
4.2.1.	Placental perfusion with physiological IgG levels .....	77
4.2.2.	Fully monoclonal human IgG2-anti-RANKL antibody crosses the placenta ....	77

4.2.3.	Monoclonal IgG1-anti HER2 antibody is unable to cross the placenta .....	82
4.2.4.	HER2 receptor is expressed in the term placenta.....	83
4.2.5.	Syn 1436 a peptide inhibitor for FcRn .....	87
5.	Discussion.....	89
6.	Conclusion .....	105
7.	References.....	107
8.	Appendix.....	132

## Abbreviations

<b>ANOVA</b>	Analysis of variance
<b>AP</b>	Antipyrine
<b>Apo A-1</b>	Apolipoprotein A-1
<b>Apo E</b>	Apolipoprotein E
<b>Apo M</b>	Apolipoprotein M
<b>BC</b>	Breast cancer
<b>BRCA1/2</b>	Tumour suppressor genes breast cancer 1 and 2
<b>BSA</b>	Bovine serum albumin
<b>CAA</b>	Chloroacetamide
<b>CD163</b>	Scavenger receptor cysteine-rich type 1 protein M13
<b>DLS</b>	Dynamic light scattering
<b>DMEM</b>	Dulbecco's modified eagle medium
<b>DAPI</b>	4',6-Diamidin-2-phenylindol
<b>EBSS</b>	Earl's buffered salt solution
<b>ELISA</b>	Enzyme-linked immunosorbent assay
<b>FBS</b>	Foetal bovine serum
<b>FcRn</b>	Neonatal Fc Receptor
<b>FDR</b>	False discovery rate
<b>FITC</b>	Fluorescein
<b>FM</b>	Foetal maternal ratio
<b>G418</b>	Geneticin
<b>GFP</b>	Green fluorescent protein
<b>HCl</b>	Hydrochloric acid
<b>HDL</b>	High-density lipoprotein
<b>HER2</b>	Human epidermal growth factor receptor 2
<b>HMEC1</b>	Human microvascular endothelial cell line 1
<b>HPLC</b>	High-performance liquid chromatography
<b>HRP</b>	Horseradish peroxidase
<b>HSA</b>	Human serum albumin

<b>HSA Iyo</b>	Human serum albumin lyophilized
<b>IgG</b>	Immunoglobulin $\gamma$
<b>KEGG</b>	Kyoto Encyclopaedia of Genes and Genomes
<b>LAMP1</b>	Lysosomal-associated membrane protein 1
<b>LC</b>	Liquid Chromatography
<b>LC-MS/MS</b>	Liquid Chromatography-Mass Spectroscopy / Mass Spectroscopy
<b>LFQ</b>	Label free quantification
<b>LOD</b>	Limit of detection
<b>LOQ</b>	Limit of quantification
<b>mAbs</b>	Monoclonal antibodies
<b>NP</b>	Nanoparticle
<b>NTA</b>	Nanoparticle tracing analysis
<b>OsO<sub>4</sub></b>	Osmium tetroxide
<b>PABC</b>	Pregnancy associated breast cancer
<b>PS</b>	Polystyrene nanoparticle
<b>PLGA</b>	Poly (lactic-co-glycolic acid)
<b>PBS</b>	Phosphate buffered saline
<b>QC</b>	Quality control
<b>RANKL</b>	Receptor activator of nuclear factor kappa B ligand
<b>RIPA buffer</b>	Radio immunoprecipitation assay buffer
<b>TBE</b>	Tris/Borate/EDTA buffer
<b>TCEP</b>	Tris(2-carboxyethyl) phosphine
<b>TEER</b>	Trans epithelial resistance
<b>TEM</b>	Transmission electron microscopy
<b>TFE</b>	2,2,2-Trifluoroethanol
<b>TRITC</b>	Tetramethylrhodamine

## 1. Introduction

Parts of this chapter were already published or adapted from the candidate's work (1).

In human reproduction, the placenta, as the essential organ for maternal-to-foetal transport, fulfils several roles to sustain development of the foetus during gestation (2). During gestation, the placenta develops to match the needs of the unborn (3). The placenta at term is build up by a placenta specific cellular layer the syncytiotrophoblasts, facing the maternal blood stream, the placental stroma and its components and the placental foetal endothelium facing the foetal blood stream. The syncytiotrophoblasts are unique regarding the absence of cellular borders between them. Nevertheless, paracellular routs exist at this barrier like trophoblastic denudations (4) and trophoblastic channels (5) potentially allowing small molecules to bypass the barrier. The syncytiotrophoblasts are in contact with the maternal bloodstream and form the first barrier between maternal and foetal circulation in the placenta. Beneath the basolateral membrane of the syncytiotrophoblasts is the placental stroma. The stroma consists of fibroblasts and tissue-resident macrophages, the so-called Hofbauer cells. In the stroma embedded are the feto-placental blood vessels, with the continuous feto-placental endothelium which is in contact with the foetal bloodstream (6,7). These cellular areas together form the majority of placental tissue, thereby building up the barrier between mother and child. The barrier of the placenta has several functions, two among others are the acquisition of passive immunity of the foetus by the transport of immunoglobulin G (IgG) from mother to foetus (8) and the partial protection of the foetus from nanomaterials (9). To overcome this function of the barrier would enable foetal in utero therapy with nanoparticles (NP) (10,11).

Nevertheless, IgGs and NPs both bear potential dangers of fetotoxicity (12,13). Knowledge on fetotoxic properties of NPs based predominantly on rodent models. Examples for such NPs are ZrO<sub>2</sub>, Cu, Ag, TiO<sub>2</sub> and polystyrene (PS) which all impact the placenta (14–18). The range of adverse effects on the placenta and the foetus covers a spectrum from cellular to organ impairments, foetal growth restrictions, and neuronal damage of the offspring (14–18). How these observations in rodents may translate to humans is unknown. Recently, the trans-placental crossing of titanium dioxide has been shown in humans *in vivo*, which was already

indicated by *ex vivo* placental perfusion (19). How these results proven *in utero* exposure may affect the children in long term is unknown.

An example of natural occurring IgG-mediated fetotoxic events is the Rhesus factor (Rh) incompatibility between mother and foetus resulting in haemolytic disease. This adverse event is still a global problem in 2020 (20). Nanoparticles and IgGs are both not transferred via channels or transporter proteins, concerning their size. Several macromolecular routes of cellular NP-uptake were reported as reviewed by Yameen et al. (21) including phagocytosis (22), clathrin-mediated endocytosis (23), clathrin-independent endocytosis (24), caveolae-mediated endocytosis (25), and macropinocytosis (26) in a size-dependent manner. Furthermore, specific receptors are mediating the uptake of NPs. Examples of such NP-uptake enhancing receptors are folate receptor (27), transferrin receptor (28), epidermal growth factor receptors (29), prostate-specific membrane antigen receptor (30), low-density lipoprotein receptor (31), and the neonatal Fc receptor (FcRn) (32). Additionally, non-receptor proteins can promote NP-uptake, as shown recently by tumour homing peptide decorated liposomes which accumulated in the placenta (33). After uptake, NPs were detected in various cellular compartments like endosomes and lysosomes (34), endoplasmic reticulum (35), Golgi apparatus (36), mitochondria, and the nucleus (37). Moreover, cells react partially with exocytosis to NP uptake, e.g., by forming secretory vesicles, glucose transporter 4 containing vesicles, and the melanosome (38). Nevertheless, individual intracellular processing routes depend on NP material and properties.

IgG handling at cellular barriers mainly involves the FcRn. After IgG uptake that can end in vesicles, containing the FcRn the IgG can be intracellularly recycled or transferred across the respective barrier. Discriminating factors for intracellular recycling and transfer are not fully understood in all tissues (39). The placental IgG processing is partially understood in the syncytiotrophoblast and was also linked to FcRn (39).

The *ex-vivo* perfusion of a placenta is an approach which combines the research fields of IgG and NP placental transfer, and is considered as the most reliable model for such experiments (8,40,41)

### **1.1. The human *ex vivo* placental perfusion model**

The placenta itself is highly species-specific, and the selectivity in transfer and transport for different substances, e.g. IgG, is different between the species (42,43). Therefore, placental

transfer studies are frequently performed with the *ex vivo* placental perfusion model, which is considered as the gold standard for such studies (44). The method was developed by Panigel et al. in 1967 (45) and was subsequently modified by Schneider et al. in 1972 (46). In labs across Europe, perfusion setting is build up by a perfusion chamber, two magnetic pumps, liquid sampling ports, gas exchange membranes or gas conditioned enclosures (47–50).

In addition, several analytical instruments like a blood gas analyser are interconnected to the perfusion equipment. These devices verify metabolic parameters of the tissue during the experiments. The perfusion chamber keeps the placental tissue in place and additionally keeps it at body temperature. The magnetic pumps recirculate formulated media thereby simulating foetal and maternal blood circulations.

Further, maternal and foetal media needs to be conditioned with gas mixtures to mimic CO<sub>2</sub> and O<sub>2</sub> partial pressures, as it exists *in vivo*. The usage of pressure sensors is less frequent but allows additional information on total foetal vascular backpressure. Figure 1 depicts a scheme of the used perfusion setting for this thesis.

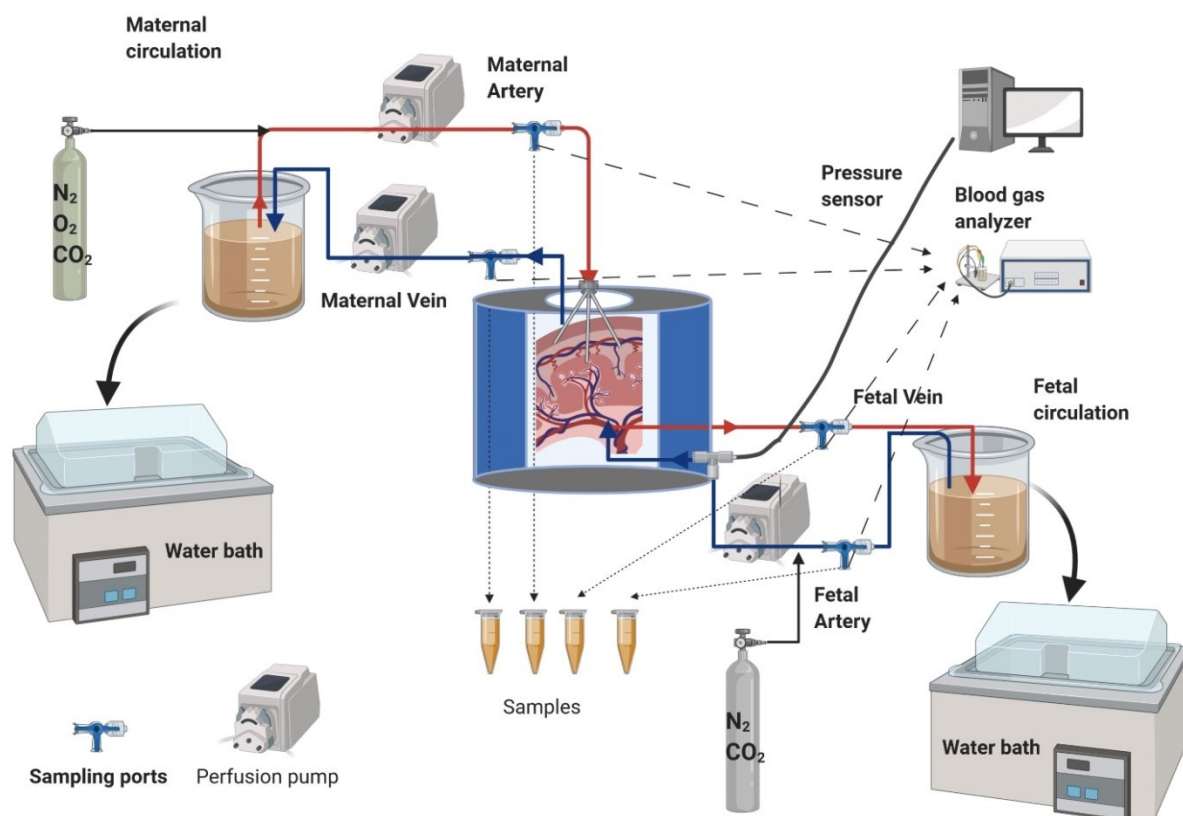


Figure 1. Scheme of the *ex vivo* placental perfusion setting as used at the Medical University of Graz. (Created with BioRender.com)

Beside to general similarities in the instrumentation of the worldwide used model several adaptations are described and mainly linked to the specific experimental objective. The perfusion media and the applied flow rates in maternal and foetal circulation may differ and these adjustments depend on the research question of each laboratory. For example, for NP perfusion experiments media based on Dulbecco's modified eagle's medium (DMEM) (51), Krebs buffer (52), even autologous maternal and foetal blood with TC199 medium (53) and others (54–56) are described in the literature.

Perfusion media for studies with IgGs included M199 (57), RPMI 1640 (58), NCTC 135 (59), eagle's minimum essential medium (EMEM) (60), and buffered saline (61).

Frequently, specific media were diluted with buffers such as Earl's buffered salt solution (EBSS) (56,59) or sodium bicarbonate buffer and contained heparin as anticoagulant (44,57). Media formulations contain additionally added antibiotics and bovine albumin (56,57) or human serum albumin, ranging from 1.8 g/l (62) to 40 g/l (51,63). Of note, the used albumin concentrations could vary between maternal and foetal media. Additionally, dextran in concentrations between 8 g/l (64) and 30 g/l is added to the medium in order to set osmolality of the solution (65). Applied flow rates in the maternal circulation range from 2 ml/min (61) to 25 ml/min (66) historically, nowadays applied flow rates of 12 ml/min (59) to 20 ml/min are frequently described (65). On the foetal side flow rates were more aligned, ranging between 2.8 ml/min (67) to 6 ml/min (65).

The applied flow in maternal and foetal circulation is a key benefit of the perfusion experiment, next to the tissue's intact barriers (68). Flow affects uptake- and NP's transfer processes at cellular barriers (69,70). The specific anatomical structure of a term placenta is responsible for the non-laminar flow in the intervillous space (71). The flow combined with recent used media (56,72–75) in the perfusion model is of high relevance as it was shown that these parameters affect the placental transfer of small molecule drugs (73,76). All these aspects were considered in the performed study, which aimed to investigate the effect of different media compositions on the transfer of NPs by the *ex-vivo* placental perfusion model.

## 1.2. Definitions of nanoparticles

Nanoparticles and nanomaterials are, by definition, in at least one dimension less than 100 nm in size (77). Each year several thousands of metric tons of natural formed NPs and five to six magnitudes fewer engineered NPs enter the environment (78). In the last decades, engineered NPs get in the focus of research, which is in line with an increased production, and usage of such particles. These engineered NPs are applied in several fields e.g. industrial, consumer, or medical applications. In the medical field, engineered NPs enable a new spectrum of cellular targeted approaches, e.g. cancer imaging or cancer therapy (79,80). In pregnancy, engineered NPs possess the capability for targeted treatment of the foetus in utero (10,11). Next to these opportunities, NPs can reach the human food chain and other life aspects due to an unavoidable environmental release. The unintentional exposure to engineered NPs may be potentially harmful to humans, especially for mothers and their unborn (81–83).

This study focused on the examination of NPs, which are constructed from two polymers; polystyrene and poly(lactic-co-glycolic acid) (PLGA) (84,85) (Figure 2).

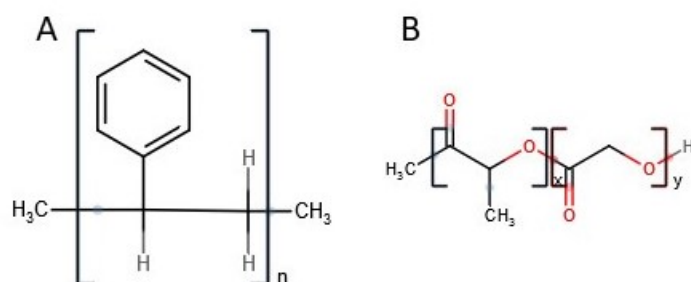


Figure 2. Chemical structure of (A) polystyrene and (B) poly (lactic-co-glycolic acid)

These two polymers are very different concerning their biodegradability. Polystyrene degrades at very slow rates over the years in the environment (86) whereas PLGA is biodegradable and can be tailored regarding its degradation time and, therefore, drug release profile for being used as a drug delivery system (87). Polystyrene is one of the most commonly produced industrial polymers, frequently found as a contaminant in the environment (88,89). PLGA is already used in drug formulations due to its properties and its usage in the field of NP drug formulation will likely increase in the future (81). PLGA NPs were shown to cross BeWo b30 cell layers, a frequent used alternative placental barrier model (85,90–92)

The adverse role of PS NPs in humans is under scientific discussion and cannot be concluded to this point (84,93,94). It is known that PS NP can cross the *ex vivo* perfused placenta but not understood (56). Already known PS NPs properties relevant for their uptake and transfer at the human placental barrier are their surface charge (95–97) and their size (84,96–98). An issue that was not addressed so far is the formation of a biocorona at the PS NP surface and its further impact on the interaction with the human placenta.

### **1.3. Biocorona definition and overview**

Nanoparticles exposed to a biological fluid or medium are readily surrounded by biomolecules which result in the formation of a corona with biomolecules (99). In general, biocoronas are composed of proteins, lipids and nucleic acids (99–101). It has been shown that protein composition on NP surfaces depends on the NP material and alters NP properties (102) (Figure 3). Further, the protein biocorona composition on NP surfaces depends on the used matrix in which they are dispersed (103). These proteins on NP surfaces will be referred to as protein biocorona in the rest of the thesis. The protein biocorona is a dynamic construct which is immediately formed in a matrix, but undergoes quantitative changes over time (104). This dynamic in the protein biocorona composition becomes even more versatile if the NPs are exposed to flow like they would be *in vivo* (105). Besides, the interaction with cells or tissue further alters the composition of the protein biocorona (106). The composition of the protein biocorona also proved to be species-specific (107). The protein composition of the biocorona highly determines the NP uptake mechanism into a target cell (103,108).

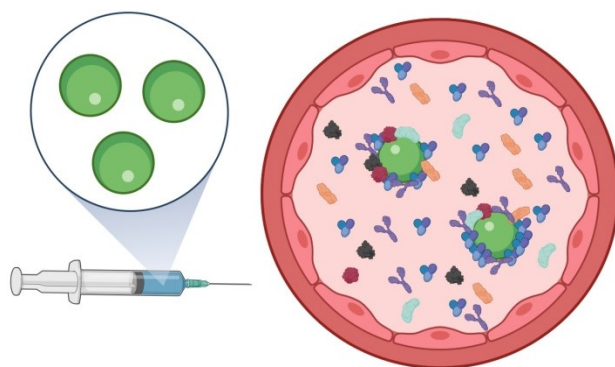


Figure 3. Scheme of NP in a pharmaceutical solution (e.g. water for injection) and the same NP after administration into a blood vessel surrounded by a biocorona. (Created with BioRender.com)

Further, the protein composition can alter the biological effects of NP by mitigating toxicity or triggering immune responses (109). Besides, the protein composition can lead to cellular responses such as a pro-inflammatory response or a response to oxidative stress (110,111). The protein biocorona formation can severely counteract targeting approaches with molecules engineered to the NPs surface as these targeting molecules can be obscured by the biocorona(112). Other reported aspects are protein biocorona dependent changes in the drug release profile of NPs drugs recently summarized by others (113). These changes can enhance, decrease, or delay drug release or potentially alter the drug's pharmacokinetics depending on the biocorona proteins.

All the aspects mentioned above of the protein biocorona can be applied to various NP materials but depend on the NP properties and need to be clarified case by case nowadays. Unquestionably, these aspects affect all kinds of NPs independent of their origin and intended purpose. Therefore the already performed research of others (97) on the transfer of PS NPs in the human placenta was extended by introducing four different media leading to different protein biocoronas within this study.

#### **1.4.Role of immunoglobulin $\gamma$ during pregnancy**

IgGs have a unique role during human gestation, as they can cross the human placenta (8). The foetal detectable IgG concentration is linked to the gestational age, equals, or succeeds the maternal IgG concentration at term and is IgG subclass dependent (114). Due to this placental transfer of IgG, the foetus acquires a maternal derived humoral passive

immunization lasting for the first months of life (115). It was demonstrated that specific maternal vaccinations during pregnancy could positively contribute to neonatal health as rising antibody levels are forwarded to the foetus, guaranteeing protective IgG levels during the first months postpartum (116).

Furthermore, the use of antibody-based therapeutic approaches for various chronic diseases is scientifically discussed for their potential as therapeutics during pregnancy (117,118). The adverse effects of placental IgG transfer are linkable with autoimmunity diseases and alloimmune disorders resulting in pregnancy complications, lifelong impairments of the neonate and death (115). A clinical example is the earlier in chapter 1 mentioned the Rh (D) incompatibility. This complication occurs between mothers that are rhesus negative and their rhesus positive children. The Rh incompatibility is still a challenging pregnancy complication with incidence rate of 1% (119). The therapeutic introduction of anti-D antibodies during pregnancy could reduce the incidence rate to 0.2% of incompatible rhesus pregnancies in rhesus negative mothers (119). Next to physiological occurring challenges therapeutic antibodies more frequently used in the management of severe malignancies. The portfolio of such antibodies covers already all IgG subclasses from 1-4, protein constructs from humanized to full human and newer proteins like bi-specific antibodies (120). The usage of IgG as a cancer treatment is well established, e.g. Trastuzumab for breast cancer (121). Nevertheless Trastuzumab bears several risks on a case report basis and is therefore frequently contraindicated during pregnancy in the general therapeutic scheme (122). The evaluation of risks associated with IgG therapeutics during pregnancy is complex in animal models and cannot be translated well to humans. When the placenta of the most commonly used animal models such as rodents or non-human primates is compared with the human placenta several differences are relevant. Developmental differences are given between rodent and human placentae e.g. in the barrier structure, the structure of the chorion and the significance of the yolk sac. Regarding the barrier structure, trophoblasts in humans are hemomonochorial, whereas in most rodents they are hemotrichorial. The chorion in human placenta forms villi, which differs from the labyrinth found in rodent placenta to increase the exchanged area between mother and offspring. Especially the inverted yolk sac placenta in rodents, which plays a relevant role in IgG transfer for them during their short gestation times, differs from the irrelevance of the yolk sac in human IgG transfer during the much longer gestation period (123). Non-human primate placenta shares the most functions with the

human placenta. Nevertheless, shorter gestation times as well as other not investigated aspects (123) may lead to deviations in the animal model versus the human observations to an unknown degree (124).

### 1.4.1. Immunoglobulin $\gamma$

Immunoglobulin  $\gamma$  (IgG) is the fraction of immunoglobulins in with the highest concentration in blood (125). There are four subclasses of IgG named 1-4 described, and their relative concentration decreases in the order from IgG1 having the highest and IgG4 the lowest plasma concentration (126). The physiological IgG protein itself contains two identical gamma ( $\gamma$ ) heavy chains and two identical light chains (126). The heavy chain contains three constant domains (CH1, CH2, and CH3) and a variable region (VH) (127). The light chain contains one constant domain (CH1), which can be of a kappa or lambda subtype and a variable region (VL) (126). These heavy and light chains form the two regions, fragment crystallisable (Fc) and fragment antigen-binding (Fab), linked by the hinge region (Figure 4). Differences between the IgG subtypes are mainly presented in the hinge region and CH2 domain, defining their binding affinity to receptor (126). Especially the IgG binding of the Fc fragment to one specific receptor, which is described in chapter 1.4.2 can be hold responsible for the ability of IgG to cross the placenta.

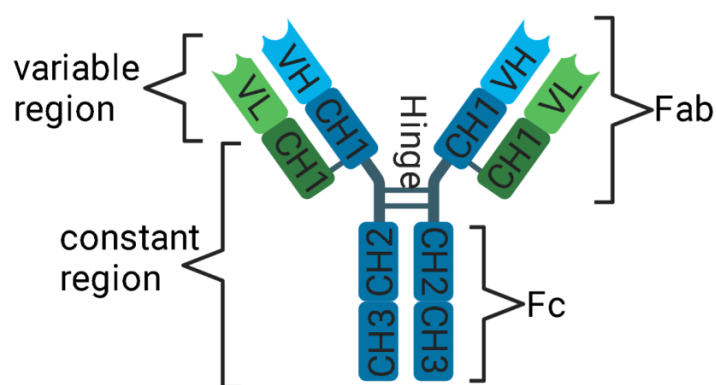


Figure 4. Scheme of a human IgG. The heavy chain constant domains CH1-CH3 are presented in dark blue, the heavy chain variable domain VH in light blue. The light chain constant domain CH1 is presented in dark green, the light chain variable domain VL in light green. The two Fc fragments (CH2 and CH3) are linked with the two Fab fragments (CH1 and VH) via the hinge region. IgGs are of high relevance for humoral immunity in humans as

they interact with effector molecules like Fc- $\gamma$  receptors, Fc receptor-like receptors and complement components (C1q) (128). (Created with BioRender.com)

#### 1.4.2. The neonatal Fc-receptor facilitator of placental IgG transfer

The presence of an IgG transferring receptor was first proposed by Brambell half a century ago, based on his work on IgG transfer from mother to offspring in various mammals (129). It took another 30 years until the receptor was finally confirmed in intestines of neonatal rats, where the receptor got its name neonatal Fc receptor (FcRn) (130) with subsequent confirmation of expression in the human placenta (131). The receptor is a heterodimer consisting of two subunits, the large p51 subunit and a noncovalent bound  $\beta$ -2 microglobulin (Figure 5A), characterized by a low binding affinity to Fc-domain of IgGs at pH 7.4 and high binding affinity at slightly acidic pH (132). FcRn was identified as a critical receptor for the long plasma lifetime and IgG transport across cells (133,134). Next to IgGs, FcRn binds to albumin, thereby stabilizing albumin concentrations significantly in blood (135). FcRn binds IgGs in a ratio of 2:1 (136), albumin in a ratio of 1:1 (137) (Figure 5B), and recycles albumin more efficiently than IgG (6:1) (138). The localization of FcRn in placental tissue has been described in syncytiotrophoblasts, Hofbauer cells and the foetal endothelium (64).

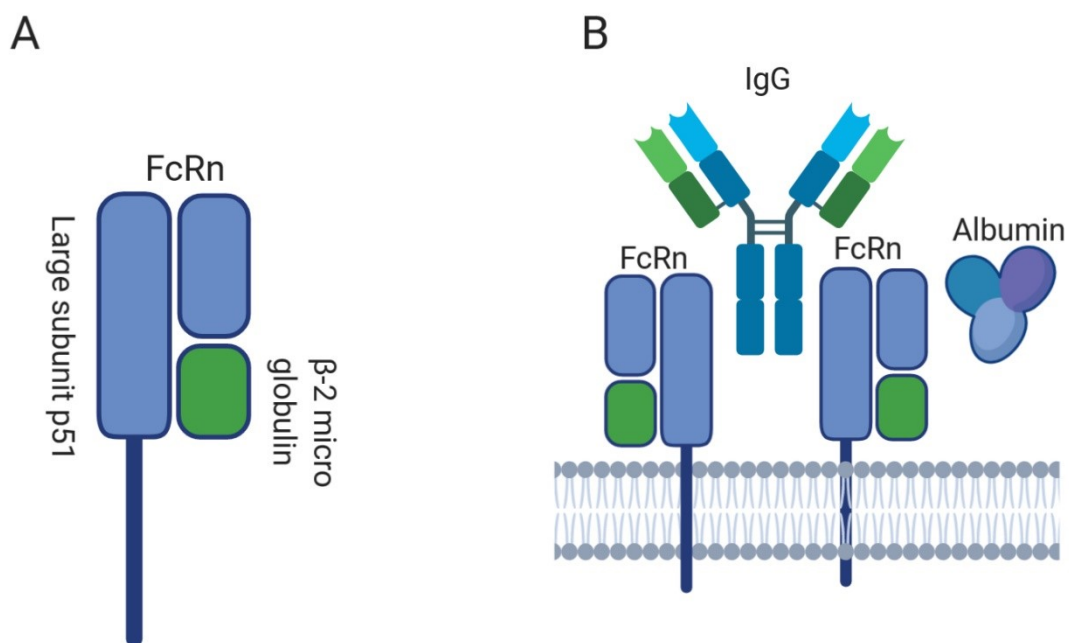


Figure 5. Build-up of FcRn (A) and with its binding partners IgG and albumin (B). (Created with BioRender.com)

It was shown that the IgG specific transport capacity across the placenta correlates with the binding affinity of FcRn to the Fc of the respective investigated IgG (60,62,63) and shows species variations in binding (139,140). Experiments with therapeutic Fab-fragments alone showed no transplacental transfer, indicating the relevance of the Fc binding site of IgGs (141). Nevertheless, the binding affinity of IgGs to FcRn seems not solely responsible for regulating IgG transfer as IgG2 shows high affinity to FcRn but low placental transfer (142).

Of note, the importance of maternal to foetal IgG transfer was long expected and was recently proven (57). Nevertheless, the mechanisms how FcRn discriminates between the recycling and the transfer of IgG in the placenta are not known. As a potential discriminating factor between placental recycling and transfer IgG glycosylation has been introduced (143,144). Recycling and transfer functions of FcRn also highlight its role as a critical player in autoimmune disease. The inhibition of the receptor could lead to new therapeutic opportunities by reducing adverse autoantibodies or alloantibodies during pregnancy(145).

### **1.4.3. Immunoglobulin based biopharmaceutics**

In the last decades, immunoglobulin based biopharmaceuticals were developed continuously, and ~ 70 monoclonal antibodies entered the pharmaceutical market with an expected market volume between 130 and 200 billion US\$ in 2022 (146). IgG-based biopharmaceutics can be separated into three types regarding their origin: chimeric, humanized, and human. Chimeric antibodies have murine origin where the constant regions within the IgGs are biotechnical exchanged with human constant regions (147). The antigen-binding site of humanized antibodies was still raised in a host organism with subsequent modifications in the antibody construct to reduce immunogenic effects within patients (148). Modern monoclonal antibodies have a fully human protein structure, including human glycosylation patterns (149). Within the generated therapeutic monoclonal antibodies, a trend towards fully human IgG1 antibodies was observed (150). The fields of application cover therapies e.g., cancer, Crohn's disease, multiple sclerosis, and osteoporosis (120). The wide variety of therapeutic applications of monoclonal antibodies makes them promising and dangerous at the same time without drug entity-specific investigations.

#### **1.4.4. IgG2- anti-RANKL antibody**

The maternal supply and placental transfer of nutrients also include metabolic changes in maternal metabolism and physiology to sustain the growth and development of the offspring. One of these changes occurs in the maternal breast glands and bone metabolism that can further lead to severe associated diseases like osteoporosis (151) or cancer (152,153).

Especially breast cancer (BC) is one of the more common cancers during gestation, reflected by incidence rates up to 7.4 per 100.000, which accounts for up to 4% of total breast cancer cases in women below 40 years (152,154,155). From metastatic breast cancer patients, up to 80% develop, additionally bone metastases (156). Osteoporosis and BC derived bone metastases are linked by RANK and RANKL, a receptor ligand pair belonging to the tumor necrosis factor family. Besides their essential function in bone, by stimulating the differentiation of osteoclasts, RANKL prepares the mammary gland for lactation. In particular it mediates proliferation of mammary gland progenitor cells that carry mutations in the tumour suppressor genes breast cancer 1 and 2 (BRCA1/2), and modulates hormone-driven breast cancers (157).

A human monoclonal IgG2 was generated to directly inhibit these functions of RANKL in diseases as therapeutic approach (158). Next to the previously mentioned aspects on the mechanisms and usage of IgG based therapeutics during pregnancy, the IgG2-anti-RANKL antibody may potentially be in some specific cases beneficial for pregnancy-associated malignancies (159,160). Nevertheless, adverse effects were reported on the offspring in animal models when the mother was exposed to anti-RANKL antibodies (161–163).

#### **1.4.5. A biopharmaceutical IgG1-anti-HER2 antibody as therapeutic agent for HER2 positive breast cancer**

The incidence rate for breast cancer rises to 15 -35 cases per 100.000 deliveries if the first year post-partum is included (164,165). The prognosis of pregnancy-associated breast cancer is similar to non-pregnant women if age and disease stage are matched and standard treatment is applied (166). In general, treatments during pregnancy should be close to treatments of non-pregnant women (167). To balance the therapeutic strategy by maximising maternal benefit and minimising foetal harm is mandatory in breast cancer health care of pregnant women. Especially as pregnancy termination does not improve breast cancer outcome (167).

Around 15-20% of all breast cancer patients are tested positive for HER2 protein that promotes the growth of cancer cells (168). In pregnancy-associated breast cancer cases, HER2 overexpression may be slightly more frequent than in non-pregnant patients of the same age (169). The receptor HER2 belongs to a family of tyrosine kinase receptors that form homo or heterodimers. They play a role in regulating proliferation and differentiation in several tissues, including the mammary gland and the human placenta (170).

The expression of HER2 in breast cancer takes advantage of a targeted therapeutic approach with monoclonal antibodies against HER2.

However, HER2 is also expressed in the placenta and various foetal tissues *in utero* (171–173). The first therapeutic monoclonal antibody against HER2 was the IgG1-anti-HER2 antibody. The IgG1-anti-HER2 antibody is a humanized IgG 1 used as adjuvant therapy in breast cancer with great success (174). Nevertheless, the usage of the IgG1-anti-HER2 antibody during pregnancy is contraindicated as case studies reported adverse effects for the foetus (122,175). During gestational administration of IgG1-anti-HER2 antibody the development of oligo- or anhydramnios was the main observed complication at the end pregnancy (176). Exposure to IgG1-anti-HER2 antibody during the first trimester did not affect the neonate (177). The IgG1-anti-HER2 antibody-dependent formation of oligo and anhydramnios was placed in proximity to foetal kidney impairment (178) as the foetal kidney expresses HER2 (172). Further, it was reported that oligo or anhydramnios is reversible if IgG1-anti-HER2 antibody therapy was discontinued during gestation (176). Nevertheless, if complications were detectable in neonates after IgG1-anti-HER2 antibody exposure during gestation, it could lead to lethal outcomes postnatal (179).

The direct transfer of IgG1-anti-HER2 antibody from mother to foetus was investigated in a pregnant baboon model where IgG1-anti-HER2 antibody crossed the placenta within 2 hours (180). Human data on the placental transfer of IgG1-anti-HER2 antibody is missing so far.

## 2. Hypothesis and Objectives

Nanoparticles are diverse in their transfer and uptake at the placental barrier in dependency of their material. The interaction of drug and biomolecules can change the cellular and tissue interaction properties further. Due to the ability of PLGA NP to cross cells we hypothesized that pharmaceutically used polymer NPs like PLGA are transferred across the placental barrier. We also hypothesized that *de novo* surface modifications like pharmaceutical exposure and plasma protein adhesion on NP might alter the placental transfer of these NP. To test these hypotheses, *ex vivo* placental perfusion experiments and further analytical methods were used.

Further, we estimate that therapeutically IgG, relevant to disease in the vicinity of pregnancy, cross the placental barrier as IgG's cross the placental barrier physiologically. As pregnancy associated breast cancer and pregnancy associated osteoporosis are rare but severe malignancies, therapeutic antibodies with a potential application to both diseases were chosen as models. It is known that IgG1 is the IgG subclass that crosses the placenta best and that IgG2 is for so far unknown reasons limited in placental transfer. To test this hypothesis, the focus was to analyse IgG1 anti-HER2 antibody and an IgG2 anti-RANKL antibody processing and transfer at the placenta *in-vitro* and *ex vivo*. The investigation should help making animal model data more comparable to human data for therapeutic IgG processing during pregnancy.

### **3. Material and Methods**

In order to improve reading fluency of the materials and methods section, information on the manufacturers of chemicals, instruments, and software packages are documented in tables in the appendix (page 129-138).

#### **3.1. Ethical approval**

All performed studies were approved by the ethical committee of the Medical University of Graz (24-529 ex 11/12) and refer to the sub-study protocols C, E, F, G, and H. Ethics complied with the declaration of Helsinki guidelines. All donors provided written informed consent. Mothers with uncomplicated pregnancies after spontaneous delivery or caesarean section at term (>38<sup>th</sup> weeks of gestation) donated placental tissue.

#### **3.2. Dual *ex vivo* placental perfusion**

##### **3.2.1. Subjects, tissue collection and handling**

Received placentas from successful experiments were from uncomplicated pregnancies at term (38-42 weeks) within 30 min after given birth by caesarean section (N=35) or spontaneous delivery (N=31) from the Department of Obstetrics and Gynaecology, Medical University of Graz.

Exclusion criteria for this thesis included placentas from women with a parity >5, a history of chronic hypertension, hyperlipidaemia, renal or liver disease, heart disease, or pregnancy-induced complications (e.g., preterm labour, preeclampsia). The average clinical characteristics of the donor mothers and characteristics of the donated tissues were given in Table 1 for the respective experimental settings.

Table 1 Subject characteristics of used placentas

	<b>Gestational age [week]</b>	<b>Maternal age [a]</b>	<b>Placental weight [g]</b>	<b>Foetal weight [g]</b>	<b>Pre-pregnancy BMI [kg/m<sup>2</sup>]</b>	<b>Cotyledon wet weight [g]</b>
<b>80 nm PS control medium [N=3*+2]</b>	38.7±0.4	30.2±5.1	517±113	3349±455	21.8±3.1	22.9±9.9
<b>80 nm PS plasma medium [N=3*+2]</b>	39.4±1.2	35±5.2	628±138	3319±366	24.1±4.1	18.7±7.9
<b>80 nm PS HSA medium [N=2*+6]</b>	39.6±0.7	31.6±1.8	675±109	3717±257	21.3±1.5	24±8.6
<b>80 nm PS HSA lyo. Medium [N=1*+2]</b>	39.9±1	32±1.6	547±29	3157±186	21.1±2.2	23.7±1.9
<b>80 nm PS IgG medium [N=2*+1]</b>	39.2±0.8	34.3±2.6	577±110	3637±260	24.3±1.7	29.1±8
<b>100 nm PLGA [N=1*+2]</b>	38.7±0.3	24.8±1.9	544±16	3340±285	23.8±4.3	11.5±0.4
<b>500 nm PS control medium [N=4*+2]</b>	39.1±0.8	28.6±5.4	532±91	2993±177	24.1±4.1	20.3±6.1
<b>IgG2-anti-RANKL antibody 27 µg/ml + serum + IgG [N=2*+1]</b>	39.0±0.5	31.4±2.3	754±305	3212±427	21.9±4.5	22.5±3.2
<b>IgG2-anti-RANKL antibody 27 µg/ml [N=3*+2]</b>	39.6±1.1	28.8±3.8	684±140	3676±483	23.0±2.3	23.8±8.4
<b>IgG2-anti-RANKL antibody 6 µg/ml [N=4*+1]</b>	39.3±1.2	31.4±4.3	580±146	3426±504	25.3±4.5	22.7±5.9
<b>IgG2-anti-RANKL antibody 0.1 µg/ml [N=2*+3]</b>	40.1±0.8	26.6±3.0	566±81	3468±542	23.6±5.3	18.7±4
<b>IgG1-anti HER2 antibody 42 µg/ml 2h [N=1*+2]</b>	37.6±2.3	26.3±5.1	683±301	3242±809	27.7±4.7	24.5±1.4
<b>IgG1-anti HER2 antibody 42 µg/ml 6h [N=5*]</b>	39.5±1.3	28.7±6.2	790±49	3881±583	24.3±2.9	22.8±5.9
<b>Human IgG 10 mg/ml 6h [N=1*+2]</b>	39±1	37.3 ± 2.8	586±51	3503±473	30.5±2.8	19±6.8

(N=x\* indicates number of placentas from caesarean section)

## Processing of placental tissue

Before starting a perfusion experiment, at least one tissue sample, including decidua and tissue from the chorionic plate was isolated from a residual cotyledon of the donated placenta. The sample was gently washed in PBS for 2 min under constant motion. After the end of the perfusion experiment, at least one tissue sample was additionally cut out from the perfused tissue area. The sampled tissues were dissected, washed and transferred into 4% formalin solution for fixation. Tissue was fixed between 24 and 72h. Thereafter, tissues were dehydrated in an ascending ethanol concentration before embedded in paraffin. Embedded tissue blocks were stored in the dark at room temperature until further processing.

### 3.2.2. Applied perfusion media

Five different perfusion media were used namely, (i) control, (ii) plasma, (iii) HSA, (iv) IgG, and the (v) IgG2-anti-RANKL antibody medium (Table1). If not subsequently further specified, these media were used for NP and IgG placental transfer studies. The basis of all media was a 2:1 mixture of DMEM and EBSS respectively, supplemented with 1.33 g/l D-Glucose and 250 mg/l Amoxicillin, further called basic medium. Table 2 summarizes the additional supplements of the five media as well as the added concentrations of the respective NPs or biopharmaceuticals to the maternal circulation. The control medium was in proximity to literature (56,72); the other media were specifically composed of several additives related to the research question.

Medium with plasma was supplemented with non-pregnant female human citrate plasma from a pool of donors (N=2). Argatroban, a specific thrombin inhibitor, was added to prevent the restart of the coagulation cascade in plasma during perfusion experiments. Argatroban dose finding was performed *in vitro* by using medium containing 10% human citrate plasma diluted in basic perfusion medium. Medium was stirred in glass beakers on a magnetic steering plate thereby simulating the primary mechanical stress in maternal and foetal reservoirs during perfusion. Argatroban, a specific thrombin inhibitor, was used as a supplement at a concentration of 33µg/ml for coagulation prevention. For competitive IgG2-anti-RANKL antibody experiments, pooled serum of pregnant women was used in the maternal circulation. The serum pool was generated over several weeks by collecting low volumes of residual serum after routine diagnostic examinations of likely more than hundred women. For the same set of experiments a pool of non-pregnant female serum was used in the

foetal circulation (N=3). To generate serum out of the citrate plasma the coagulation cascade was restarted by adding 20% w/v CaCl<sub>2</sub> into plasma in a ratio of 1:100 (v/v of CaCl<sub>2</sub>/plasma); after 60 min of incubation coagulated proteins were removed by centrifugation and residual serum was used for experiments.

Table 2. Composition of applied perfusion media

	<b>Control medium</b>	<b>Plasma medium</b>	<b>HSA medium</b>	<b>IgG medium</b>	<b>IgG2-anti-RANKL antibody medium</b>
<b>Dextran [g/l]</b>	10	0	0	0	0
<b>BSA [g/l]</b>	5	0	0	0	0
<b>HSA [g/l]</b>	0	40	40	0	40
<b>Human polyclonal IgG [g/l]</b>	0	0	0	10	10
<b>Plasma [v/v%]</b>	0	8.6	0	0	0
<b>Argatroban [µg/ml]</b>	0	33	0	0	0
<b>Serum of pregnant donor pool [v/v%]</b>	0	0	0	0	1
<b>Serum of non-pregnant donor [v/v%]</b>	0	0	0	0	1

### 3.2.3. Dual *ex vivo* placental perfusion setting

The used perfusion setting is based on publications by Schneider *et al.* (46,181) and was further developed by Hirschmugl *et al.* in our lab (182). The experimental perfusion setup is shown in Figure 6.



Figure 6. *Ex vivo* placental perfusion setting as used for this thesis. 1) foetal reservoir 2) pump for foetal circulation 3) pump for maternal backflow 4) perfusion gases 5) glass heat exchange coil 6) gas exchange membrane 7) foetal arterial sampling port 8) perfusion chamber 9) pressure sensor catheter 10) maternal arterial sampling port 11) maternal reservoir

### **Preparations of the tissue**

The maximum of time between delivery of the placenta and further manipulation of the tissue should not exceed 20 min. First, the tissue was examined macroscopically for lesions. A cotyledon without lesion, which was supplied by one chorionic artery and one chorionic vein, was selected, if necessary the amnion was removed. A steel cannula with tubes was inserted in selected artery and vein and fixed by surgical suturing. The tubes in foetal artery and vein deviated in size. The tubes in the vein had a greater diameter, to minimize pressure inside the placental tissue during the experiments. The foetal vessels were flushed with 37°C warm basis medium without additives. If necessary, a ligation of surrounding or branching vessels at the particular cotyledon was performed. Subsequently, the placenta was transferred to the holder of the perfusion apparatus and excessive tissue was removed. The tube for the foetal artery was connected to the upfront operational perfusion pump with a flow rate of 100 ml/h. Flow rate was stepwise increased by 20 ml/h steps and finally reached 3 or 4 ml/min depending on the subsequent experiment. Time intervals between the stepwise flow increases depended on

the measured foetal vasculature backpressure and varied therefore in the individual experiments. Afterwards, the establishment of the maternal circulation took place by inserting a manifold with three connected blunt cannulas by gently pushing them through the decidua to place the cannulas inside the intervillous space. A measured increase in pO<sub>2</sub> between fetal artery to the fetal vein indicated appropriate placement of the maternal cannulas. Mismatches in this criterion lead to a relocation of the maternal cannulas. Flushing the placenta, with open circulation, for at least 30min reduced residual maternal blood components. This perfusion phase was always the first phase and did not differ between all experiments independent of the subsequent investigated question.

### Technical features

A flow rate of 12 ml/min maternal and 4 ml/min foetal was used in the 500 nm PS NP perfusion experiments. In all other perfusion experiments, flow rates of 9 ml/min maternal and 3 ml/min foetal were used. All experiments except the AP washout experiments were carried out in a double closed circulation setting. Gas partial pressures in media were equilibrated with gas exchange membranes. Media in the maternal circulation was equilibrated to 75% N<sub>2</sub>, 20% O<sub>2</sub>, 5% CO<sub>2</sub> and media in the foetal circulation to 95% N<sub>2</sub>, 5% CO<sub>2</sub>.

Samples of 1.5 ml were collected during each experiment set (Table 3) at defined time points from maternal and foetal arteries and veins, respectively (Table 4). One experimental set contained additionally chloroquine to prevent acidification of endosomes as described in more detail in chapter 3.2.4.4. Sampling started within 1 min after the main experiments started with sampling in the foetal circulation, which is the declared 0 min time point. This slight delay and initial sampling was purposefully done to allow the maternal media to overcome the void volume between sampling port and reservoir.

Table 3. Information on differently composed and used media during experiments

Experiments	Control medium	Plasma medium	HSA medium	IgG medium	IgG2-anti-RANKL antibody medium
500 nm PS (40 µg/ml)	X	-	-	-	-
80 nm PS (40 µg/ml)	X	X	X	X	-

<b>80 nm PS (40µg/ml) + Chloroquine (100µM)</b>	-	-	X	-	-
<b>100 nm PLGA (40 µg/ml)</b>	X	-	-	-	-
<b>IgG</b>	X	-	-	-	-
<b>IgG2-anti-RANKL antibody</b>	X	-	-	-	X
<b>IgG1-anti HER2 antibody</b>	X	-	-	-	-

Table 4: Time points of sampling during different perfusion experiments

<b>Time points [min]</b>	<b>500 nm PS</b>	<b>100 nm PLGA</b>	<b>80 nm PS</b>	<b>80 nm PS Chloroquine</b>	<b>IgG</b>	<b>IgG2-anti-RANKL antibody</b>	<b>IgG1-anti HER2 antibody (A/B)</b>
<b>0</b>	X	X	X	X	X	X	A/B
<b>15</b>	X	X	X	X	-	X	A
<b>30</b>	X	X	X	X	X	X	A
<b>45</b>	X	X	X	X	-	X	A
<b>60</b>	X	X	X	X	X	X	A
<b>90</b>	X	X	X	X	X	X	A
<b>120</b>	X	X	X	X	X	X	A+B
<b>150</b>	-	-	-	X	X	-	-
<b>180</b>	X	X	X	X	X	X	-
<b>210</b>	-	-	-	-	X	-	-
<b>240</b>	X	X	X	-	-	X	B
<b>300</b>	X	X	X	-	-	-	-
<b>360</b>	X	X	X	-	-	-	B

A) IgG1-anti HER2 antibody in 150 ml of medium and 120 min continued perfusion. B) IgG1-anti HER2 antibody in 300 ml of medium and 360 min continued perfusion.

## **Sample processing**

All experiments and subsequent analysis with fluorescent NPs were performed in the dark. All sampled media with NPs were stored at 4°C overnight before further analysis. PS NP-containing media were never frozen for long term preservation due to the product description's to avoid freezing of PS NP, with exception of proteomics PS NP samples for batch processing. The same procedure was applied for PLGA NP. Samples from polyclonal IgGs and biopharmaceutical IgG1 and IgG2 experiments were centrifuged at 3000 g for 10 min. Supernatants were transferred to new tubes and were frozen at -80°C until respective batch processing.

### **3.2.3.1. Quality level of perfusion experiments**

First, foetal outflow must equal or exceed 95% of foetal inflow within 10 min. Second, maternal circulation was established, by gently inserting a manifold with three connected blunt cannulas by puncturing the decidua to place the cannulas inside the intervillous space. A flow of 12 ml/min or 9 ml/min, justification given in chapter 1.2.3, was constantly applied in the maternal circulation. A higher pO<sub>2</sub> in foetal vein compared to foetal artery indicated an appropriate placement of the maternal cannulas. If no increase in pO<sub>2</sub> in the foetal vein was observed maternal cannulas were relocated. Subsequently, the placenta was flushed, in open circulation, for at least 30 min to reduced residual maternal blood components. This flushing of the tissue was always the first phase of perfusion and did not differ between all experiments independent of the subsequent protocol.

### **Viability of perfused tissue**

The monitoring of pO<sub>2</sub>, pCO<sub>2</sub>, glucose and lactate concentrations, and pH with a blood gas analyser during the experiments allowed inline monitoring of tissue viability but also, if needed, interventions during the perfusion experiment to balance mentioned metabolic parameters. Additionally, documentation of these parameters was part of the quality assessment in all experiments. Table 4 summarizes also the sampling plan for the viability samples of each set of experiments. Blood gas analyses of the collected samples were immediately implemented in order to minimize the effect of gas partial pressure equilibration with ambient air. If the pH exceeded 7.5 in the maternal or foetal artery samples, pH was adjusted with citric acid to obtain physiological ranges. If the pO<sub>2</sub> or pCO<sub>2</sub> decreased and pH rose to 7.5, in the foetal or maternal artery, the gas exchange membranes were exchanged

during the experiments. Further, the foetal vessel backpressure was recorded continuously by introducing a digital catheter pressure sensor into the foetal arterial tubing with a Y-connector. Average foetal perfusion pressure in foetal vasculature was kept below 65 mbar without pressure peaks above 80 mbar to reduce the risk of vasculature rupture.

### **Criteria of a successful perfusion experiment**

Each experiment was validated in regards to reproducibility according to literature (4). All experiments were assessed and needed to pass several quality criteria: i) perfusion of foetal circulation was established within 30 min after delivery of the placenta; ii) the foetal volume recovery was at least 95% within 10 min during the washout phase; iii) O<sub>2</sub> transfer from maternal to foetal circulation was detectable by a higher O<sub>2</sub> partial pressure in foetal vein compared to foetal artery; iv) the difference in media volume between maternal and foetal circulation was below 30 ml (5 ml/h) at the end of the perfusion experiment; v) the antipyrine F/M ratio (AP) determined was at least 0.3 within 30 min of perfusion time; vi) glucose was consumed, and lactate was formed, vii) the pH in both circulations equilibrated between 7.2 and 7.5 and viii) the foetal vessel backpressure was below an average of 65 mbar without pressure peaks above 80 mbar.

#### **3.2.3.2. Antipyrine**

Antipyrine, a small molecule drug that crosses membranes by passive diffusion in a flow-dependent manner, is a frequently used substance in perfusion experiments (46). It serves as indicator for the exchange area between maternal circulation and placental tissue (183).

Basic medium with 100 µg/ml AP was used for the maternal to foetal AP transfer studies, which were performed in open circuits. Foetal media contained no AP and the same flow rates were applied as in the respective perfusion experiments with the compound of interest. Samples of 1.5 ml were collected from the foetal vein, maternal artery, and vein at 0, 10, 20, and 30 min perfusion time. All AP samples were centrifuged at 3000 g; supernatants were collected and stored at -20°C until analysis.

In one set of experiments, the maternal to foetal antipyrine transfer took place before the main experiment with 500 nm PS NPs started. For all other experiments, perfusion of AP was started after tissue was perfused with the compound of interest.

AP wash out perfusion experiments were performed in order to assess the required time to remove AP from the perfusion setting and the placental tissue (N=3). The applied flow rates were 12 ml/min and 4 ml/min in maternal and foetal circulation, respectively. After AP was perfused for 30 min a subsequent washout period of 60 min followed, using basic medium, in a double open circuit setting. For AP quantification, 1.5 ml samples were taken every 5 min from maternal and foetal vein.

Antipyrine concentrations were determined in maternal and foetal perfusates by HPLC according to Annola *et al.* (5). Briefly, 100  $\mu$ l of perfusate was mixed with 100  $\mu$ l methanol, vortexed, and centrifuged at 12000 rpm for 15 min. The upper phase was transferred to a new tube and mixed with 150  $\mu$ l acetonitrile, vortexed, and centrifuged. The antipyrine standard curve included concentrations ranging from 5  $\mu$ mol/l to 1 mmol/l. AP levels in the supernatants were determined by HPLC. For the measurement, 10  $\mu$ l sample or standard was injected and run at isocratic flow (0.2 ml/min) at room temperature in a mobile phase of 20 mM KH<sub>2</sub>PO<sub>4</sub> in water, mixed 1:1 with acetonitrile. Antipyrine was quantified by a UV-detector at 255 nm. The foetal to maternal (FM) AP ratio was calculated and only perfusion experiments with a FM ratio above 0.30 within 30 min were declared as successful, and included for further analysis.

### **3.2.4. Applied compounds**

#### **3.2.4.1. Polystyrene 500 nm**

The 500 nm PS NPs were perfused for 6 h using two different protocols. The aim was to investigate the influence of AP on the transfer of PS NPs in control medium. First, the tissue was perfused with AP before the perfusion of the PS NPs started (N=3). After 30 min of AP perfusion, the experiment was continued with control medium containing 40  $\mu$ g/ml of 500 nm PS NPs. Second, the perfusion with 40  $\mu$ g/ml 500 nm PS NPs was performed before AP was applied (N=3). The flow rate for these experiments was 12 ml/min in the maternal and 4 ml/min in the foetal circulation.

#### **3.2.4.2. Polystyrene 80 nm and biocorona**

To study the influence of a biocorona on maternal to foetal transmission of 80 nm PS NPs four differently formulated media (control (N=5), plasma (N=5), HSA (N=5), IgG (N=3)) were used as published (1). Further, perfusions with medium based on lyophilized human

HSA (N=3) were performed in analogy to the HSA medium experiments. The formation of the biocorona on NPs was executed by using 1.2 ml of PS NP stock solution (1% w/v) incubated either in 26 ml of citrate plasma, 60 ml of HSA solution (200 g/l), 30 ml of IgG solution (100 g/l) or control medium for 15 min at 37 °C. This preincubated protein NP solutions were further diluted with the respective medium that contained the remaining supplements to a final volume of 300 ml. A dilution was mandatory to decrease the viscosity of the preincubated media and to increase nutrients in order to run perfusion experiments under physiological conditions. Finally, this medium contained 40 µg/ml of PS NPs and was used at the beginning of the experiment in the maternal compartment. In contrast, the foetal media lacked PS NPs but was identically composed as in the maternal circulation. The applied flow rates were 9 ml/min and 3 ml/min at the maternal and foetal site respectively. Further, one placenta was perfused with 80 nm PS NPs in plasma medium for 3h which was then fixed under perfusion for electron microscopy. An additional placenta was perfused without PS NPs for 3h with subsequent perfusion fixation for electron microscopy.

#### **3.2.4.3. Poly(lactic-co-glycolic acid)**

Control, medium with 40 µg/ml of 100 nm PLGA NPs labelled with Texas red (184) (kindly provided by Prof. Gabor and Prof. Wirth from the Institute of Pharmaceutical Technology, University of Vienna) were used in this set of experiments (6 h, N=3). The experimental setting applied here was (i) double recirculating (closed) perfusion; (ii) 300 ml medium on each side of the placenta and without PLGA NPs on the foetal side; (iii) The flow rate was 12 ml/min in maternal-and 4 ml/min in the foetal circulation. AP transfer was studied after perfusion of PLGA NPs. The PLGA NP experiments did not meet the strict QC criteria of the other perfusion experiments performed within this thesis, as in the PLGA NP experiments a high volume shift from the foetal to the maternal circulation, representing a leakage rate between 8 and 33 ml/h, was observed in all experiments. Furthermore, in this experimental set the wet weight of the perfused cotyledons clearly deviates from the other experimental sets.

#### **3.2.4.4. Human neonatal Fc-receptor and chloroquine**

As IgG and HSA are binding partners of FcRn, the potential involvement of FcRn in the PS NP transfer in the presence of HSA and chloroquine to prevent acidification of endosomes, was investigated by perfusion experiments (N=3) (185). The introduction of chloroquine aimed for the partial inhibition of potential pH depended transfer mechanisms of PS NPs, as

IgG and HSA binding to FcRn depends on slight acidic pH values. These experiments were split into two phases and in all settings, 300 ml of media were used for both circulations. Initial a 3h perfusion phase with 40 µg/ml PS NPs with HSA medium was performed to establish a reference NP transfer kinetic in the individual cotyledon. Subsequently, during a 30 min washout period, with open circulations, PS NPs in the tissue and perfusion system was depleted. For this washout phase, a PS NP free HSA medium with 100 µM chloroquine was used. After the washout, new HSA medium containing 100 µM Chloroquine and 40 µg/ml PS NPs were applied to the perfusion system for further 3h. To identify potential deviations in transfer kinetics with/without chloroquine PS NPs concentrations were measured and compared.

#### **3.2.4.5. Immunoglobulin**

In order to validate the used *ex-vivo* placental perfusion setting for antibodies, IgG maternal to foetal transfer was experimentally determined (N=3). First, all endogenous IgG in placental tissue was depleted during an extended 120 min washout phase before IgG perfusion started. After the washout, samples were taken from maternal and foetal vein to quantify the remaining IgG outflow from the placenta. In all experiments, (210 min) control medium supplemented with 10 g/l of pharmaceutical polyclonal human total IgG was applied. IgG samples were quantified by ELISA.

#### **IgG2-anti-RANKL antibody**

##### **Perfusion experiments with IgG2-anti-RANKL antibody**

A dose-dependent placental transfer of Denosumab was carried out with control medium supplemented either with 27 µg/ml, 6 µg/ml, or 100 ng/ml of Denosumab for 240 min (186–188) (N=5 per group). Samples were taken as shown in Table 4, with additional sampling of 25 ml perfusion media at the end of the experiment from maternal and foetal reservoirs. Samples were centrifuged at 3000 g for 10 min and subsequently stored at -80°C in 1.5 ml or 10 ml (samples at the end of perfusion) aliquots until LC-MS/MS batch processing.

##### **Competitive perfusion experiments with the IgG2-anti-RANKL antibody**

In the presence of competing IgGs trans-placental transfer of 27 µg/ml IgG2-anti-RANKL antibody was assessed by using HSA/IgG medium supplemented by 10% pooled pregnant serum in the maternal circulation (N=3). In the foetal circulation, the same medium additionally supplemented with 10% non-pregnant serum instead of pregnant serum and

without IgG2-anti-RANKL antibody was used. Samples were centrifuged at 3000 g for 10 min and subsequently stored at -80°C as 1.5 ml or 10 ml (samples at the end of perfusion) aliquots until LC-MS/MS batch processing or RANKL ELISA analysis.

### **IgG1-anti HER2 antibody**

In the first set of experiments the transfer of 42 µg/ml IgG1-anti HER2 antibody was investigated with control medium (150ml) for two hours [N=3]. In the second set of experiments, perfusion time was increased to 6 h, and perfusion volume was increased to 500 ml, again containing 42 µg/ml IgG1-anti HER2 antibody [N=5]. Samples were centrifuged at 3000 g for 10 min to remove erythrocytes; supernatants were collected and stored at -80°C until ELISA quantification.

## **3.3.Characterization of Nanoparticles**

### **3.3.1. Biocorona formation**

Formation of a biocorona on the surface of PS NPs was performed by adding 1200 µl 80 nm PS NP stock solution to 2.6 ml female citrate plasma or 6 ml HSA solution or 3 ml IgG solution for 15 min at 37°C. These suspensions were further diluted to a final volume of 30 ml after the 15 min incubation to equal to the maternal perfusion media.

### **3.3.2. Nanoparticle tracing analysis (NTA)**

Nanoparticle Tracking Analysis (NTA) is one of the few methods, which visualizes and measures NP in suspension. 80 nm PS NP stock was sonicated for 3 min. The sonicated stock was diluted in control, plasma, HSA, IgG media and water to reach a concentration of 400 ng/ml and was incubated for 15 min at 25°C. Nanoparticles were visualized with a laser beam (488 nm). Data was recorded by camera at a slider gain of 15, and camera levels of 9, except for plasma medium where camera level was adjusted to 5. PLGA NPs were processed and measured like PS NPs in control medium. Five technical replicates were applied.

### **3.3.3. Dynamic light scattering (DLS) and Zeta potential**

For DLS measurements 80 nm PS NP and 500 nm PS NP stock solutions were sonicated for 3 min, diluted in control-, plasma-, HSA- IgG medium, and PBS to reach a concentration of 40 µg/ml. Additionally, 500 nm PS NPs were prepared in double-distilled filtered water with and

without 3mg/ml AP to reach a final concentration of 40 µg/ml. To allow biocorona formation, the PS NPs were incubated 15 min before each measurement in the respective medium, as described (1). For the DLS measurement 500 µl of the samples were transferred into single use semi micro cuvettes. Refraction index of the PS NPs was set as polystyrene latex beads. Viscosity of the media was set to water. All measurements were performed in technical triplicates at 25°C.

For zeta potential measurements 80 nm PS NPs were diluted to 1 µg/ml in the same media. The 500 nm PS NP stock was diluted to 1 µg/ml in control medium, control medium with 0.1 mg/ml AP, water, water with 3 mg/ml AP and PBS. To allow biocorona formation, the NPs were incubated 15 min before each measurement in the respective medium. Disposable folded capillary cells were filled with sample and after 2 min of equilibration time zeta potential was measured. Measurements were performed three individual times with a minimum of 10 replicates and a maximum of 100 runs in each measurement.

The PLGA NP stock solution was sonicated for 3 min and diluted 1:1000 in plasma medium for DLS measurements. Further, the handling of PLGA NPs was in accordance to PS NP processing.

### **3.3.4. Transmission electron microscopy**

To validate NP size, and shape of 100 nm PLGA NPs and 500 nm PS NPs, respective NP stock solutions were aspirated in semipermeable cellulose-capillaries. A subsequent fixation step in 2% paraformaldehyde/ 2.5% glutaraldehyde in 0.1 M cacodylate buffer was performed for 2 h. Afterward, capillaries were washed in 0.1 M cacodylate buffer for 2h with subsequent staining in 2% osmium tetroxide solution for an additional 2h. Samples were washed overnight at 4°C in 0.1 M cacodylate buffer. Samples were dehydrated in an ascending ethanol row, 50%, 70%, 80%, 96% for 30 min, and two times for 15 min in 100% ethanol. Embedding was performed for 1 h in propylene oxide followed by 3 h in a mixture of propylene oxide and TAAB resin (1:1). Samples were transferred in a new propylene oxide TAAB resin mixture and stored overnight at 4°C. The next day, samples were changed to TAAB for 90 min at 45°C for PS NPs and 37°C for PLGA NPs two times. Polymerization was performed at 60°C for PS NPs and 37°C for PLGA NPs. Ultra-thin sections (70 nm) were generated and investigated with an FEI Tecnai 20 at 80 kV.

To validate the NP size, and shape of 80 nm PS NPs and PLGA NPs were natively applied to a carbon membrane grid, liquid was gently removed, and TEM pictures were taken with an FEI Tecnai 20 at 80 kV.

Placental tissues were fixed with of 2% formaldehyde, 2% glutaraldehyde in 0.1 M sodium cacodylate buffer, during perfusion with maternal and foetal flow rates of 100 ml/h for 30 min. The fixed cotyledon was isolated, weighted, and ten cubes with a side length of ~1 mm were resected from different areas of the cotyledon. Cubes were transferred into the same buffer for additional fixation and stored overnight at 4°C. Samples were transferred in 2% osmium tetroxide (OsO<sub>4</sub>) and washed in 0.1 M cacodylate buffer.

The cubes were dehydrated in an increasing ethanol row (50%, 70%, 80%, 96%, 100%, 100%, 15 min per concentration). Subsequently, the cubes were placed into propylene oxide as an intermedium and embedded in TAAB embedding resin. Thin sections were made at 70 nm thickness with a Leica UC 6 ultramicrotome. The sections were visualized at an acceleration voltage of 80 kV with a Zeiss EM 900 transmission electron microscope.

### **3.3.5. Fluorochrome analysis**

All used NPs contained a fluorochrome. The fluorescence of the respective NPs was quantified in the respective media by using a fluorescence plate reader.

At the beginning of the study PS NPs loaded with a “green” emitting chromophore and PS NPs with a “pink” emitting chromophore were tested in control perfusion medium. This medium was collected from the maternal circulation after 3 h washout perfusion. The medium was enriched with residual blood components, and placental derived biomolecules that may interfere with the fluorescence read out. The same experiments were performed with BODIPY FL, and Texas red labelled PLGA NPs. The limit of detection (LOD) and the limit of quantification (LOQ) emanated from the results of a concentration series, 0.5, 1, 1.5, 2, 5, 15, 25, 35, 50, and 75 µg/ml, of NPs containing the respective dye. The series was measured in quadruplicates with a chromophore dependent filter set (485/520 nm or 544/590nm). Further, 12 blanks were used on each individual 96 well plates to generate a bassline for the sensors noise and calculate the standard deviation of the blank. Calculations of LOD and LOQ based on guidelines of the international council for harmonization of technical requirements for pharmaceuticals for human use (ICH) (189):

$$LOD = \frac{3.3 * \textit{standard deviation of the blank}}{\textit{Slope of the concentration series}}$$

$$LOQ = \frac{10 * \textit{standard deviation of the blank}}{\textit{Slope of the concentration series}}$$

Based on these validation results, the NP concentration was quantified indirectly with a FluoStar Optima fluorescence plate reader; excitation wavelength of 544 nm and emission wavelength of 590 nm. 80 and 500 nm pink labelled PS NPs, and 100 nm PLGA NPs Texas red labelled were quantified in triplicates. Each maternal and foetal sample was vortexed and three aliquots of 200 µl were transferred to non-binding black F-bottom 96 well microplate. Standards of respective NPs (1, 5, 15, 35, 75 µg/ml) in the respective perfusion medium, served as a reference for each experiment. Obtained signals were background corrected to foetal 0 min sample of each experiment, which contained no NPs. Linear regression model was used as model fit for NP quantification.

To exclude any destructive effects of AP on the 500 nm PS NPs 10 ml of control medium with and without 100 µg/ml AP were gently mixed in glass beakers on a magnetic stirrer for 5 h to achieve similar mechanical stress as encountered in the perfusion setup. The PS NP concentration was 40 µg/ml. Light conditions during steering were similar to perfusion light conditions to avoid bleaching of the chromophores. After the five hours, the residual PS NPs containing media were filtered through 20 nm syringe filters. The fluorescence of 100 µl aliquots from the filtrates was measured in triplicates to determine the leaked chromophore amount. The leakage results were compared between each other with paired student's t-test.

### **3.4. Quantification of IgG2-anti-RANKL antibody and IgG1-anti HER2 antibody**

#### **3.4.1. ELISA**

All collected perfusion and cell culture samples were centrifuged at 3000 g to remove residual erythrocytes and cell debris. Perfusion sample (1000µl) or cell culture supernatants (as indicated in the respective sections) were collected and stored at -80°C until quantification.

#### **ELISA for total IgG**

Samples were diluted with sample buffer 1:10000 (foetal) and 1:10000000 (maternal), before analysis, all collected samples were determined as triplicates according to the protocol. The inter CV was 10.4% for the replicates.

### **ELISA based Assay RANKL**

The saturation of IgG2-anti-RANKL antibody with RANKL was quantified indirectly, after placental perfusion experiments. In the assay, maternal and foetal perfusion samples from start and endpoint were analysed. Maternal perfusion samples were diluted 1:27 into RANKL free perfusion medium. Subsequently, dilution of maternal samples was 1:100 and of foetal samples, 1:1 in serum/IgG medium, spiked with free recombinant RANKL (20 pg/ml and 10 pg/ml, respectively). Samples were mixed for 2h with an overhead shaker to enable the binding of the IgG2-anti-RANKL antibody and RANKL. Aliquots of the samples (150 µl) and the serum/IgG medium (150 µl) were analysed by enzyme-linked immunosorbent assay (ELISA) to detect remaining free recombinant RANKL. The readout was blanked against serum and compared to the standard curve and serum/IgG medium with 20 pg/ml RANKL. These values indicate the amount of pharmacologically active and, therefore, functional IgG2-anti-RANKL antibody after the experiments. ELISA analysis followed the manufacturer protocol at 450 nm. The inter CV was 3.2% for the replicates.

### **ELISA for IgG1-anti HER2 antibody**

10 µl of foetal perfusates and 10 µl of 1:50 diluted maternal perfusates were used to meet the ELISA's analytical range. The handling of the samples was performed with regard to the manufacturer's protocol. Spectra Max 250 UV plate reader (450 nm) was used to determine IgG1-anti HER2 antibody levels. The inter CV was 9.6% for the replicates. Because of the expected low IgG1-anti HER2 antibody concentrations in the FcRn depended cell culture experiments for IgG recycling the ELISA was adjusted. Adjustments compared to the manufacturer's protocol were a dilution of the 72 collected supernatants 1:1 instead of 1:10 in the assay buffer. Further, the incubation time for the enzyme link chromophore reaction was doubled to generated detectable chromophore ranges. The remaining parts of the assay were performed as described by the manufacturer. ELISA had an intra CV of 11.5% and an inter CV of 3.6% in this adjusted setting.

## 3.5. Proteomics

### 3.5.1. Sample processing and LC-MS/MS analysis of nanoparticles

Preparatory procedure of collected maternal and foetal perfusates was published (1). To investigate the differences of biocorona proteins on PS NPs surfaces, 6 ml of maternal and foetal medium after 360 min tissue perfusion and 2 ml of non-perfused PS NPs pre-incubated with plasma medium were collected and processed. In order to remove cellular debris and un- or weakly bound proteins all samples were centrifuged for 10 min at 5000 g at 4°C. The supernatant was collected and immediately processed as published by Docter et al. (190) except for the used centrifugal force (21000 g). The gathered pellets were stored at -80°C until LC-MS/MS analysis.

#### 3.5.1.1. LC-MS/MS analysis 80 nm PS protein biocorona

The used LC-MS/MS method was published (1). Biocorona proteins bound to PS NPs were dispersed in TFE-digestion buffer (25% 2,2,2-trifluoroethanol (TFE) in 50 mM Tris-HCl, pH= 8.5) followed by a centrifugation step (15300 g, 4°C, 10 min.). 10 mM tris(2-carboxyethyl) phosphine (TCEP) and 40 mM chloroacetamide (CAA) were used for reduction and alkylation for 1 hour at 37°C. Samples were diluted to 10% TFE with 50 mM ammonium bicarbonate and digested using rLysC in a protein: enzyme ratio of 100:1 at 37 °C for 3.5 hours.

Subsequent, a second digestion with modified trypsin protein: enzyme ratio of 50:1 at 37°C was performed overnight. Enzymatic digestion was stopped with 5% formic acid to reach 0.1% final concentration of peptide. The resulting peptide solution was filtered through a 10 kDa cut-off filter to remove the NPs and injected into a nano-HPLC equipped with a C18, 5 µm, 100 Å, 5 x 0.3 mm enrichment column and an Acclaim PepMap RSLC nanocolumn (C18, 2 µm, 100 Å, 500 x 0.075 mm). Peptide concentration was increased on the enrichment column for 6 min at a flow rate of 5 µl/min with 0.1% heptafluorobutyric acid as isocratic solvent. Separation by chromatography was performed on a nanocolumn at a flow rate of 300 nl/min<sup>-1</sup> at 60°C using subsequent gradient; solvent A: 0.1% formic acid in water; solvent B: acetonitrile containing 0.1% formic acid; 0-6 min: 4% B; 6-94 min: 4-25% B; 94-99 min: 25-95% B. 99-109 min: 95% B; 109.1-124 min: 4% B. The maXis II ETD mass spectrometer was operated with the captive source in positive mode employing the following settings: mass

range: 200-2000 m/z, 2 Hz, capillary 1300V, dry gas flow 3 L/min with 150°C. nanoBooster 0.2 bar, precursor acquisition control top17 (CID).

### **Mass Spectroscopy data processing.**

The LC-MS/MS data were analysed by Data Analysis software from Bruker, using the Sum Peak algorithm, and by MaxQuant 1.5.8.3 searching the public Swissprot database with taxonomy Homo sapiens (downloaded on 02.03.2017) and common contaminants (20233 sequences). Carbamidomethylation on Cys was entered as a fixed modification, oxidation on methionine as variable modification. Detailed search criteria were used as follows: trypsin, max. missed cleavage sites: 2; search mode: MS/MS ion search with decoy database search included; precursor mass tolerance +/- 0.006 Da; product mass tolerance +/- 40 ppm; acceptance parameters for identification: 1% PSM false discovery rate (FDR); 1% protein FDR. Besides, an intensity based quantitation including the match between runs feature of MaxQuant was performed (191) requiring a minimum of 2 quantified razor and unique peptides. The software Perseus version 1.6.12.0 was used for further data processing. Intensities were log<sub>2</sub> transformed and reduced to proteins detected in all samples of at least one sampling cohort (4 valid in a group of 4, plasma, maternal or foetal), reflecting a defensive data inclusion strategy.

Qualitative comparison of the protein distribution between groups was done with Venny (Oliveros, J.C. (2007-2015) Venny (<https://bioinfogp.cnb.csic.es/tools/venny/index.html>)). For quantitative investigations, the intensity data was normalized by median subtraction for each respective LC-MS/MS run to align data points around the zero point of log<sub>2</sub> transformation. Further, missing data points were imputed within the software Perseus. Briefly, missing values were replaced with random values taken from a shifted Gaussian distribution of all valid values (width of 0.3 and downshift of 1.8 separately for each column), in order to simulate an intensity value for low abundant protein groups. Statistical comparison was done by a multiple t-testing approach with a permutation based FDR to detect significant differences between the sampling groups. Additionally, the relative distribution of significantly enriched proteins in foetal biocoronas was calculated based on relative intensity of the respective proteins compared to total intensity.

The mass spectrometry proteomics data were made available at the ProteomeXchange Consortium (<http://proteomecentral.proteomexchange.org>) via the PRIDE partner repository (192) with the dataset identifier PXD018160.

### **3.5.1.2. Data handling and analysis**

#### **Functional analysis of proteomics data**

The functional analysis of the isolated biocorona proteins were carried by using three online databases. The databases were DAVID: Functional Annotation tool (build 6.8), STRING: functional protein association network (version 11), and the Reactome Pathway database (Reactome browser version 3.6, Reactome database release 70). Due to differences in the recovery rate of the individual proteins in the databases and the different calculation models in the databases, all three tools were used and compared for pathway analysis. The gene names of 642 significant proteins on maternally isolated NPs were analysed. For comparing the three most likely results for biological processes in the STRING and DAVID database, or pathways in the Reactome database, a table is provided (Table 9) with the false discovery rate output from each database.

#### **Intracellular pathway proposal**

The significant enriched proteins of the maternally isolated PS NPs after perfusion were compared with the Kyoto Encyclopaedia of Genes and Genomes (KEGG) pathway database and additional publications (193–202). Out of the 642 proteins, 144 were structured in a proposed intracellular processing cascade to emphasise how the placental tissue could interact with 80 nm PS NPs.

### **3.5.1.3. Western Blot of plasma incubated nanoparticles**

As a complementary approach to the proteomics analysis, plasma medium was incubated with 40 µg/ml 80 nm PS NPs, plain plasma medium, and plasma was used for western blotting. One ml of PS NP containing medium was loaded on one ml of 0.7 M sucrose in a 2 ml Eppendorf tube. For the pure plasma medium, the approach was carried out ten times and pooled to enrich the investigated proteins. The tubes were centrifuged for 15min at 21000 g to generate either a PS NP-protein or a pure protein pellet. The pellets were resuspended in 2 ml of PBS and centrifuged again this washing step was repeated three times. Supernatant was discarded. The pellet was resuspended in 100 µL of PBS, for the plain plasma medium tubes

were vortexed and pooled, and finally centrifuged to get a pellet. Pellets were treated in RIPA buffer before western blotting. As a positive reference, human plasma used for the plasma medium was treated in RIPA buffer as well. The treated pellet proteins were loaded onto Biorad Mini-Protean TGX 4-20% precast gel/10 wells/50 $\mu$ l. Proteins were transferred onto nitrocellulose membranes using the TransBlot Turbo system from Biorad. Membranes were blocked for one h in 5% non-fat milk in TBE buffer was used for blocking the membranes. Membranes were incubated with antibodies against Apo A1, Apo B, which were also present in the proteomics results and Apo M, which is part of the HDL NP, and therefore could be an indicator if HDL was co-isolated, overnight. Membranes were developed using an ECL chemiluminescence substrate in a Vilber Fusion FX camera system for the semi-quantitative analysis.

### **3.5.2. Sample processing and LC-MS/MS analysis of IgG2-anti-RANKL antibody**

The IgG2-anti-RANKL antibody was enriched with protein G affinity columns from collected perfusion samples. In details, one ml of sample (27  $\mu$ g/ml, 6  $\mu$ g/ml) and 5 ml (0.1  $\mu$ g/ml) of the respective samples were loaded on the affinity columns. Further processing was performed as described in the manual. Due to technical changes in the nano-LC equipment, the analytical method changed between the first analysis batch (27  $\mu$ g/ml) and the second analysis batch (6  $\mu$ g/ml). The liquid chromatography-tandem mass spectrometry (LC-MS/MS) method was further adapted for the experiments with the lowest IgG2-anti-RANKL antibody concentration (0.1  $\mu$ g/ml), the third analytical batch in order to increase sensitivity.

#### **Sample preparation for LC-MS/MS**

For tryptic digest, approx. 50  $\mu$ g protein of protein G purified perfusion products were precipitated with four volumes of acetone at -20°C overnight. The precipitate was solubilized in 50  $\mu$ l 25% 2,2,2-Trifluoroethanol (TFE) in 50 mM Tris-HCl (pH 8.5), reduced with 10 mM Tris(2-carboxyethyl)phosphine (TCEP) and alkylated with 40 mM chloroacetamide at 95°C for 10 min. The solution was diluted to 10% TFE with 50 mM ammonium bicarbonate. Protein was digested by adding one  $\mu$ g of Promega modified trypsin and shaking overnight at 550 rpm at 37°C. The resulting peptide solution was acidified by adding 5% formic acid to get 0.1% end concentration.

### **3.5.2.1. LC-MS/MS method for 27 µg/ml IgG2-anti-RANKL antibody perfusion samples**

Peptides were separated by nano-HPLC (Dionex Ultimate 3000) equipped with an enrichment column (C18, 5 µm, 100 Å, 20 x 0.1 mm) and an Acclaim PepMap RSLC nanocolumn (C18, 2 µm, 100 Å, 500 x 0.075 mm) (all Thermo Fisher Scientific, Austria). Samples were concentrated on the enrichment column for 5 min at a flow rate of 15 µl/min with 0.1% formic acid as isocratic solvent. Separation was carried out on the nanocolumn at a flow rate of 400 nl/min at 60°C using the following gradient, where solvent A is 0.1% formic acid in water and solvent B is acetonitrile containing 0.1% formic acid: 0-5 min: 2-5% B; 5-70 min: 5-25% B; 70-90 min: 25-55% B; 90-100 min: 55-95% B; 100-110 min: 95% B; 110-111 min: 95-5% B; 111-125 min: 5% B. The Bruker maXis II ETD mass spectrometer was operated with the captive source in positive mode with following settings: mass range 200 - 2000 m/z, 2 Hz, precursor acquisition control top17, capillary 1300V, dry gas flow 3 l/min with 150°C, nanoBooster 0.2 bar.

### **3.5.2.2. LC-MS/MS method for 6 µg/ml IgG2-anti-RANKL antibody perfusion samples**

The LC-MS/MS method changed according to a new nanoLC-Setup, which should minimize dead-volumes and spray problems, leading to more stable measurements over time. Peptide samples were subjected to an additional offline desalting step using C18 Bond Elut OMIX® pipette tips before directly injecting onto an Aurora Series Emitter nanocolumn with CSI fitting (C18, 1.6 µm, 120 Å, 250 x 0.075 mm) (IonOpticks, Melbourne, Australia). Separation was carried out at room temperature at a flow rate of 300 nl/min using the following gradient, where solvent A is 0.1% formic acid in water and solvent B is acetonitrile containing 0.1% formic acid: 0-18min: 2% B; 18-107 min: 2-35% B; 107-108 min: 35-95% B; 108-118 min: 95% B; 118-118 min: 95-2% B; 118-133 min: 2% B.

The Bruker maXis II ETD mass spectrometer was operated with the captive source in positive mode with following settings: mass range 150 - 2200 m/z, 4 Hz, precursor acquisition control top20, capillary 1600V, dry gas flow 3 l/min with 150°C, nanoBooster 0.2 bar.

### **3.5.2.3. LC-MS/MS method for 0.1 µg/ml IgG2-anti-RANKL antibody perfusion samples**

The nanoLC method was the same as described in the previous chapter 3.3.6.

The IgG2-anti-RANKL antibody concentration decreased to 1/60<sup>th</sup> in contrast to the previous batch. Therefore, the MS/MS settings were changed to the scan mode parallel reaction monitoring PRM (CID) for absolute quantification of the target peptide (R.LEPEDFAVFYCQQYGSSPR.T) on the MS/MS level. For that purpose, a calibration curve ranging from 0.05 – 10 fmol on column of the heavy peptide standard (R.LEPEDFAVFYCQQYGSSPR.T), <sup>13</sup>C<sup>15</sup>N labelled, delta mass+16 Da (Thermo Fisher Scientific, Vienna, Austria), spiked into a foetal perfusate matrix was measured right after the original samples. The Bruker maXis II ETD mass spectrometer was operated with the captive source in positive mode with the following settings: mass range: 150 - 2200 m/z, 3 Hz, capillary 1600V, dry gas flow 3 l/min with 150°C, nanoBooster 0.2 bar.

For fragmentation of the light and heavy target peptide (charge 3+), previously measured peptide m/z were added to a PRM mass list using a width of 3 m/z and calculated collision energies. Furthermore, a mass of 300.00 with a width of 0 and collision energy of 5 eV was added to obtain full MS spectra.

### **3.5.3. LC-MS/MS data analysis**

The LC-MS/MS data were analysed by the Data analysis software (Bruker) using the Sum Peak algorithm for all experiments.

Results of experiments with 27 µg/ml and 6 µg/ml IgG2-anti-RANKL antibodies were further analysed with Bruker Proteinscape 4.0, in particular, by using the Swissprot database, including common contaminant-, homo sapiens- as well as the IgG2-anti-RANKL antibody peptide sequences. Carbamidomethylation on Cys was entered as fixed modification, oxidation on methionine as variable modification. Detailed search criteria in the created Swissprot database were used as follows: trypsin, max. missed cleavage sites: 2; search mode: MS/MS ion search with decoy database search included; precursor mass tolerance +/- 10 ppm; product mass tolerance +/- 0.05 Da; acceptance parameter for identification: 1% protein false discovery rate (FDR).

Data of the 0.1 µg/ml samples were processed with MSConvertGUI. MSConvertGUI (203) was used to generate .mgf files, which were searched by Proteome Discoverer 1.4. (Thermo Fisher Scientific, Vienna, Austria) and Mascot 2.4.1 (MatrixScience, London, UK) against a database containing the IgG2-anti-RANKL antibody sequences, the database Swissprot human, and all common contaminants. Carbamidomethylation on Cys was entered as a fixed modification, oxidation on methionine as variable modification. Detailed search criteria were used as follows: trypsin, max. missed cleavage sites: 2; search mode: MS/MS ion search with decoy database search included; precursor mass tolerance +/- 10 ppm; product mass tolerance +/- 0.05 Da. Resulting .dat files were used to build a spectral library in Skyline (version 4.1.0.11796) (204) and quantify the light and heavy target peptide on the MS/MS level in the raw data (Bruker .d-files) of the same samples as used for generating the .mgf files for the spectral library and of the calibration curve.

Detailed Skyline settings were: retention time prediction +/- 2.5 min of the target peptide (measured retention time 98.97 min); pick peptides matching library; filter for 6 ion transitions from  $m/z > \text{precursor}$  (y,b,p); ion match tolerance 0.5  $m/z$ ; method match tolerance 0.005  $m/z$ ; use only scans within 10 min of predicted retention times.

Transition areas of accepted peptides (threshold  $\geq 3$  out of 6 matched transitions with  $s/n$  ratio  $>5$ ) were exported to an excel sheet and product ions summed up per sample. Transition areas linear regression was applied to the calibration curve, and the resulting equation used to quantify the light equivalent in samples.

## 3.6. Microscopy

### 3.6.1. Fluorescence Microscopy of 500 nm PS particles

To localize PS NPs in placental tissue 4 µm thin sections were cut from collected and embedded tissues blocks (3.2.1). The thin sections were processed by removing paraffin with xylene and a descending alcohol series for tissue rehydration. Tissue sections were embedded on slides with a DAPI-containing embedding medium. Due to the high autofluorescence of syncytiotrophoblast in the placenta, no specific staining was identifiable for the rudimentary localization of 500 nm PS NPs at or in the syncytium. Nanoparticle localization was analysed with a fluorescence microscope with a connected digital camera by making pictures at DAPI,

a FITC, and a TRITC filter settings. Software Axiovision V 4.8.2.0 was used to merge the pictures.

### **3.6.2. Microscopy of IgG2-anti-RANKL antibody & IgG1-anti HER2 antibody**

Tissue sections were generated of placental tissue before perfusion experiments started and perfused tissue samples after respective experiments. Tissue blocks spanned from the chorionic plate to the decidua was generated. Tissue was washed under gentle shaking in PBS for 30 sec and was subsequently fixed for 18-24 hours at 4°C in 4% paraformaldehyde. Fixed tissue was transferred into PBS and stored at 4°C until paraffin embedding. For further processing, 5 µm tissue sections generated and were mounted on glass slides and deparaffinized directly with a xylene and ethanol gradient.

#### **Immunohistochemistry of RANKL & HER2**

Immunohistochemistry was performed with placental tissue sections collected before perfusion. All washing steps were performed with 1x Tris/Borate/EDTA buffer (TBE) containing 0.1% Tween 20. Staining was performed at room temperature. Slides were washed six times for 1 min, followed by a hydrogen peroxide block for 10 min. Slides were again washed five times with subsequent blocking of background staining with Ultra V Block for 5 min. Incubation of slides with primary antibody against RANKL or HER2 diluted 1:100, and antibody against CD163, diluted 1:500, was performed for 120 min followed by four times washing. Primary antibody enhancer was applied for 20 min, followed by four washing steps with subsequent application of horseradish peroxidase (HRP) polymer for 30 min in the dark. Slides were washed four times and incubated with AEC Single Solution for 10 min. After four washing steps, with double distilled water, counterstaining with Mayer's Haematoxylin was done for 2 min. Slides were rinsed for four min with tap water and mounted afterward with Aquatex mounting medium.

#### **Semi quantitative immunohistochemistry of RANKL**

The few strongly coloured, thus RANKL positive areas in tissue sections before perfusion were counted under the microscope. The investigated tissue areas were collected from the middle of a cotyledon [N=5]. These collected cross-sections of placental tissue span from the chorionic plate to the decidua. Next to the staining of RANKL the tissue was

immunohistochemically stained with an anti-CD-163 antibody, a macrophage marker. The CD-163 staining should clarify whether the RANKL expressions sites in the term placenta are originating from the main macrophage population in the tissue. The tissues areas were roughly classified based on placental structure in terminal villus, intermediate villus, and stem villus. Each area was designated to one of these micro anatomical structures. Additionally, the RANKL staining distribution was classified into three cellular compartments: (i) syncytiotrophoblast, (ii) placental stroma, and (iii) foetal endothelium. In some cases, the areas could not be assigned to one specific compartment, resulting in repeated counting. As the complete tissue area of each investigated slide was used for the semi- quantitative analysis the dimensions of this area was roughly estimated with a ruler. The distribution of stained areas per mm<sup>2</sup> was calculated as well as the distribution percentage in the villous structures and cell compartments [N = 5 placentas].

### **Immunofluorescence IgG1-anti HER2 antibody experiments**

The presence and localization of HER2, and subsequent HER2, FcRn, and LAMP1 in perfused and corresponding non-perfused placental sections was investigated by immunofluorescent staining. Sole HER2 was stained with a polyclonal rabbit anti-HER2 antibody. Co-localization of HER2, FcRn, and LAMP1 was investigated with monoclonal mouse, and polyclonal rabbit antibodies, in dilutions 1:50, 1:100, 1:100, and 1:50, respectively.

The slide were prepared at 60°C overnight with followed paraffin removal with xylene (2-times, 10 min), and rehydration within a decreasing ethanol row.

For staining, slides were rinsed with 1x TBE +0.1% Tween 20 for five min three times. Primary antibodies were diluted 1:100 with antibody diluent containing background reducing components. The incubation of primary antibodies was performed for at least 90 min at room temperature or 4°C overnight. Slides were washed three times with 1x TBE +0.1% Tween 20. A primary antibody enhancer was applied for 20 min at room temperature. Slides were washed three times with 1x TBE +0.1% Tween 20. Secondary fluorescent antibodies were diluted with before mentioned antibody diluent and incubated in humidified staining chambers for at least 90 min at room temperature. Slides were washed three times with 1x TBE +0.1% Tween 20. Slides were mounted with DAPI containing mounting media. The slides were stored at 4°C until microscopic investigation.

## 3.7. Cell Culture Experiments

### 3.7.1. BeWo transwell cell experiments

For these experiments, BeWo c24 (205) cells and hFcRn transfected BeWo c24 ((205) clone five) cells, both kindly provided by Isabella Ellinger (Institute for Pathophysiology and Allergy Research, Medical University of Vienna, Austria) were used. The transfected cells contained a mutation to generate resistance to Geneticin (G418), an antibiotic interfering with protein synthesis by blocking 80s ribosomes (206).

Both BeWo c24 Cells were expanded in 75cm<sup>2</sup> flasks with DMEM high glucose (4.5 g /l), 10% FBS, Glutamax (100 x), penicillin-streptomycin-neomycin antibiotic mixture (100 x). For hFcRn transfected BeWo c24 additionally 0.25 mg/ml G418 was added to generate the transfection selection medium which denies the growth of cells which lost the transfect. Cells were grown at 37°C and 21% O<sub>2</sub> and 5% CO<sub>2</sub>. Flasks were split at ~80% confluence to reduce the seeding of cell clusters, leading to the formation of a cellular multilayer instead of a monolayer.

BeWo c24 and hFcRn BeWo c24 clone five were seeded at a concentration of 50000 cells per well in 12 well transwell plates, leaving one well empty as blank reference.. Transepithelial resistance (TEER) was measured every 24 h, followed by media change in each well. For the TEER measurement, the electrode was inserted into the bottom and top well without touching the cell layer. Electrode was rinsed with ethanol followed by distilled water after each measured well. Cells were cultivated for three to four days to reach at least a TEER of 55 [ $\Omega$ .cm<sup>2</sup>] (207) before cell culture experiments started.

After an appropriate TEER was attained, cells were washed three times with HBSS, followed by 1h starvation. Thereafter cells were pre-incubated for 30 min either with control medium (4 wells), or with HSA medium (4 wells), or with HSA medium containing 100  $\mu$ M Chloroquine (4 wells) (N=3). Each well was supplied with 500  $\mu$ l and 1500  $\mu$ l of HSA or control medium in the top and bottom of the wells, respectively. Polystyrene NPs were incubated for 15 min at 37°C in HSA or control medium to allow biocorona formation in analogy to perfusion experiments. Medium was removed, and 80 nm PS NP containing medium (40  $\mu$ g/ml) was applied. Wells already pre-incubated with Chloroquine were additionally supplemented with 100 $\mu$ M Chloroquine in order to decrease interaction of PS

NPs with Chloroquine. Cells were incubated for 6h at 37°C, 21%O<sub>2</sub> and 5%CO<sub>2</sub> for the PS NP transfer experiments subsequently medium from the top and bottom, well compartments were individually collected and NP fluorescence was measured.

### **3.7.2. Endothelial cell culture assays**

To test the peptide inhibitor SYN 1436 (208) for FcRn a set of three cell culture experiments were performed. Human microvascular endothelial cell line 1 (HMEC1) (209) isolated from human foreskins, and stable transfected with hFcRn and green fluorescent protein were used. These cells were kindly provided by Wayne I. Lencer from Harvard Medical School (209).

For HMEC1 cells MCDB131 medium supplemented with 10% FCS, 2 mM L-Glutamine, 25 µg/ml streptomycin, 25 U/ml penicillin, 10 ng/ml human epidermal growth factor (hEGF), 1 µg/ml hydrocortisone, 5 µg/ml blasticidin and 100 µg/ml G418 was used.

#### **FcRn-dependent recycling of IgG1-anti HER2 antibody and IgG**

The herein used experimental setup is based on a published protocol and was performed in triplicates containing three technical replicates each (210). Briefly,  $5 \times 10^5$  HMEC1 cells per well stably expressing HA-hFcRn-EGFP were seeded into 24-well plates and cultured for 2-3 days with previously described MCDB131 medium until grown to confluency. The cells were washed twice and starved for 1 h in Hank's balanced salt solution (HBSS) and pre-incubated with different FcRn inhibitor Syn 1436 concentrations ( 2.5, 5, 7.5, 10 nM equally to 7.75, 15.5, 23.25, and 31ng/ml of inhibitor, for 30 min in 250 µl HBSS, adjusted with 0.1 M HCl to pH 6). Subsequently, buffer was removed and cells were incubated for 4 h with IgG1-anti HER2 antibody or polyclonal human IgGs (412 nM, 60 µg/ml) and different inhibitor concentrations in buffer at pH 6. The respective cell control conditions used here were: (i) cells without IgG1-anti HER2 antibody or IgGs and inhibitor, (ii) with IgG1-anti HER2 antibody or IgGs and without inhibitor and (iii) IgG1-anti HER2 antibody or IgGs and with inhibitor (250 nM). After incubation buffer was removed and the cells were washed four times with ice-cold HBSS (pH 7.4) and pre-warmed (37°C) DMEM without FCS and without supplements were added to enable the recycling of intracellular accumulated IgG1-anti HER2 antibody. After 4 h supernatants were collected and IgG1-anti HER2 antibodies or IgGs were determined by ELISA to measure the amount of intracellular recycled antibodies.

### **3.8. Statistical analysis**

Descriptive statistics were used to analyse the data of NP quantification. Categorical results (perfusion time, maternal/foetal side, type of media) were presented as absolute and relative frequencies, continuous data (PS NP concentration  $\mu\text{g/ml}$ ) as means, and standard deviations. A linear mixed model assessed the relationship between the quantity of transported PS NPs and the independent variables (perfusion time, maternal/foetal side, type of media). The model included a random intercept for every successful placental perfusion experiment. Tissue perfusion time was considered as a repeated factor, and all the other variables were entered as fixed effects. An autoregressive heterogeneous covariance structure was used. Between perfusion time, maternal/foetal side, and type of media pairwise interactions, as well as a three-way interaction, were analysed and considered in the model, if significant. The statistical analyses were performed with SAS software.

Further two-tailed paired t-test, one way ANOVA, and repeated measures 2 Way ANOVA with subsequent Holm-Sidak multiple comparisons or Tukey's multiple comparison were used to analyse NP characterization data, PS NP concentrations in perfusate, IgG2-anti-RANKL antibody RANKL scavenging capacity and cell culture data as indicated in the corresponding results. The software GraphPad Prism was used for the analysis. Data were reported as mean  $\pm$ SD or mean  $\pm$ SEM, as indicated. Normality of perfusion data was given within groups and was tested by Shapiro-Wilk test.

Results below  $p < 0.05$  were considered as significant.

## **4. Results**

### **4.1. Placental perfusion of nanoparticles**

#### **4.1.1. Characteristics of polystyrene nanoparticles**

##### **Polystyrene nanoparticles show media dependent heterogeneity in size**

NTA measurements revealed correlations between size of PS NPs and composition of media. Comparing the NP size in the protein-containing media to water, the NPs showed an increased hydrodynamic diameter in respect of peak size in the media (Table 5).

Table 5. Hydrodynamic diameter of 80 nm PS NP main fraction is presented next to the mode sized of measured NP.

	<b>Medium</b>	<b>Hydrodynamic diameter, main fraction peak max. [nm]</b>	<b>Mode NP sized [nm]</b>
<b>80 nm PS</b>	Control medium	115	114.6 ± 2.7
	Plasma medium	107	107.8 ± 41.6
	HSA	104	57.3 ± 21.5
	IgG	105	110.2 ± 6.1
	Water	80	83.8 ± 5.5

In all different media, except water, multiple peaks with different NP sizes could be detected (Figure 7). Of note, mean NP size, representing the average of all detected NPs, would overlap the observation of multiple NP fractions. The mode, on the other hand, focuses on the most frequent detected NP fraction. Therefore, the mode presentation of the data allowed getting information on the most prominent NP fraction that interacts with the placenta during perfusion experiments.

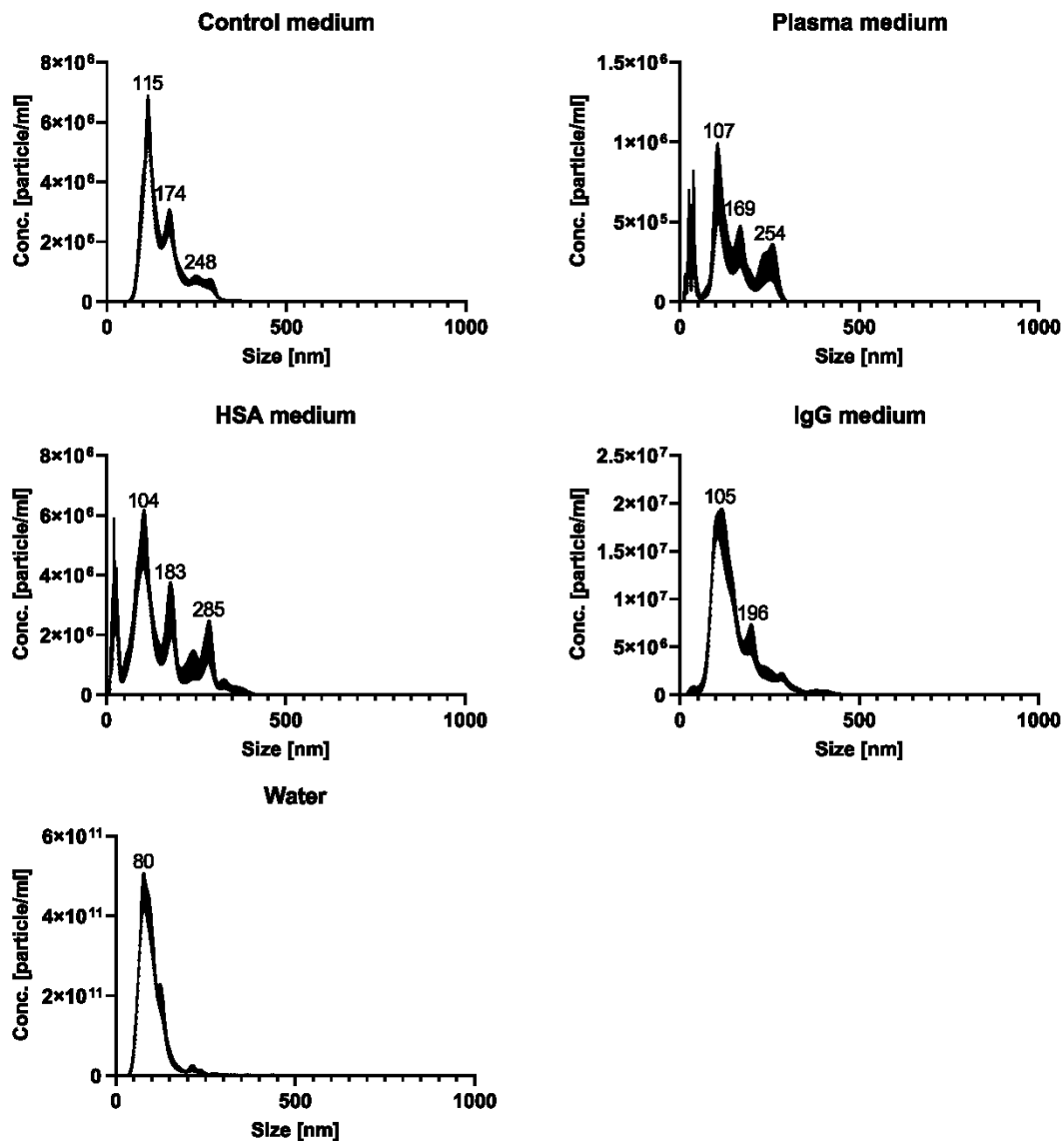


Figure 7 Perfusion media influence the size of 80 nm PS NP in NTA. Average size distribution of 80 nm PS NP in different media and water (N=5 for all media and water). In all media the highest peak in the graphs represents the determined PS NP size which varies from 80-115nm. Modified graph from (1).

Nevertheless, the data distribution detected in HSA medium, containing fractions between 20 and 30 nm, which were below the NP size, negated the statistical identification of the most relevant PS NP fraction by using the mode of the data. The smaller fractions had a higher concentration in some of the experiments than the potential PS NP fraction. The combined

mode readout by the software resulted then analysis in a mode of 57.3 nm for the experiments, which does represent neither the observed smaller fractions nor the PS NPs.

### **Dynamic light scattering is limited suitable as analytical tool in perfusion media**

Dynamic light scattering (DSL) is a complementary approach for NP size determination, especially for NP with monodisperse homogeneous NP size distributions in media free of macromolecular additives.

With the methodology, reliable data for 80 nm and 500 nm PS NP was determined in the protein-free media (Table 6).

Table 6. Table shows the mean size of the main peak of the DLS measurements with the respective PDI in different media

	<b>Medium</b>	<b>Mean size main peak <math>\pm</math>SD[nm]</b>	<b>PDI</b>
<b>80 nm PS</b>	Control medium	992.7 $\pm$ 206.6	0.69
	HSA	188.4 $\pm$ 113.2	0.76
	IgG	197.7 $\pm$ 82.40	0.65
	Phosphate buffered saline	87.63 $\pm$ 2.94	0.07
	Plasma medium	150.3 $\pm$ 81.34	0.50
<b>500 nm PS</b>	Control medium	874.7 $\pm$ 214.6	0.32
	HSA	573.0 $\pm$ 208.7	1.00
	IgG	879.4 $\pm$ 301.0	1.00
	Phosphate buffered saline	461.98 $\pm$ 5.24	0.05
	Plasma medium	925.1 $\pm$ 323.7	0.98
	Water with AP	451.57 $\pm$ 2.27	0.05
	Water without AP	460.27 $\pm$ 4.07	0.04

The determined NP sizes 87.63 $\pm$ 2.94 nm and 461.98 $\pm$ 5.24 meet the manufacturer's specifications for both 80 and 500nm PS NPs in phosphate buffered saline, respectively. Differences between 500 nm PS NPs in water with and without AP was not observed. In the

macromolecule containing media, the detected main peak NP size was increased compared to NPs in PBS. Especially in the control medium, the only medium containing dextran, the particle size was increase to  $992.7 \pm 206.6$  nm. In PBS, one peak was observable compared to two and more peaks in the perfusion media. Therefore, the main peak was reported in Table 6 for the experiments with perfusion media. An example of data distribution of 80 nm PS NPs in IgG medium is given in Figure 8. Data on NP size in the other perfusion media was also diverse, as indicated by the high standard deviations in macromolecule containing media.

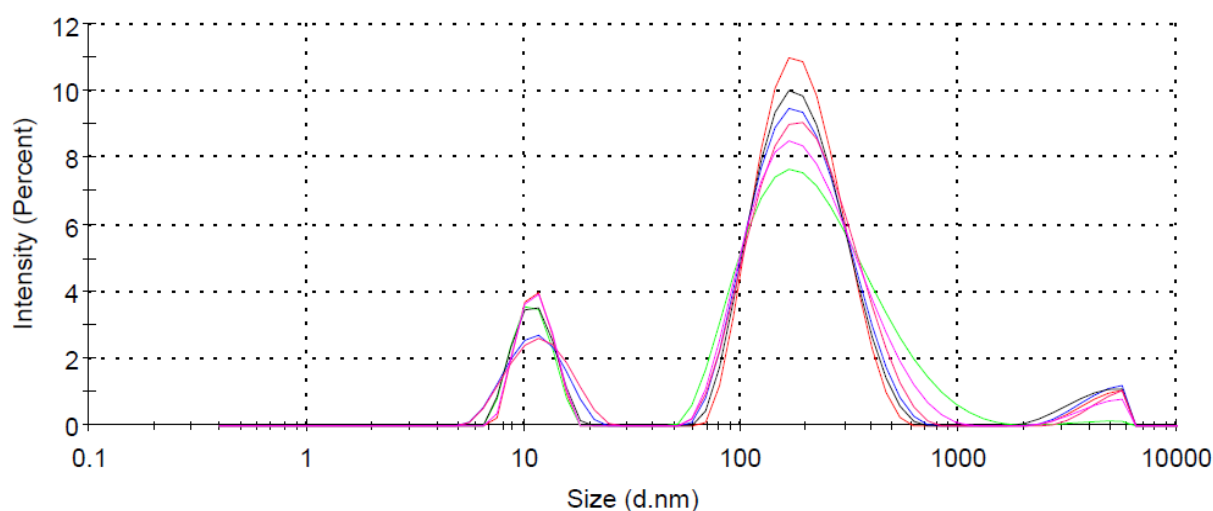


Figure 8 80 nm PS showed a broad size distribution in IgG medium. NP size recorded by DLS (N=3). Three different base line separated particle fractions could be detected.

The polydispersity index (PDI) is a relevant value calculated from the obtained data for DLS data interpretation. This PDI allows estimating the uniformity of the measured sample in regards to NP size distribution. A PDI of 0.00 would indicate uniform NPs with no size variations, while a PDI of 1 would indicate a completely heterogeneous NP size distribution. A heterogeneous size distribution can lead to biased interpretation of some data if NP sizes are too close to each other. Results of 80 nm PS NPs in PBS and 500 nm PS NPs in PBS as well as water with and without AP showed a homogeneous NP size distribution indicated by PDI. The PDI was between 0.5 and 0.76 for 80 nm PS NPs in macromolecule containing media. The data of 500 nm PS NPs resulted in a PDI between 0.32 and 1 in the macromolecule containing media. Therefore, for both PS NP types the DLS results showed a heterogeneous size distribution in the perfusion media.

### **Zeta potential indicates biocorona formation on polystyrene nanoparticles**

Zeta potential displays the accumulation capacity of ions of the medium, close to the NP surface. It states the electrostatic stabilization of NPs in suspension, which is a determinant of agglomeration. The measurement of the zeta potential of 80 nm and 500 nm PS NPs used in various media is depicted in Table 7.

Table 7. Zeta potential of 80 nm and 500 nm PS NPs in different perfusion media. All data are presented as mean  $\pm$ SD (N=3).

	<b>Medium</b>	<b>Zeta potential <math>\pm</math>SD [mV]</b>
<b>80 nm PS</b>	Control medium	-13.23 $\pm$ 0.91
	HSA	-9.61 $\pm$ 0.85
	IgG	-3.54 $\pm$ 0.63
	Phosphate buffered saline	-27.63 $\pm$ 0.72
	Plasma medium	-7.05 $\pm$ 0.64
<b>500 nm PS</b>	Control medium	-11.53 $\pm$ 0.04
	Control medium AP 0.1 mg/ml	-13.27 $\pm$ 0.17
	Water without AP	-29.05 $\pm$ 7.72
	Water with 3mg/ml AP	-59.32 $\pm$ 12.24
	Phosphate buffered saline	-30.43 $\pm$ 1.01

The zeta potential reference data generated in PBS showed for 80 nm and 500 nm PS NPs moderate negative charges, -27.63 $\pm$ 0.72 mV and -30.43 $\pm$ 1.01 mV, respectively. Polystyrene NPs suspended in the perfusion media showed all an increase in zeta potential. Results were between -13.23 $\pm$ 0.91 mV in control medium and -3.54 $\pm$ 0.63 mV in IgG medium.

**Antipyrine changes zeta potential of 500 nm polystyrene nanoparticles but not the particle size**

Zeta potential of 500 nm PS NPs in water was -29.05 $\pm$ 7.72 mV and decreased significantly to -59.32 $\pm$ 12.24 mV in water containing 3 mg/ml AP (p=0.008) (Figure 9 A). The addition of AP to control medium changed the zeta potential from 11.53 $\pm$ 0.04 mV without AP to -

13.27±0.17 mV with AP, which was not significant different (Table 7). Further, the measurements of 500 nm PS NPs in water with and without AP were not significant different in respect of NP size (Table 6, Figure 9 B).

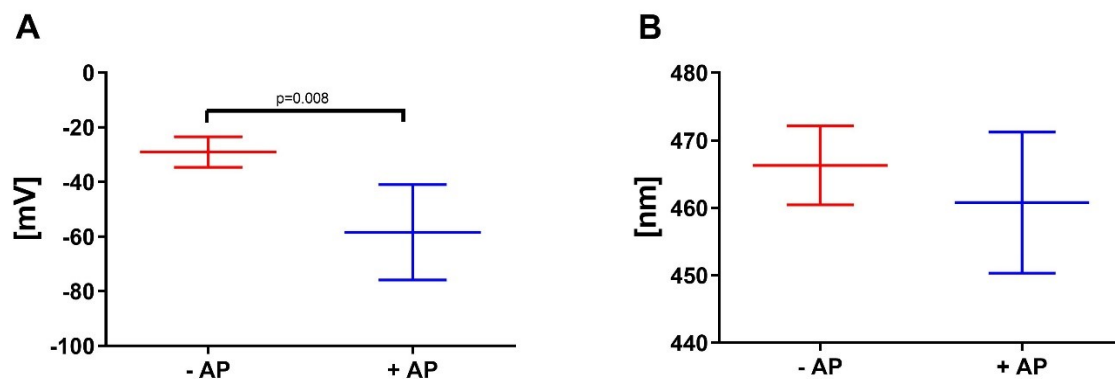


Figure 9. Antipyrine changes zeta potential of 500 nm PS NPs particles in water but not their size. A) Zeta potential of 500 nm PS NPs in water in the presence and absence of AP. Red graph represents particles in water. Blue graph shows particles in the presence of three mg/ml of AP in water. B) Particle size of 500 nm PS NPs in water in the presence and absence of antipyrine. The blue graph represents NPs measured in the presence of three mg/ml antipyrine. The red graph shows NPs measured in the absence of antipyrine (N=3). Statistical analysis was performed with paired t-test.

### Transmission electron microscopy (TEM) confirms sphericity and size of polystyrene nanoparticles

TEM allows beside an evaluation of the NP size an analysis of the NP shape as well. TEM is another complementary approach for NP size determination. Further, these data served as a reference for subsequent approaches to detect 80 nm PS NPs within the placental tissue after perfusion. The tested stock solution of 80 nm PS NPs contained NP in the size range of around 50 nm to 100 nm in TEM (Figure 10 A). The 500 nm PS NPs from the stock solution were uniform in their size and around 460 nm in diameter (Figure 10 B). The observed shape of PS NPs was spherical.

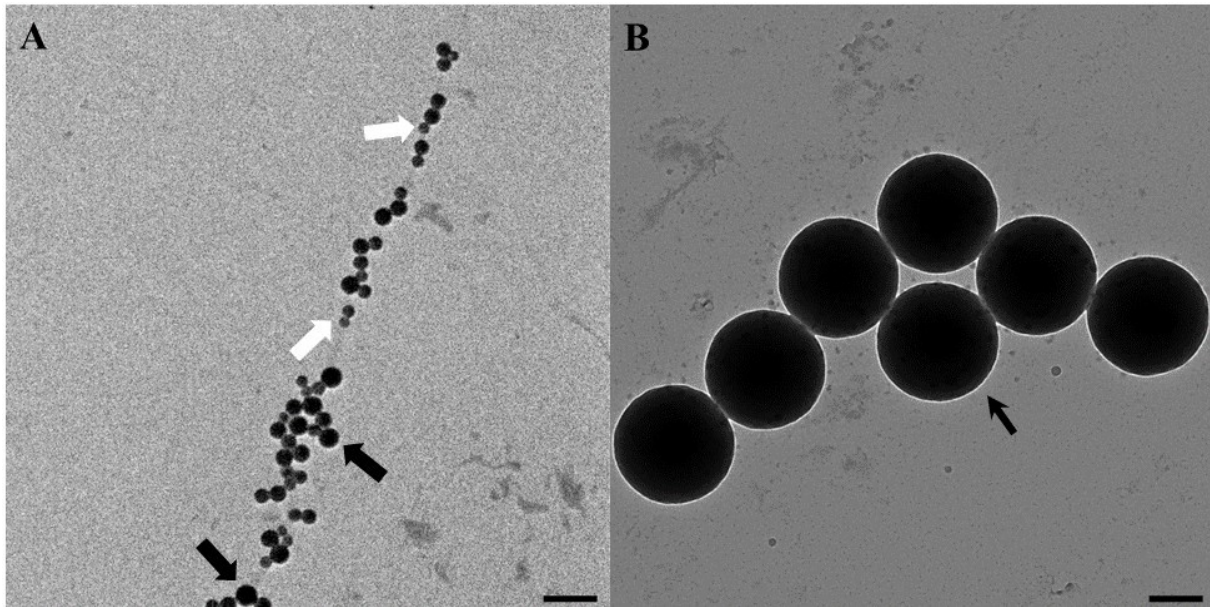


Figure 10. Polystyrene NP show minor size deviations in TEM. Representative TEM pictures of native 80 nm and embedded 500 nm PS NPs. A) The heterogeneous distribution of the 80 nm PS NPs ranging from 50 nm, white arrows, to 100 nm, black arrows, is depicted. Observed NPs were spherical. B) The homogeneous distribution of the spherical 500 nm PS NPs was visible indicated by the black arrow. Scale bar represents 200 nm (N=1 for both PS NP sizes).

#### 4.1.2. Characteristics of PLGA nanoparticles

The NTA measurements of PLGA NPs in control perfusion medium resulted in a mean NP size of  $125 \pm 56$  nm. The plotted data indicates a different most frequent NP size with a maximum at 85 nm (Figure 11). In such measurements, NP with increased size or agglomerates influence the mean leading to mean data that deviate clear from the most frequent particle size. Discrimination between more distinct NP size fractions was not possible as a plethora of individual peaks across the whole size range.

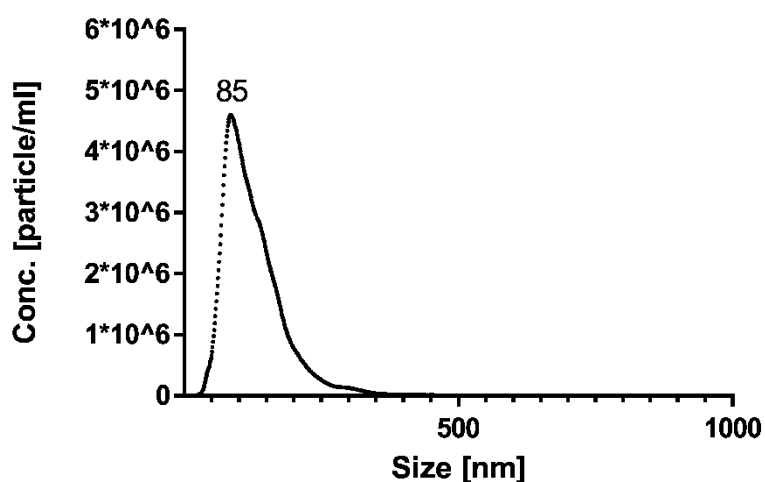


Figure 11. PLGA NPs in control medium showed a broad but monodisperse distribution. Average size distribution of PLGA NPs in control medium measured with NTA (N=3). A broad size distribution was detected with a maximum at 85 nm.

The determination of PLGA NP size in plasma medium by DLS resulted in a size of  $28.86 \pm 0.6$  nm and a PDI of 0.48.

### **Transmission electron microscopy indicates sphericity and reveals material dependent fragility of PLGA NP**

The embedded PLGA NPs were not detectable in the electron microscope. The observed PLGA NPs after native application in the electron microscope were, in the best case, partially visible as spherical structures (Figure 12 A). It appeared that incorporated fluorescent dye in the PLGA NPs leak out of the NP into the TEM grid membrane. The more frequent observation was dendritic like structures that were distinctly different in electron density from the TEM grid membrane (Figure 12 B). Within these dendritic structures, areas with higher electron density occurred.

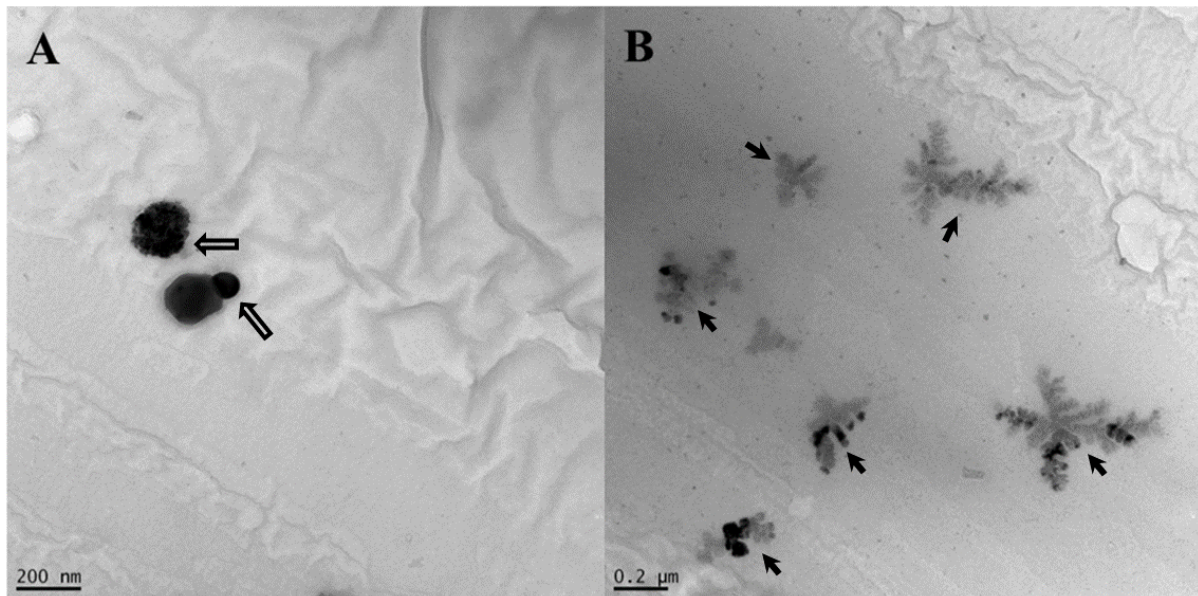


Figure 12. Native applied PLGA NPs lose their structural integrity in the electron microscope. A) The blank arrows point towards the electron dens visible remains of burst PLGA NPs. The slightly lesser electron dense areas next to the spherical remnants show the leaking dye from within the NP. B) The solid arrows point to supposed remnants of burst PLGA NPs. The visible grey presented structures were most likely recrystallized Texas red dye. In the structures, darker areas were occasionally visible, which were presumably fragments of the PLGA NPs. (N=9)

#### 4.1.3. Perfusion settings influence perfusion outcome for NPs

##### *Antipyrine attenuates placental uptake of 500 nm polystyrene particles during perfusion*

The first sets of experiments with control medium demonstrated a constant decrease over time of the 500 nm PS NPs fluorescence in the maternal circulation if the placenta was exposed to AP before. NP levels decreased from the start concentration of  $26.7 \pm 10.2 \mu\text{g/ml}$  to  $13.3 \pm 7.2 \mu\text{g/ml}$  after 360 min. In contrast to the second experimental setting, in which AP was added at the end of the perfusion, the initial fluorescence signal of PS NPs was  $34.8 \pm 1.9 \mu\text{g/ml}$  and only slightly changed to  $32.0 \pm 8.8 \mu\text{g/ml}$  at the end of the perfusion (Figure 13). In foetal circulation fluorescence signal was increasing during 360 min to  $0.7 \pm 0.4 \mu\text{g/ml}$  in experiments without AP exposure and to  $0.5 \pm 0.2 \mu\text{g/ml}$  in experiments with AP exposure of the tissue. During these experiments, a glucose consumption of  $0.18 \pm 0.06 \mu\text{mol/g/min}$  and a lactate formation of  $0.52 \pm 0.39 \mu\text{mol/g/min}$  can be reported.

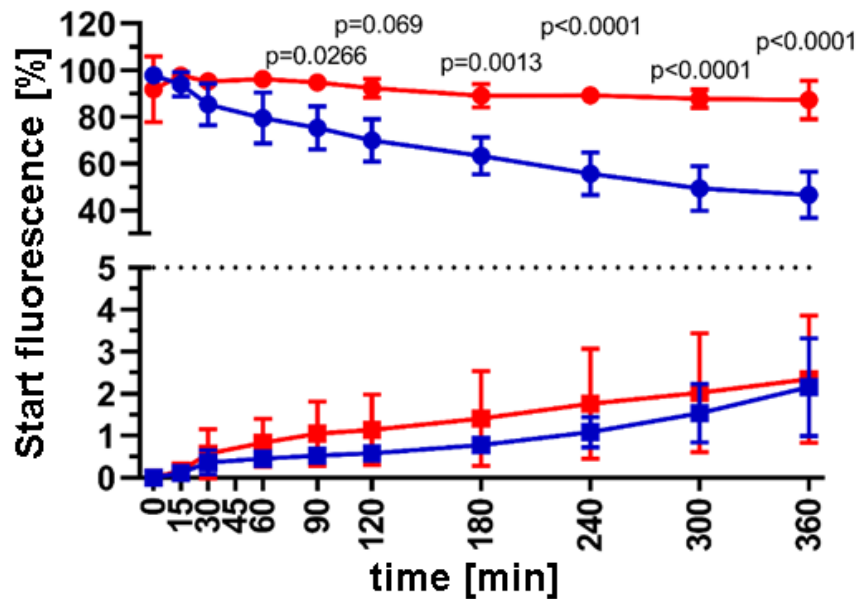


Figure 13. Antipyrine in the perfusion medium leads to a decreased detection of fluorescence in maternal circulation during perfusion experiments with 500 nm PS NPs. The upper part of the split y-axis shows the relative detected fluorescence of PS NPs over time in maternal artery. The lower part of the split y-axis shows the relative detected fluorescence of PS NPs over time in foetal artery. Perfusions were performed with control medium before AP perfusion phase (red) and with control medium after AP perfusion phase (blue). Data were normalized to maximal maternal PS NP fluorescence intensity during perfusion and were presented as % of this max intensity. One-Way-ANOVA was used for statistical analysis, and p values were given for significant different results between the groups at the respective time point. (N=3)

### Antipyrine impacts fluorescence characteristics of 500 nm polystyrene nanoparticles

A significant increase of the relative fluorescence of 500 nm PS NPs after one and five hours was detectable if control medium contained no AP ( $p=0.024$  and  $p=0.018$  respectively). The leakage of fluorescent dye from the NPs in the AP-containing control medium was  $2.53 \pm 0.06\%$  of the detected fluorescence of the respective NPs before the experiment (Figure 14).

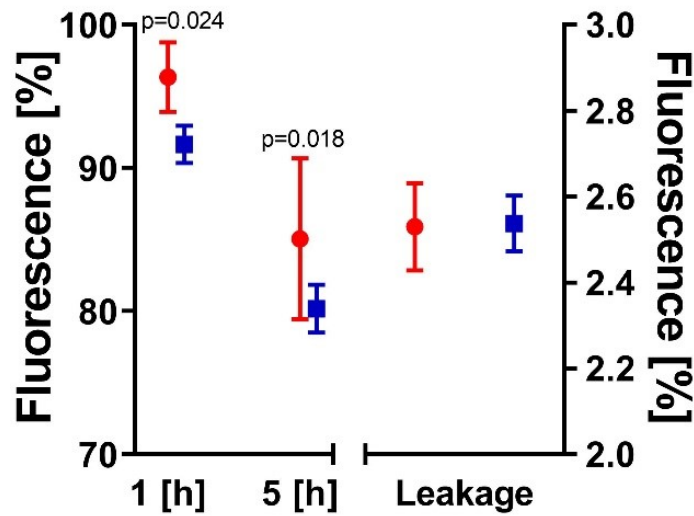


Figure 14. Fluorescence bleaching and leaking phenomenon of PS NPs with AP in control medium. The red dots represent PS NPs suspended in medium without AP. The blue dots show PS NPs in the presence of 100 µg/ml AP. Left panel of the graph shows significantly different fluorescence of PS NPs after 1 and 5 hours of steering in the respective medium in the dark compared to the initial fluorescence at 0 h. The right panel of the graph shows the detected fluorescence in filtrated NP free medium after 5 h of steering in the dark. The data, normalized to the PS NPs fluorescence starting signal, were analysed with Two-Way ANOVA (N=3).

### **Antipyrine changed the fluorescence pattern in placental tissue after perfusions with 500 nm polystyrene nanoparticles**

Fluorescence microscopy revealed a different fluorescence pattern after 500 nm PS NP perfusion depending on the time point of the AP perfusion. Tissue samples from experiments without AP show a low number of red-labelled NPs adhering to the apical syncytiotrophoblast membrane. Tissue samples from experiments where AP was used before the 500 nm PS NP perfusion showed red adhering NPs at the syncytiotrophoblast membrane. Additionally, bright greenish sharp localized areas were detectable within the syncytiotrophoblast cell layer but not in deeper cell layers of the placental tissue (Figure 15).

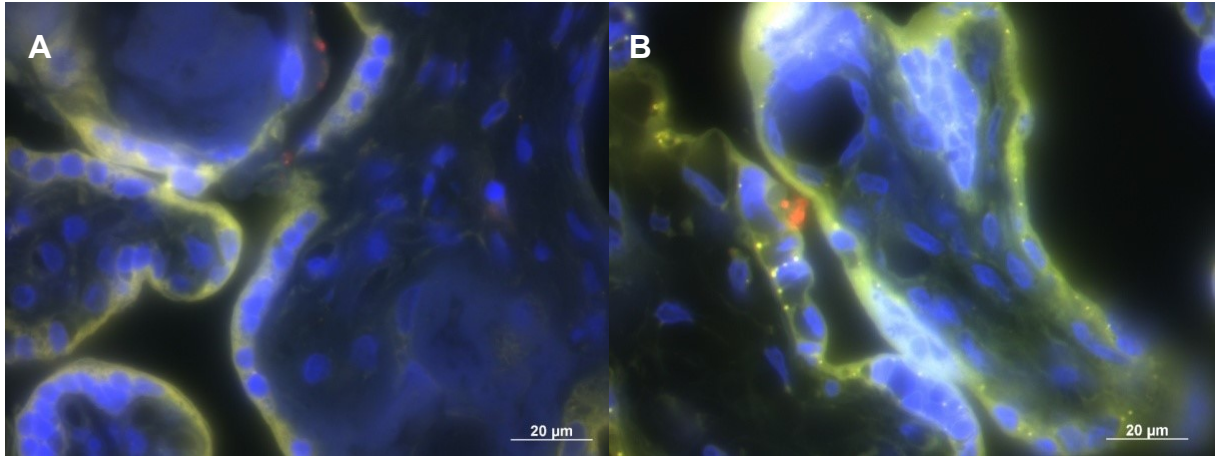


Figure 15. The presence of AP during 500 nm PS NP perfusion experiments showed fluorescent structures in the syncytium. The pictures show term placental sections where the tissue was exposed to AP after (A) or before (B) 500 nm PS NP perfusion experiments. The syncytium shows green/yellow auto-fluorescence, with a blue DAPI nuclei staining and the red-labelled 500 nm PS NPs after 6 h perfusion. A) Representative tissue section of a perfusion experiment in which AP was used after the NP experiment. Red fluorescence is localized visible at the syncytium to a minor extend. B) Representative tissue section of a perfusion experiment in which AP was used before the NP experiment. Red fluorescence can be detected at the syncytium. Further, spherical bright green presented fluorescence areas could be observed in the syncytium (N=1).

The AP washout perfusion experiments, where the placentas were perfused for 30 min with medium containing 100  $\mu\text{g/ml}$  AP with a subsequent media change to AP free medium in both circulations, showed an exponential decline of AP (Figure 16).

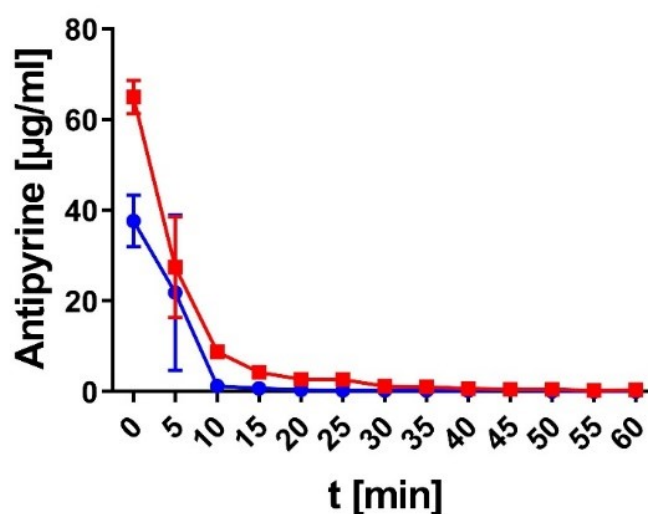


Figure 16. Antipyrine exponentially decreases during wash out phase of the placenta. The red graph represents the maternal vein. The blue graph demonstrates the foetal vein. Data presented as means with SEM (N=3).

Antipyrine could be detected in the collected washout medium for 20 min in the foetal circulation and for 30 min in maternal circulation.

### **Fluorophores with emission above 550 nm were superior to fluorophores emitting below 550 nm in regards to sensitivity of particles quantification sensitivity in perfusion media**

For PS NPs loaded with a green chromophore (ex 488 nm, em 520 nm), the LOD in pre perfused medium containing, blood cells and placental released factors, medium was 48.65 µg/ml and the LOQ 147.68 µg/ml. The PS NPs loaded with a pink chromophore (ex 560 nm, em 580 nm) had a LOD of 0.08 µg/ml and a LOQ of 0.27 µg/ml. BODIPY FL containing PLGA NPs had a LOD of 24.44 µg/ml and a LOQ of 74.08 µg/ml. Texas red containing PLGA NPs had a LOD of 0.3 µg/ml and a LOQ of 1.14 µg/ml. In summary, the "green" chromophores can be detected less sensitive than "red" chromophores in perfusion media after perfusion. Therefore, using "red" chromophores increased the sensitivity of NP detection in the perfusion media up to 500 times more sensitive.

### **Perfusion media composition directly effects total foetal vasculature backpressure**

Interestingly, the differently composed media influenced foetal vasculature backpressure (Figure 17). The two media containing pharmaceutical HSA, plasma, and HSA medium, had

a significant decreased foetal backpressure during 80 nm PS NP perfusion experiments compared to control medium (both  $p < 0.0001$ ), respectively  $25.1 \pm 3.2$  mbar,  $33.1 \pm 4$  mbar and  $45.4 \pm 3.5$  mbar. No statistical differences in pressure could be found between the control medium and the IgG ( $42.1 \pm 4.7$  mbar) as well as the lyophilized HSA medium ( $45.7 \pm 3.3$  mbar). By comparing plasma medium with HSA medium a significant difference between both was present ( $p = 0.0192$ ). The comparison of HSA medium with the HSA lyo medium, which differ by the presence of pharmaceutical stabilizers in HSA medium, resulted in a statistical difference ( $p = 0.0009$ ).

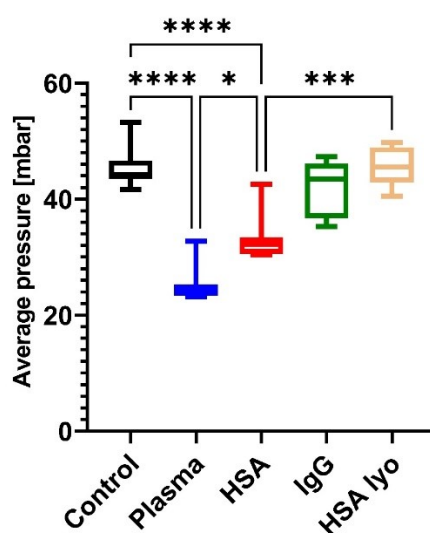


Figure 17. Composition of perfusion media influences foetal vasculature backpressure. Mean foetal vasculature backpressure during the perfusion experiments with 80 nm PS NPs. Plasma medium (N=5) backpressure significantly differs from control (N=5) ( $p < 0.0001$ ) as well as does HSA medium (N=5) differ from control ( $p < 0.0001$ ). Plasma medium differed significant from HSA medium ( $p = 0.0192$ ). HSA medium differed significantly from HSA lyo medium (N=3) ( $p = 0.0009$ ). IgG medium (N=3) and HSA lyo medium showed no significant decrease in foetal backpressure compared to control. Data was analysed with 2-Way ANOVA with a subsequent Tukey's multiple comparison test.

#### 4.1.4. PLGA particles cross the placenta

The perfusion experiment with 100 nm PLGA NPs in the control medium showed a pronounced NP decrease in the maternal circulation by  $20.7 \pm 4.9\%$  within 120 min. In two of

the three performed experiments, a turning point from NP uptake to NP secretion out of the tissue between 120 and 240 min was observed. During the perfusion experiments, a higher volume shift from fetal to maternal circulation occurred as noted before in chapter 3.2.4.3. This volume shift did not influence the antipyrine QC marker in any experiment that would lead to the exclusion of the experiments. In the foetal circulation, PLGA NP concentration increased until 180 min (Figure 18). It has to be noted that in regards of volume shift from foetal to maternal circulation none of the experiments with PLGA NPs met the QC criteria applied for all perfusion experiments. During these experiments, a glucose consumption of  $0.14\pm 0.11$   $\mu\text{mol/g/min}$  and a lactate formation of  $0.44\pm 0.26$   $\mu\text{mol/g/min}$  can be reported.

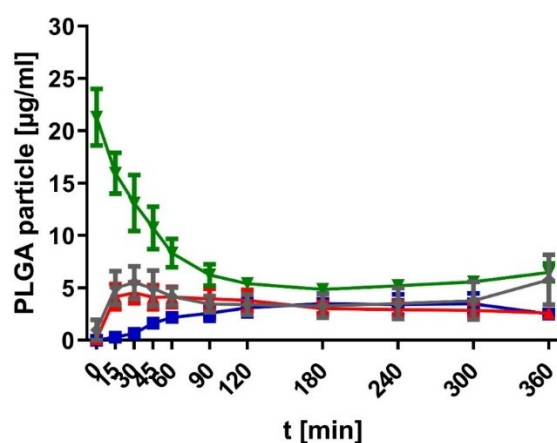


Figure 18. PLGA NPs crosses the human placenta effectively. Nanoparticle concentrations in maternal artery (green) decrease immediately after perfusion started. In maternal vein (grey) PLGA NP concentration stabilizes after 60 min. In foetal artery (blue) transfer of PLGA NPs is monitored. The foetal vein (red) shows similar PLGA NP release characteristics to the maternal vein for the first 300 min of the experiment (N=3).

#### 4.1.5. Biocorona on 80 nm polystyrene nanoparticles changes depending on circulation and time

This chapter summarizes the results of proteomics data. Overall, four experiments leading to 12 samples were included in the study. A fifth perfusion experiment (three samples) was excluded because the labelling on the individual samples was untraceable. For the matrix reduction of the generated data, only proteins were included, which could be quantified in

four out of four samples in the plasma biocorona, foetal biocorona or maternal biocorona group (highlighted in blue, red and green in table 8). These processing identified 664 human proteins, non-human proteins from sample preparation were excluded before further analysis.

Table 8: Proteomics sample and reduction matrix

	Plasma biocorona	Foetal biocorona	Maternal biocorona
Experiment 1	X	X	X
Experiment 2	X	X	X
Experiment 3	X	X	X
Experiment 4 (excluded)	-	-	-
Experiment 5	X	X	X

The repeatedly presence of lipoproteins in the proteomics data was the basis for a complementary test of the PS NP isolation and purification protocol by western plot. Plasma medium incubated with 80 nm PS NPs and plain plasma medium was processed equally. The subsequent performed western blots for Apo A-1, Apo B, and Apo M are presented in Figure 19. For the plain plasma samples, 10 purifications had to be pooled to reach borderline detectable protein amounts. Thus, the contamination of the samples by co-isolated lipoproteins had neglectable influence.

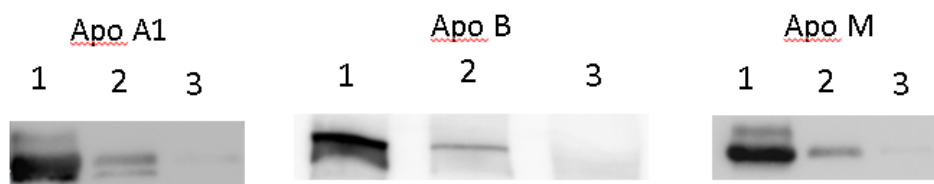


Figure 19. Examination of proteomics NP purification protocol by western blot. Western blots of apolipoproteins. Samples were loaded in the order of 1) female human citrate plasma 2) 1 mL plasma medium with 40  $\mu$ g/mL 80 nm PS NPs centrifuged through a sucrose cushion (0.7 M) 3) 10 mL plasma medium without PS NPs centrifuged through a sucrose cushion.

#### 4.1.5.1. Maternally isolated 80 nm polystyrene nanoparticles show a heterogeneous biocorona

First, the distribution of these 664 proteins between the three sample groups was investigated. Venn diagram was created to graphically represent the distribution of different proteins (Figure 20). The Venn diagram shows the qualitative distribution of the 664 proteins that were present in all measurements of the respective PS NP isolation groups. The majority of recovered proteins (96.6%) were found in the biocorona of the maternally isolated PS NPs after perfusion experiments. In comparison, only 19.4% of the proteins were identified on NPs incubated with plasma or 14.1% for isolated NPs from the foetal circuit. HSA and IgG were located on all NPs independent of isolation and sampling time point.

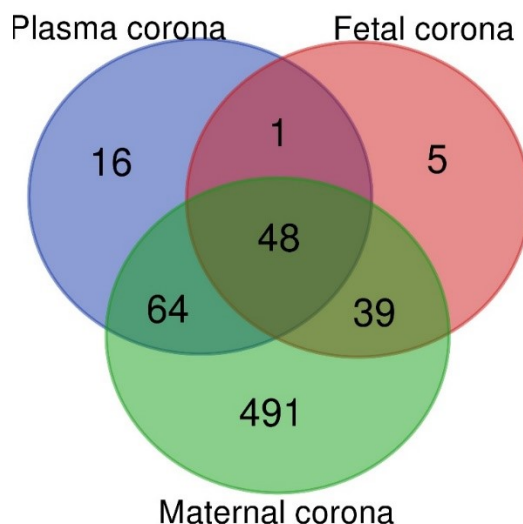


Figure 20. The protein biocorona on maternally isolated PS NPs after perfusion displayed a heterogeneous protein profile. Venn diagram of proteins that were detected in all samples of the respective PS NP proteomics analysis group (N=4 per group). Whether the qualified proteins on maternally isolated PS NP were acquired within the placental tissue during endocytosis and exocytosis events or adhered to the PS NP in maternal circulation after the proteins were released from the placenta cannot be discriminated. Venn diagram was created with VENNY (<http://bioinformatics.psb.ugent.be/webtools/Venn/>). This graph is a modification of “Supporting Figure 3” (1).

#### **4.1.5.2. Foetal isolated 80 nm polystyrene nanoparticles biocorona carry more albumin**

##### **The intensity based protein distribution on particles indicates placental transfer enhancing proteins**

In the median subtracted protein intensity approach, the intensity based proteomics data were evaluated by multiple t-tests and graphically displayed in volcano plots (Figure 21). There were no significant differences of proteins between the plasma NP biocorona and the foetal NP biocorona. Comparing the plasma NP biocorona with the maternally isolated PS NP biocorona resulted in 61 proteins significant enriched on plasma isolated NP. Comparing the foetal isolated PS NP biocorona with the maternally isolated PS NP biocorona resulted in 39 significant enriched proteins on foetal NPs.

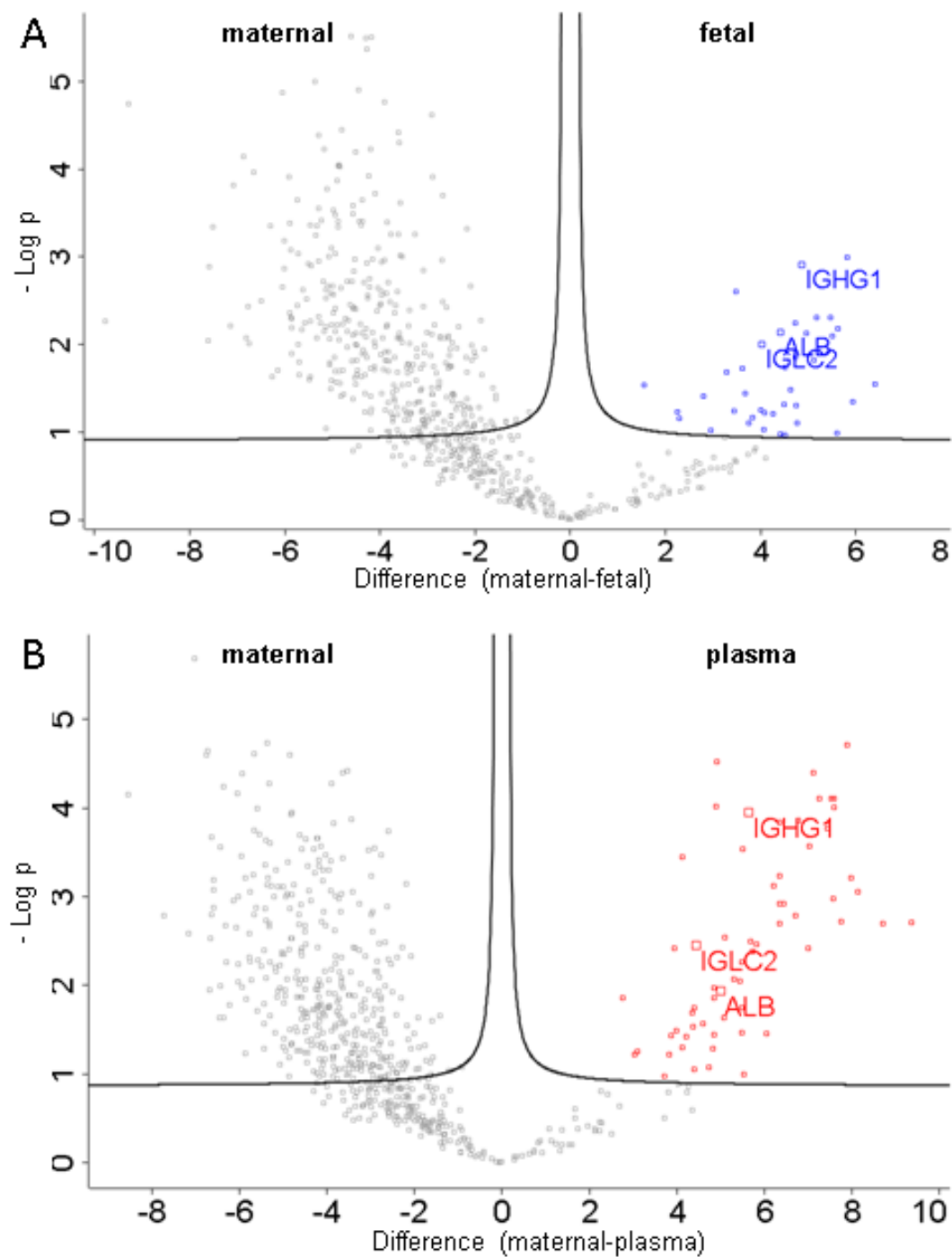


Figure 21. Analysis of proteome revealed few proteins that could act as drivers for 80 nm PS NP placental transfer. Volcano plots of proteomics data comparing significant enriched proteins in the biocorona of PS NPs isolated from plasma medium or maternal or foetal circulation after perfusion experiments. The x-axis shows the difference in log<sub>2</sub> transformed intensity data. The y-axis demonstrates the -10log transformed p values of the FDR corrected

multiple t-tests. Significantly, enriched proteins in the biocorona of plasma medium are displayed as red symbols, and those from PS NPs isolated from foetal circulation are depicted in blue. Grey symbols represent proteins significant enriched in maternally isolated PS NPs or not significant differing proteins. A) Graph compares maternal samples with the foetal samples. B) Graph compares plasma samples with maternal samples. In A and B human serum albumin, IgG-1 heavy chain C region and the constant are highlighted with their gene names (N=4). This graph is a modified version of “Supporting Figure 3: Venn diagram” (1) used under CC BY 4.0/ % information was removed, diagram was coloured and labelling was rearranged.

An overlap of 24 significant enriched proteins of plasma and foetal isolated protein biocoronas can be reported. Out of this group of proteins IgG-1 heavy chain C region, the immunoglobulin lambda light chain 2 constant and serum albumin needs to be reported (Appendix Table 11) as IgGs were known to cross the placenta and serum albumin was highly enriched on NPs crossing the placenta, these proteins were considered for further media formulations.

#### **4.1.5.3. Biocorona proteins indicate vesicular processes on maternal isolated particles**

The databases STRING, DAVID, and Reactome differed in the number of proteins, which they could process in the database. The input for all of them was 642 gene names of the maternally significant enriched biocorona proteins, which gave 638 recognized proteins in DAVID, 627 recognized proteins in STRING, and 591 recognized proteins in Reactome. The results of the three most probable biological processes or the cellular pathways of the three databases used were compared in Table 8.

Table 9. Top 3 protein hits of enriched biocorona proteins on PS particles data analysis assessed by applying different online databases namely, DAVID, STRING, and Reactome.

DAVID (protein detection 638)		STRING (protein detection 627)		Reactome (protein detection 591)	
Biological process	False discovery rate	Biological process	False discovery rate	Pathway	False discovery rate
Cell-cell adhesion	3.5E-60	Vesicle-mediated transport	8.55E-79	Neutrophil degranulation	1.11E-16
Wnt signalling, pathway, planar cell polarity pathway	5.0E-23	Establishment of localization	4.18E-71	AUF1 (hnRNP D0) binds and destabilizes mRNA	1.11E-16
NIK/NF-kappaB signalling	1.5E-20	Transport	4.18E-71	Vesicle-mediated transport	1.11E-16

Differences between the readouts of the three databases were detected. Results from STRING and Reactome pointed towards vesicular processes and vesicle mediated transport. The results from DAVID pointed more into the direction of cell signalling.

In a broader overview in Reactome the five most likely involved pathway clusters were: cellular response to external stimuli (FDR: 2.96E-14), Immune System (FDR: 2.33E-12), Vesicle-mediated transport (FDR: 1.28E-11), Metabolism of proteins (FDR: 5.15E-9) and Programmed cell death (FDR: 7.74E-9) (Figure 22).

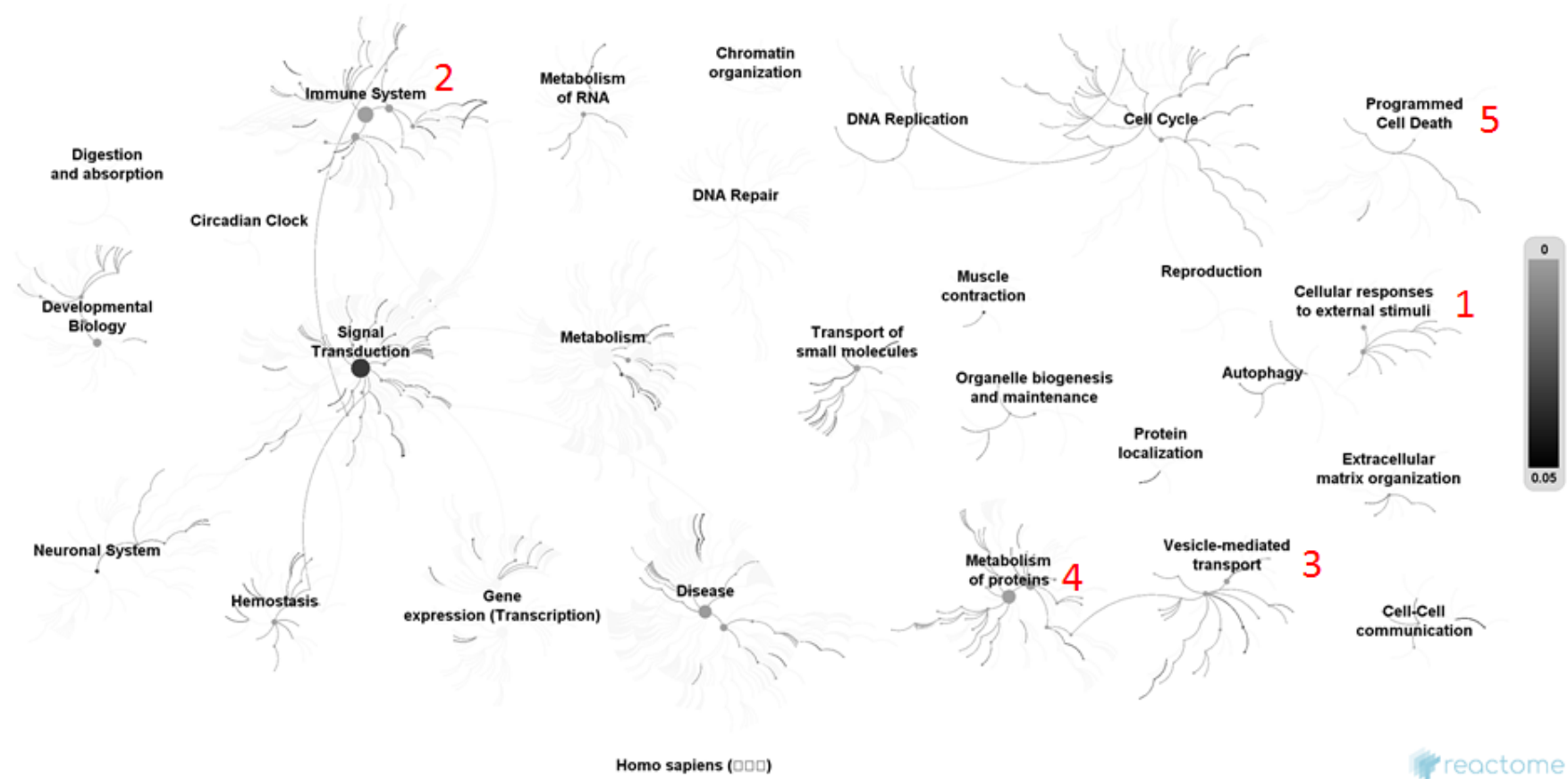


Figure 22. Overview of cellular pathway cluster of protein biocorona proteomics data. The five statistically most likely cellular pathway families were 1) cellular response to external stimuli 2) immune system 3) vesicle-mediated transport 4) metabolism of proteins 5) programmed cell death (N=4).

#### 4.1.6. 80 nm polystyrene nanoparticles were detectable in placental syncytium

The purpose of TEM approach was to identify the localization of the 80 nm PS NPs within the placental tissue. The used protocol for perfusion fixation demonstrated high-grade conservation of microstructures in the tissue after perfusion. The glycocalyx was visible at the foetal endothelium and the syncytiotrophoblast layer (Figure 23 A, B). Cellular organelles were well preserved and could be identified clearly in cells of the stroma (Figure 23 C, D).

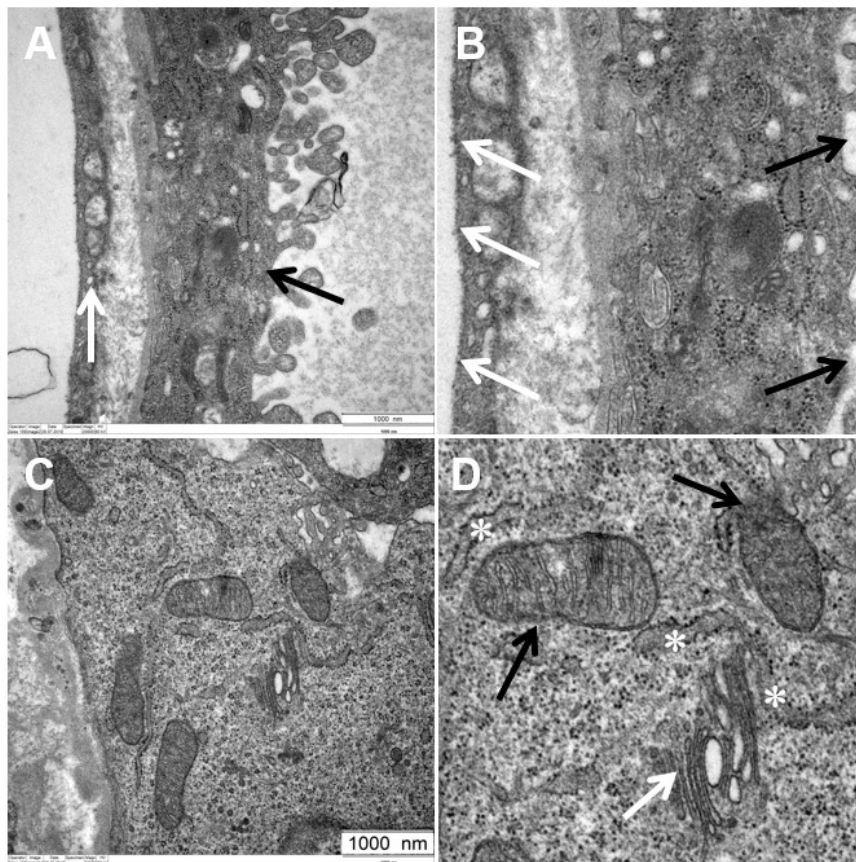


Figure 23. Applied protocol for fixation of perfused placental tissue leads to high quality ultrastructure preservation for TEM. A) Short diffusion distance between syncytiotrophoblast (black arrow) and foetal endothelium (white arrow). B) Magnification of A). The white arrows are pointing to the diffusely roughened glycocalyx at the membrane of endothelial cells. Black arrows mark the glycocalyx at the syncytium. C) A cell in the placental stroma. D) Magnification of a section in picture C). Black arrows display mitochondria. The white arrows point to a Golgi apparatus. Parts of rough endoplasmic reticulum are indicated with white stars. (N=2)

### **Detection of polystyrene particles in placental tissue is challenging and limited to degenerative organelles within the syncytiotrophoblast**

To identify the 80 nm PS NPs in the tissue the tissue sections had to be negative contrasted with uranium salt. Without negative contrasting a clear differentiation between vesicles and 80 nm PS NPs was not possible within the placental tissue due to their similarity in size and electron density. If negative contrasting was applied, the potential NPs remained brighter compared to physiological structures indicating a lower affinity to the contrasting process. The comparison of potential internalized PS NPs within likely degenerating organelles to a similar physiological structure within sections of a control experiment is demonstrated (Figure 24 A). Such PS NPs filled organelles were distinctly detectable in syncytiotrophoblasts, but not in other cells. In control as well as in PS NP perfused tissue organelles contained vesicles with varying diffuse staining of their lumen (Figure 24 B).

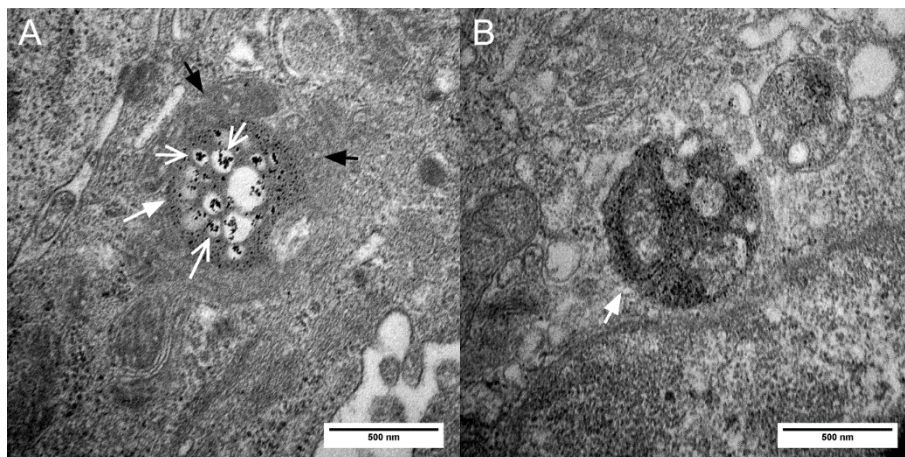


Figure 24. Polystyrene accumulates in organelles of syncytiotrophoblast. A) Organelle of syncytiotrophoblast after 80 nm PS NP perfusion with plasma medium. The filled white arrow points to an organelle, likely an autophagolysosome. In the organelle, open white arrows indicate 80 nm PS NPs visible as intense black spot localized staining from the negative contrasting. Mitochondria in proximity to the organelle are highlighted with black arrows (N=1). B) Arrow points to a similar organelle in the syncytium of a control perfusion with plasma medium without PS NP (N=1). This graph was modified from (1).

#### **4.1.7. Albumin mediates placental transport of 80 nm polystyrene nanoparticles**

The PS NP concentration in the maternal artery decreased in all four media over time. In control medium the PS NP concentration declined over time most of all, resulting in a final concentration of  $15.5 \pm 2.3$   $\mu\text{g/ml}$ . In the HSA and IgG medium the decrease in PS NP concentration was time delayed but resulted in similar final concentrations as the control with  $16.7 \pm 1.9$   $\mu\text{g/ml}$  in HSA and  $15.5 \pm 2.2$   $\mu\text{g/ml}$  in IgG medium. In plasma medium, PS NP concentration decrease over time was less pronounced leading to a final concentration of  $23.2 \pm 5.5$   $\mu\text{g/ml}$  (Figure 25). Statistical significant differences occurred after 30 min between plasma and control medium, after 180 min between plasma and HSA medium and after 240 min between plasma and IgG medium (all  $P > [t] < 0.05$ ).

Samples taken from maternal vein had initial low PS NP concentrations, explainable by the void volume within the perfusion system and the placental intervillous space. Within the first 60 min of each perfusion experiment, the placental PS NP outflow concentration reached a maximum. At later time points, the PS NP concentration in maternal outflow decreased and started to converge with the maternal inflow concentration without being equal until perfusion end.

The end point concentrations of maternal outflow were  $14.8 \pm 2.4$   $\mu\text{g/ml}$ ,  $22.7 \pm 5.6$   $\mu\text{g/ml}$ ,  $16.3 \pm 2.2$   $\mu\text{g/ml}$  and  $14.7 \pm 2.6$   $\mu\text{g/ml}$ , for control, plasma, HSA and IgG media, respectively (Figure 25).

In the foetal samples 80 nm PS NPs was observed suggesting placental transfer. At the foetal vein sampling port a media dependency in transfer was observed after 15-30 min of experimental time. After 120 min foetal PS NP outflow was nearly constant resulting in final concentrations of  $6.7 \pm 1.1$   $\mu\text{g/ml}$ ,  $9.8 \pm 2.8$   $\mu\text{g/ml}$ ,  $11.7 \pm 0.6$   $\mu\text{g/ml}$  and  $5.1 \pm 0.6$   $\mu\text{g/ml}$  in control, plasma, HSA and IgG medium respectively (Figure 25).

In the foetal artery PS NP concentration increased similar in all media within the first 60 min. As perfusion progresses, differences between the transfer rates of PS NPs in the four media were clearly detectable. In control and IgG media, PS NPs transfer was nearly balanced resulting in final PS NP concentrations of  $6.5 \pm 1$   $\mu\text{g/ml}$  and  $5.3 \pm 0.8$   $\mu\text{g/ml}$  respectively. Polystyrene NP concentration in plasma and HSA media increased with a declining kinetic until experimental end resulting in  $9.9 \pm 2.3$   $\mu\text{g/ml}$  in plasma and  $11.6 \pm 0.5$   $\mu\text{g/ml}$  in HSA medium. After 4h of perfusion PS NP concentration in the foetal artery was significant higher

during HSA medium perfusion compared to the other media (control  $p<0.0001$ , plasma  $p<0.0461$ , IgG  $p<0.0001$ ).

During the control, plasma, HSA and IgG medium experiments, a glucose consumption of  $0.14\pm 0.03 \mu\text{mol/g/min}$ ,  $0.08\pm 0.04 \mu\text{mol/g/min}$ ,  $0.14\pm 0.06 \mu\text{mol/g/min}$  and  $0.09\pm 0.03 \mu\text{mol/g/min}$  can be reported, respectively. Additionally, lactate formation was determined in control ( $0.45\pm 0.26 \mu\text{mol/g/min}$ ), plasma ( $0.28\pm 0.13 \mu\text{mol/g/min}$ ), HSA ( $0.25\pm 0.13 \mu\text{mol/g/min}$ ), and IgG ( $0.20\pm 0.09 \mu\text{mol/g/min}$ ) medium.

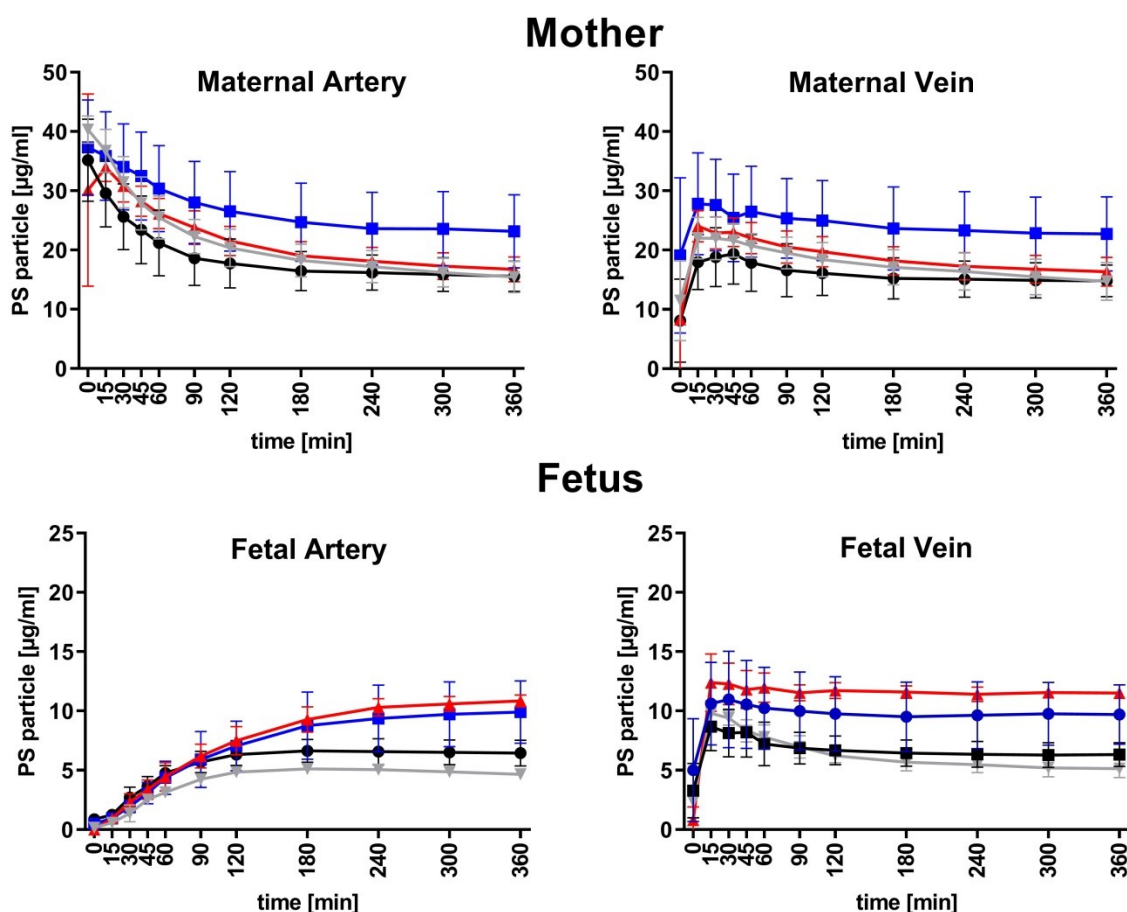


Figure 25. Perfusion media influences PS NP kinetics during perfusion experiments. Time course of PS NP concentration in the maternal artery, maternal vein, foetal artery, and foetal vein sampling ports (control, plasma, and HSA  $N=5$ ; IgG  $N=3$ ). Blue graph represents plasma medium experiments. Black graphs represent control medium experiments. Red graphs

represent HSA medium experiments. Gray graphs represent the IgG medium. Data represent mean  $\pm$ SD for each medium. This graph was taken from literature and modified (1)

### Specific protein biocoronas affect the 80 nm polystyrene particle recovery after perfusion experiments

The total recovery of PS NPs at the end of perfusion was calculated by summing up foetal and maternal detected total fluorescence signals in the media and was normalized to the maternal PS NP total start fluorescence signal representing the start concentration. By comparing different media significant differences between the 40g/l HSA containing media (plasma (88.7 $\pm$ 12.8%) and HSA 75 $\pm$ 3.6%) compared to control (59.9 $\pm$ 7 %) and IgG (54.1 $\pm$ 1.7%) medium was observed (Figure 26). The highest significant differences in PS NP recovery occurred between plasma medium to control- and IgG medium. (p=0.0007, p=0.0006 respectively).

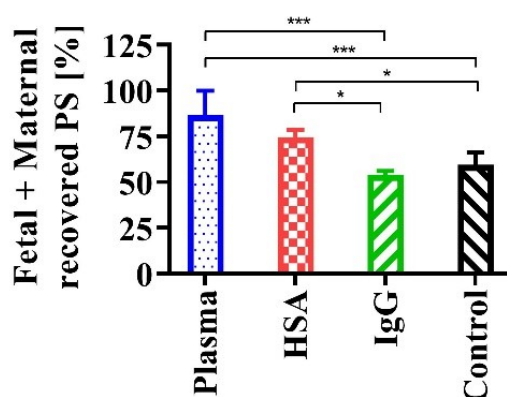


Figure 26. Total recovery of PS NPs after perfusion is media dependent. Recovery of PS NP levels from foetal and maternal circulation at showed significant differences. Plasma medium (N=5) differed from control medium (N=5) (p=0.0007) and IgG medium (N=3) (p=0.0006). HSA medium (N=5) differed from control medium (p=0.0351) and IgG medium (p=0.0178). Data was analysed with One-Way-ANOVA and Holm-Sidak's multiple comparison test. Data is presented as mean with  $\pm$ SD. This graph is a reused and modified figure of (1)

### Pharmaceutical stabilizers in HSA medium do not increase 80 nm polystyrene transfer across the placenta

In these three validation experiments, one was terminated after 180 min due to the accidental removal of the foetal cannula during sample handling. Until 180 min, no reportable differences in PS NP transfer between the pharmaceutical and the lyophilized HSA medium occurred. From 240 min onwards, the two remaining perfusion experiments showed a higher transfer rate of PS NPs in the lyophilized HSA medium compared to the HSA medium with a final foetal concentration of  $12.63 \pm 0.1 \mu\text{g/ml}$  in the foetal circuit (Figure 27). Glucose consumption can be reported with  $0.09 \pm 0.01 \mu\text{mol/g/min}$ . Lactate formation reached  $0.21 \pm 0.10 \mu\text{mol/g/min}$ .

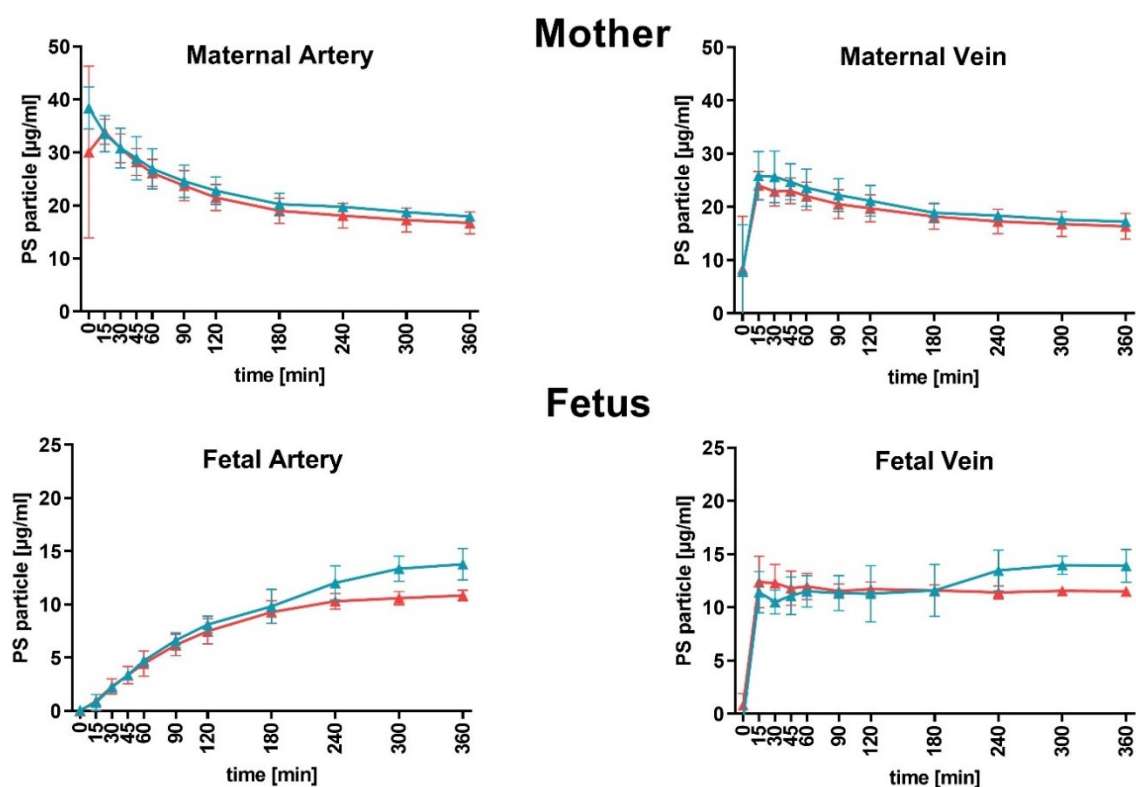


Figure 27: Pharmaceutical stabilizers do not enhance PS NP transfer across the placenta. Triangles with red lines represent PS NP concentration in HSA medium experiments (N=5). Triangles with blue lines represent PS NP concentration in HSA lyo medium experiments (N=3). In HSA lyo experiments, the PS NP transfer started to be increased after 240 min. Data represent mean  $\pm$ SD for each medium.

**Addition of chloroquine to HSA perfusion medium has no significant effect on 80 nm polystyrene particle transfer**

The introduction of chloroquine aimed for the partial inhibition of potential pH dependent transfer mechanisms of PS NPs. The experiments were split in two phases lasting 180 min were the first phase was in analogy to the 360 min HSA medium experiments in the same period (Figure 28 red). In the second phase with chloroquine containing HSA medium no significant differences to the first phase in placental uptake and transfer was detectable (Figure 28 grey). Nevertheless, trends in a delayed PS NP transfer of the placenta were indicated in the foetal artery and vein sampling ports. During these experiments, a glucose consumption of  $0.16 \pm 0.04 \mu\text{mol/g/min}$  and a lactate formation of  $0.19 \pm 0.17 \mu\text{mol/g/min}$  can be reported.

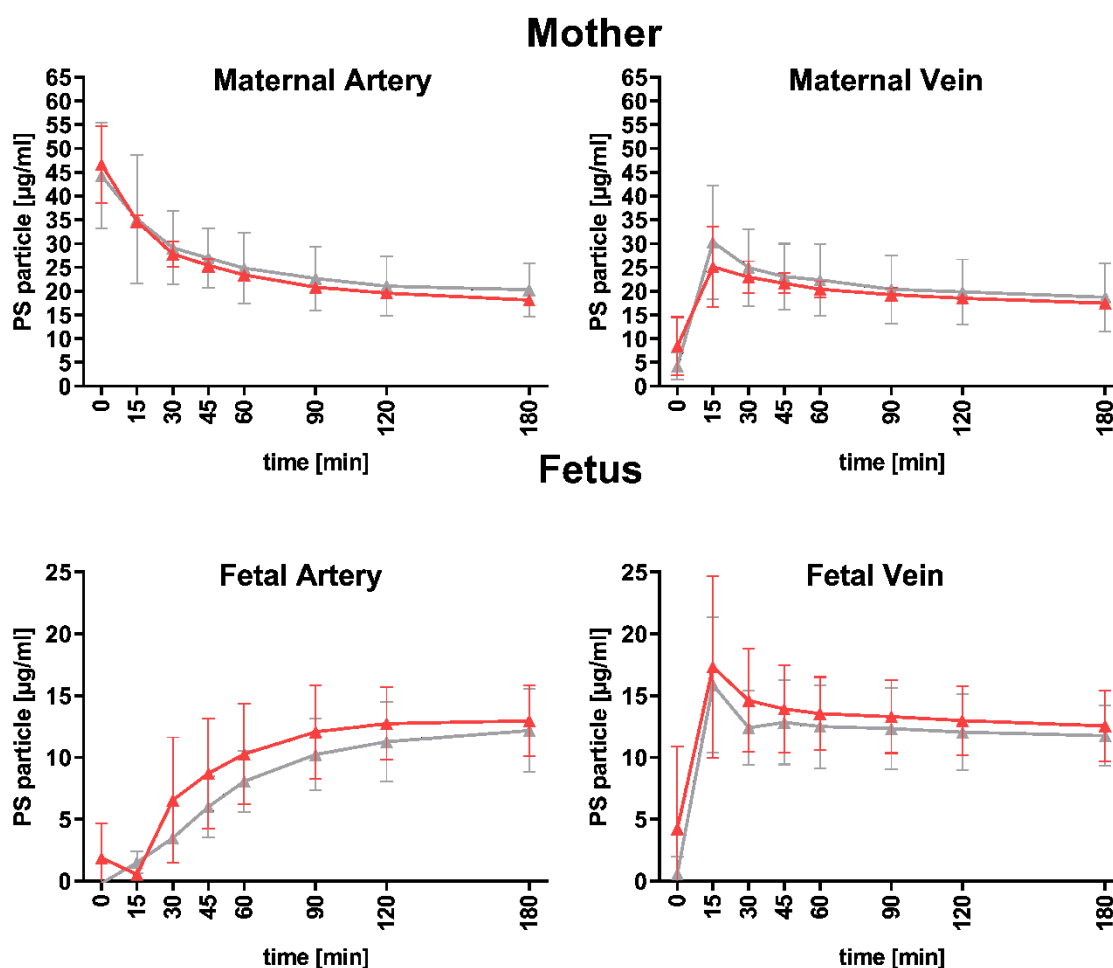


Figure 28. Polystyrene NP concentration in chloroquine perfusion experiments. Red lines represent the mean of the first 180 min of the experiments with HSA medium. Grey lines represent the second perfusion phase with HSA medium containing chloroquine (N=3). In the maternal artery, no effect of chloroquine was observed on PS NP concentration over time. In

Maternal vein, PS NP outflow is equal between both media with and without chloroquine. Polystyrene NP concentration over time in foetal artery in both media indicates a not significant delay of PS NP transfer in presence of chloroquine. Foetal vein PS NP outflow shows a not significant difference.

### **Albumin concentrations affects 80 nm polystyrene nanoparticle processing in cell culture**

The choriocarcinoma cell line BeWo, which shares mechanistic functions (211) with syncytiotrophoblast cells, and hFcRn transfected BeWo cells were used in a transwell setting (Figure 29) to investigate the influence of FcRn on the observed transfer kinetics of PS NP in HSA media. The PS NP were added at the top well and this compartment can be linked to recycling.

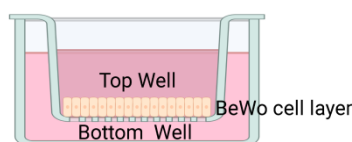


Figure 29. Scheme of the transwell setup for PS NP chloroquine experiments. The top well is the medium compartment of initial uptake and recycling. The BeWo cells represent the barrier. The bottom well contains PS NP that were transferred across the barrier during the experiment.

In not transfected (Figure 30 A, C) and transfected (Figure 30 B, D) cells a significant difference in PS NP uptake and recycling was detectable between 5 g/l BSA und 40 g/l HSA medium independent of the presence of chloroquine. The transfer and recycling of PS NPs at and across not transfected and transfected BeWo cell layers was not significant different in a cell type dependent manner (Figure 30 E, F).

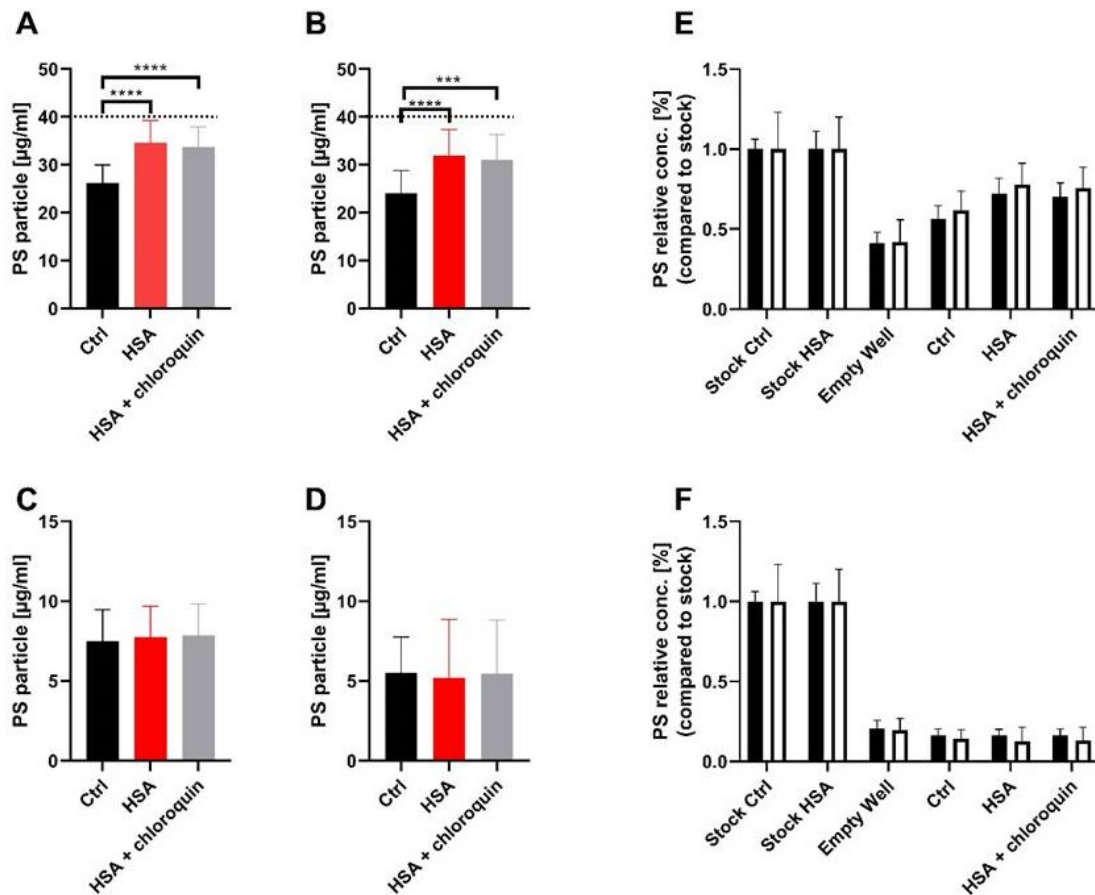


Figure 30. Albumin but not chloroquine impacts 80 nm PS NP uptake and recycling in BeWo cells. Recycling and transfer of 80 nm PS NPs was assessed in the presence and absence of chloroquine in HSA medium with BeWo and overexpressing hFcRn-BeWo- cells by a transwell system. Dashed line in A & B represents the applied PS NP concentration in the top wells at the beginning of the experiment. Polystyrene NP concentration after 6h incubation for top wells is represented in A, B & E. A) BeWo cells show significant difference between media with 0.5% BSA (ctrl) and 4% HSA. B) Transfected BeWo-hFcRn shows significant differences between 0.5% BSA (ctrl) and 4% HSA media. Polystyrene NP concentration after 6h incubation for bottom wells are represented in C, D & F. C & D) No significant medium dependent differences are detectable in the bottom compartments in BeWo and BeWo-hFcRn experiments. E & F) Between BeWo (solid black bars) and BeWo-hFcRn (empty bars) no significant differences in PS NP uptake and recycling (E) as well as transcytosis (F) was detected. Experiments with Chloroquine demonstrated a non-significant trend of a reduction in PS NP uptake and recycling and no impact on transcytosis (N=3). Data was analysed with One-Way-ANOVA and Tukey's multiple comparison test. Data are presented as mean  $\pm$ SD.

## **4.2. Therapeutic and non-therapeutic IgGs at the placental barrier**

### **4.2.1. Placental perfusion with physiological IgG levels**

Polyclonal polyvalent human IgGs in physiological concentration (10mg/ml) was used to validate the experimental setup according to published data (8). Upon an IgG washout phase of the tissue and change of perfusion media, maternally offered total IgG (10 mg/ml) was perfused for 6 hours. During these three perfusions  $3.64 \pm 2.86$   $\mu\text{g/ml}$  of IgG could be detected after 180 min and  $10.61 \pm 0.56$   $\mu\text{g/ml}$  could be detected after 360 min within the foetal circulation. These values represent a foetal to maternal ratio of  $0.0002 \pm 0.0002$  after 180 min and  $0.0012 \pm 0.0015$  reflecting the high detected deviation between the offered maternal IgG concentration of 10 mg/ml and the low  $\mu\text{g/ml}$  IgG concentrations in foetal circulation. Nevertheless, the time depending concentration increase of IgG in foetal circulation confirmed the suitability of the used placental perfusion setup. A glucose consumption of  $0.10 \pm 0.07$   $\mu\text{mol/g/min}$  and a lactate formation of  $0.19 \pm 0.10$   $\mu\text{mol/g/min}$  were observed.

### **4.2.2. Fully monoclonal human IgG2-anti-RANKL antibody crosses the placenta**

#### **IgG2 specific peptide was detected by LC-MS/MS in the foetal circulation after placental perfusion**

Concentrations of 27  $\mu\text{g/ml}$ , 6  $\mu\text{g/ml}$  and 0.1  $\mu\text{g/ml}$  were used to investigate the general possibility of placental transfer of (pharmacological active, fragmented or complex bound). The IgG2 specific peptide (LEPEDFAVFYCYQYQYSSPR), present in the variable region of the antibody, was chosen to be analysed via LC-MS/MS. The analytical LC-MS/MS setting allowed to answer the general transfer question as the analytics is independent from the pharmacological activity of the IgG2-anti-RANKL antibody which could lead to false negative results e.g. with an ELISA approach in the case of immunocomplex formation. The IgG2-anti-RANKL antibody was detected in foetal circulation after 3h in experiments with 27 and 6  $\mu\text{g/ml}$  (Figure 31). A transfer of the IgG2-anti-RANKL antibody during the 0.1  $\mu\text{g/ml}$  setting was not detected with the method as the foetal IgG2-anti-RANKL antibody concentration may be below the  $<0.125$  fmol detection limit. The calculation of the specific peptide ratio between mother and foetus resulted in a ratio of 0.03 ( $\pm 0.015$ ) and 0.41 ( $\pm 0.11$ )

in the 27 and 6  $\mu\text{g/ml}$  experiments, respectively. The glucose consumption during experiments containing 27  $\mu\text{g/ml}$  was  $0.11\pm 0.02$   $\mu\text{mol/g/min}$ , during experiments containing 6  $\mu\text{g/ml}$   $0.10\pm 0.03$   $\mu\text{mol/g/min}$  and during experiments with 0.1  $\mu\text{g/ml}$   $0.10\pm 0.04$   $\mu\text{mol/g/min}$ . Likewise,  $0.21\pm 0.16$ ,  $0.20\pm 0.14$  and  $0.21\pm 0.12$   $\mu\text{mol/g/min}$  of lactate were formed in the experimental groups containing 27, 6, and 0.1  $\mu\text{g/ml}$  of the investigated IgG2, respectively.

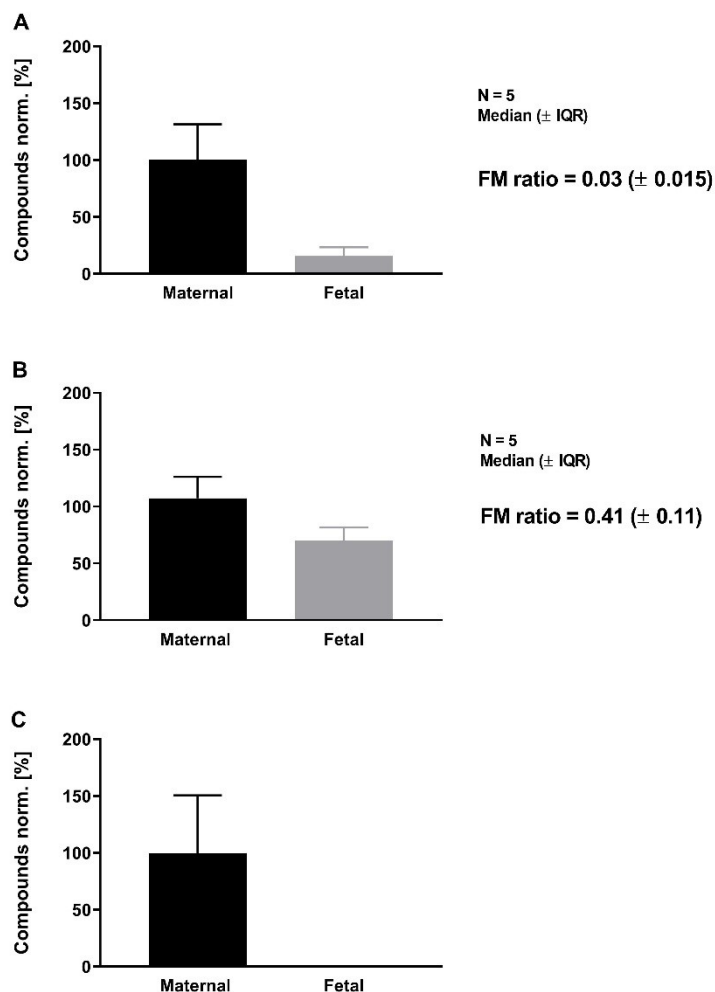


Figure 31. IgG2-anti-RANKL antibody specific peptide in the foetal circulation confirms placental transfer. Counts of the specific peptide, gathered by targeted proteomics, were normalized to the median of maternal detected specific peptide counts of the respective measurement group (N=5 per group). A) By applying 27  $\mu\text{g/ml}$  IgG2-anti-RANKL antibody the normalized peptide counts are clearly different between maternal and foetal samples. B) Experiments with 6  $\mu\text{g/ml}$  IgG2-anti-RANKL antibody normalized peptide counts deviations

were minor. C) Applying 0.1 µg/ml IgG2-anti-RANKL antibody no specific peptides could be detected in foetal samples. Data is presented as median ( $\pm$  IQR).

### **The placental transfer of functional IgG2-anti-RANKL antibody was analysed by an indirect functional assay**

The pharmaceutical activity of placental transferred IgG2-anti-RANKL antibody was assessed indirectly in competitive IgG/IgG2-anti-RANKL antibody perfusion experiments with a RANKL ELISA. The indirect assay measured the free soluble RANKL, which was spiked into the perfusion samples. Functional active IgG2-anti-RANKL antibody would bind to spiked RANKL and therefore RANKL would decrease in the ELISA. Interestingly in maternal in foetal samples the amount of detected free RANKL increased within 240 min perfusion experiments. In revers the binding capacity of the IgG2-anti-RANKL antibody decreased significant in maternal and foetal samples ( $p = 0.0209$  and  $p = 0.0134$ ) (Figure 32). During these experiments,  $0.17 \pm 0.07$  µmol/g/min glucose was consumed and  $0.28 \pm 0.15$  µmol/g/min lactate were formed.

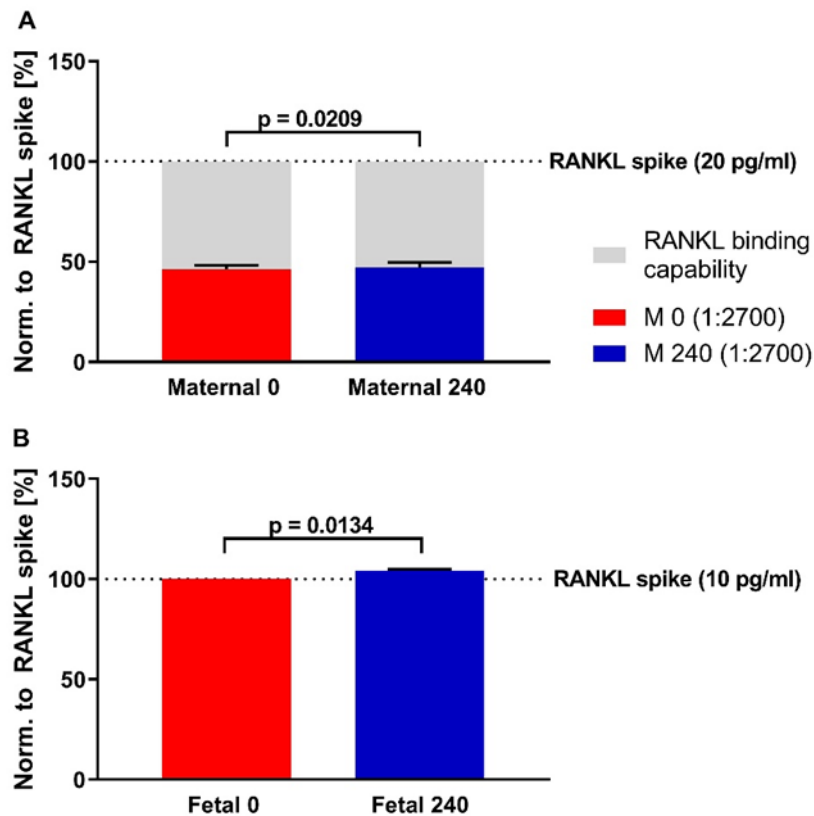


Figure 32. The placental RANKL secretion exceeds the RANKL binding capacity of IgG2-anti-RANKL after perfusion. Relative RANKL binding capability of in maternal and foetal circulation. Ex vivo perfusion experiments were performed with 27  $\mu\text{g/ml}$  IgG2-anti-RANKL antibody in maternal media. The media containing pooled pregnant serum (10%) or pooled female serum (10%) in maternal and foetal circulation, respectively. Media further contained 10 mg/ml of polyclonal human IgG in both circulations at perfusion start. RANKL binding capacity was determined from both circulations after 240 min perfusion. For analysis, samples were spiked with recombinant RANKL (20 pg/ml maternal, 10 pg/ml foetal) and remaining free RANKL was quantified by ELISA. Higher concentrations of free RANKL were detected (A) in maternal circulation and (B) in foetal circulation after placental perfusion with the IgG2-anti-RANKL antibody. Data are shown in relation to 100% RANKL spike (N=3). Statistical analysis was performed with paired t-test.

### **RANKL detected with immunohistochemistry in limited highly positive areas within the term placenta**

Expression of RANKL in immunohistochemistry from tissue collected before perfusion showed few strong positive stained areas in the term placenta for RANKL (Figure 33A). The RANKL staining was not directly at the same locations as CD163 staining. CD 163 is a marker expressed by the majority of placental macrophages in vitro (Hofbauer cells) (212)(Figure 33 B).

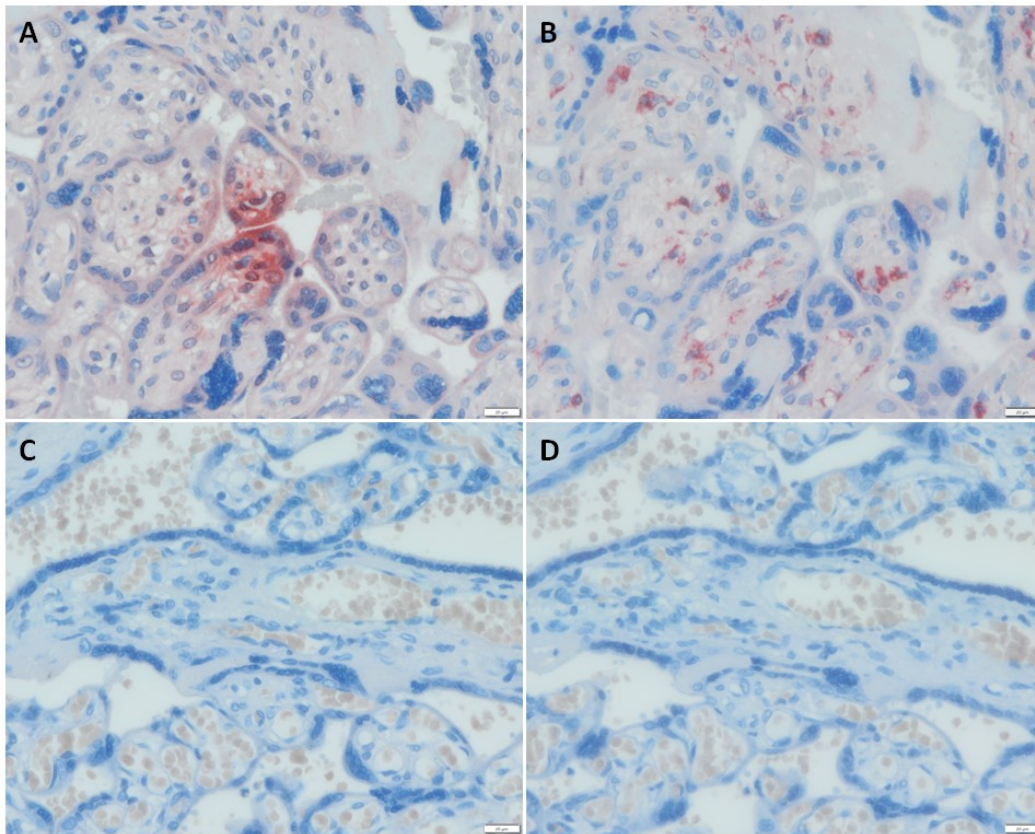


Figure 33 RANKL staining is present in few but highly positive areas in placental tissue, which are not in direct proximity to CD163 positive cells. Representative RANKL and CD 163 immunohistochemically staining in term placentas (N=5). A) Strong RANKL staining in a narrow localized area ranging from syncytium to the endothelium is depicted. The syncytiotrophoblast layer shows a slight baseline staining. B) CD163 staining in the same term placental section in the subsequent serial slide. CD163 positive Hofbauer cells are not localized in or close to the epicentre of the RANKL staining in placental stroma. C) Negative control rabbit (RANKL) D) Negative control mouse IgG (CD163).

RANKL expression in placental cross sections was very limited therefore, these areas were counted resulting in approximately 0.233 stained areas per mm<sup>2</sup> on the slides. RANKL was

detected mainly in terminal villi, and to a minor extend in the stroma of intermediate villi and stem villi (Table 9). The stained areas were predominant in the placental stroma. Syncytium and foetal endothelium were presented mainly free from strong RANKL staining. Nevertheless, RANKL was detected in the syncytium and the foetal endothelium especially in areas with small distances between maternal and foetal circulation. For quantification of RANKL distribution, such overlying areas were added in the calculation to all three cellular compartments in Table 10. A limited increased staining slightly above the unspecific background staining was observed in the syncytiotrophoblast throughout the observed tissue.

Table 10. Distribution of RANKL staining classified by different villous structures

<b>Stained areas/slide median (min-max)</b>	<b>Stained/mm<sup>2</sup> median (min-max)</b>	<b>Terminal villous [%] median (min-max)</b>	<b>Intermediate villous [%] median (min-max)</b>	<b>Stem villous [%] median (min-max)</b>
51 (42-61)	0.233 (0.167-0.321)	78 (63-83)	13 (10-23)	10 (3-14)

Table 11. Distribution of RANKL staining classified by cell type

<b>Stained areas/slide median (min-max)</b>	<b>Stained/mm<sup>2</sup> median (min-max)</b>	<b>Trophoblast [%] median (min-max)</b>	<b>Stroma [%] median (min-max)</b>	<b>Endothelium [%] median (min-max)</b>
51 (42-61)	0.233 (0.167-0.321)	28 (26-34)	44 (38-51)	28 (22-28)

#### **4.2.3. Monoclonal IgG1-anti HER2 antibody is unable to cross the placenta**

Perfusion experiments with IgG1-anti HER2 antibody were performed for 120 or 360 min. During the 120 min experiments 36 ( $\pm 7.2$ )  $\mu\text{g/ml}$ , 30.9 ( $\pm 4.8$ )  $\mu\text{g/ml}$ , 31.7 ( $\pm 5.8$ )  $\mu\text{g/ml}$ , 30.3 ( $\pm 9$ )  $\mu\text{g/ml}$ , 28.1 ( $\pm 6.3$ )  $\mu\text{g/ml}$ , and 26.8 ( $\pm 2.1$ )  $\mu\text{g/ml}$  of IgG1-anti HER2 antibody were

detected at the time points 0, 15, 30, 60, 90, and 120min in maternal circulation. During the 360 min experiments 31.9 ( $\pm 4$ )  $\mu\text{g/ml}$ , 32.5 ( $\pm 4.4$ )  $\mu\text{g/ml}$ , 31.7 ( $\pm 6.2$ )  $\mu\text{g/ml}$ , and 30.1 ( $\pm 6$ )  $\mu\text{g/ml}$  of IgG1-anti HER2 antibody were detected at the time points 0, 120, 240, and 360 min (Figure 34) in maternal circulation. During the 120 min and the 360 min IgG1-anti HER2 antibody experiments the IgG1-anti HER2 antibody concentration in the foetal circulation was below the detection limit (2 ng/ml) of the used ELISA. Tissues used for 2h experiments consumed  $0.20 \pm 0.06$   $\mu\text{mol/g/min}$  of glucose and produced  $0.30 \pm 0.19$   $\mu\text{mol/g/min}$  of lactate. During the 6h experiments  $0.08 \pm 0.04$   $\mu\text{mol/g/min}$  of glucose were consumed and  $0.21 \pm 0.14$   $\mu\text{mol/g/min}$  of lactated formed.

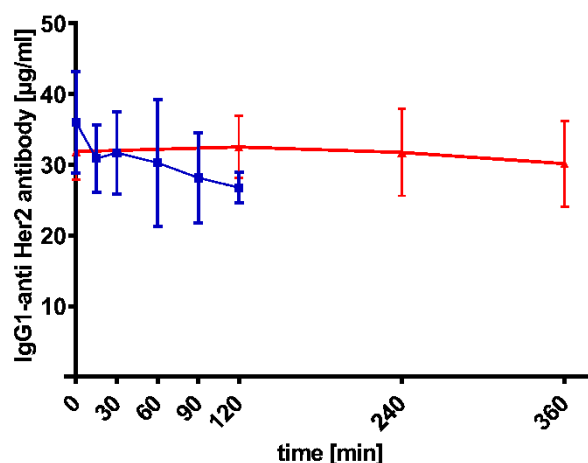


Figure 34. IgG1-anti HER2 antibody concentration in maternal circulation during perfusion experiments. Graph shows maternal IgG1-anti HER2 antibody concentrations during (blue) 120 min perfusion experiments (N=3) and (red) 360 min perfusion experiments (N=5) determined by ELISA. Data shown as mean  $\pm$  SEM of three 120 min experiments and four 360 min experiments.

#### 4.2.4. HER2 receptor is expressed in the term placenta

Immunohistochemistry staining for HER2 in unperfused term placenta showed its expression in the syncytiotrophoblast layer and to a minor degree in cells in the stroma and the foetal endothelium (Figure 35 A).

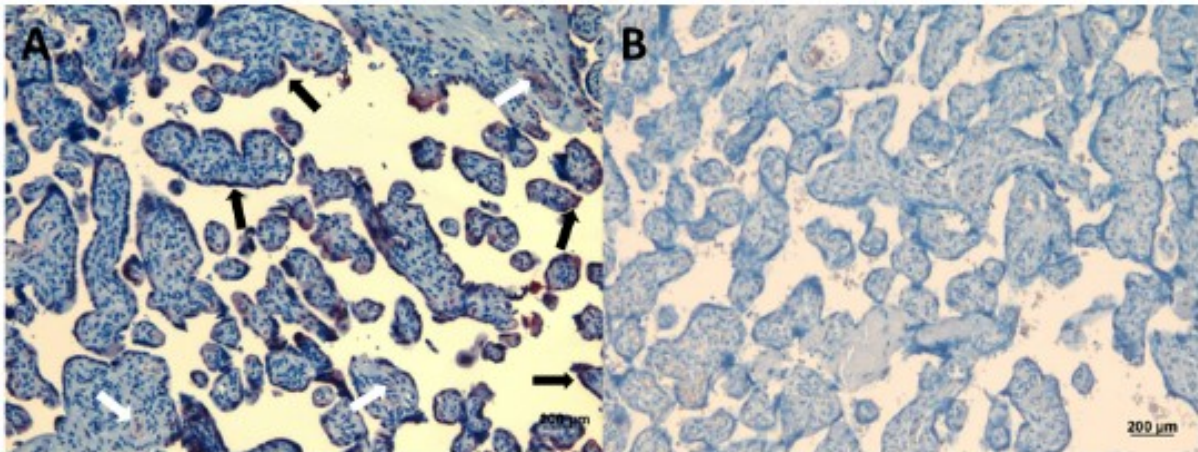


Figure 35. HER2 staining in term placenta. Representative immunohistochemistry staining of HER2 in (A) placental tissue, predominantly in the syncytiotrophoblast (solid black arrows) and to a minor extent in the foetal vasculature (hollow black arrows); (B) negative control of the same tissue (n=5).

#### 4.2.4.1. IgG1-anti HER2 antibody interactions with its antigen on the placenta

HER2 placental distribution before and after perfusion with IgG1-anti HER2 antibody was further investigated with two immunofluorescence approaches. The first approach investigated the saturation of the HER2 receptor after IgG1-anti HER2 antibody perfusion with a polyclonal HER2 antibody. As in immunohistochemistry HER2 was predominantly detectable in the syncytium, partially in the stroma cells and foetal endothelium (Figure 36 A) in unperfused placental tissue. After IgG1-anti HER2 antibody perfusion for 120 min the stainability of the receptor in the syncytium was negligible. HER2 staining in foetal endothelium was present, in stromal cells the staining seemed to be partially reduced (Figure 36 B).

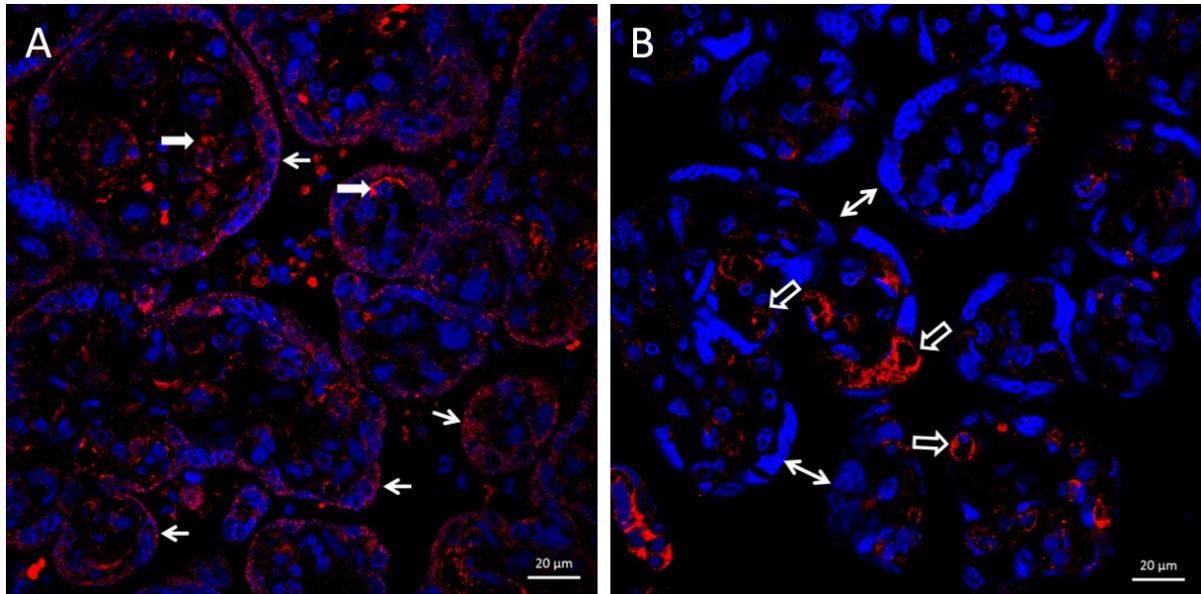


Figure 36. IgG1-anti HER2 antibody binds to HER2 at the syncytiotrophoblast. Immunofluorescence staining of unperfused (A) and perfused (B) placental tissue sections for HER2 from the same placenta (N=2). Perfusion experiments lasted for 120 min and contained 42 µg/ml IgG1-anti HER2 antibody in the maternal circulation at start of the perfusion. A) HER2 is predominantly identifiable in the syncytium (slim arrows). Further, potential endothelial cells were stained (thick arrows). B) Syncytium was not stained after IgG1-anti HER2 antibody perfusion (double arrows). HER2 staining of foetal endothelium was not affected and showed a positive staining (hollow arrows). HER2 staining was performed with a polyclonal anti HER2 antibody and is presented in red. Nuclei were stained with DAPI and are presented in blue.

### **Co-staining of HER2, FcRn and LAMP1 indicate the degeneration of IgG1-anti HER2 antibody in the placenta**

The second approach investigated the HER2, FcRn and LAMP1 staining before and after IgG1-anti HER2 antibody perfusion. To detect potential co-localization of the three proteins the antibody for HER2 was changed to a monoclonal antibody that binds at a very different antigen area than IgG1-anti HER2 antibody. Therefore, the staining results for HER2 showed different staining intensity compared to the first experimental set with the polyclonal antibody. Before perfusion, HER2 was localized in the syncytium. FcRn was present predominant in the syncytium but was detected in localized areas in the placental stroma. LAMP1 was present predominant in the syncytium (Figure 37 A, C, E). HER2 was not co-

localized with FcRn or LAMP1 before perfusion. (Figure 37 A, C). FcRn and LAMP1 showed co-localization in proximity to the apical membrane of the syncytium (Figure 37 E).

After perfusion with IgG1-anti HER2 antibody the stainability of HER2, LAMP1 and FcRn was overall decreased (Figure 37 B, D, and F). HER2 and LAMP 1 were partially co-localized in areas in proximity to the basolateral membrane of the syncytium (Figure 37 B). A co-localization of HER2 and FcRn was not observed due to the absence of stainable FcRn in the syncytium and reduced stainability of HER2. In placental stroma, FcRn was stainable in clear localized areas after IgG1-anti HER2 antibody exposure (Figure 37 D). LAMP 1 and FcRn were more frequently co-localized tending to be in closer proximity to the basolateral membrane of the syncytium after IgG1-anti HER2 antibody perfusion (Figure 37 F).

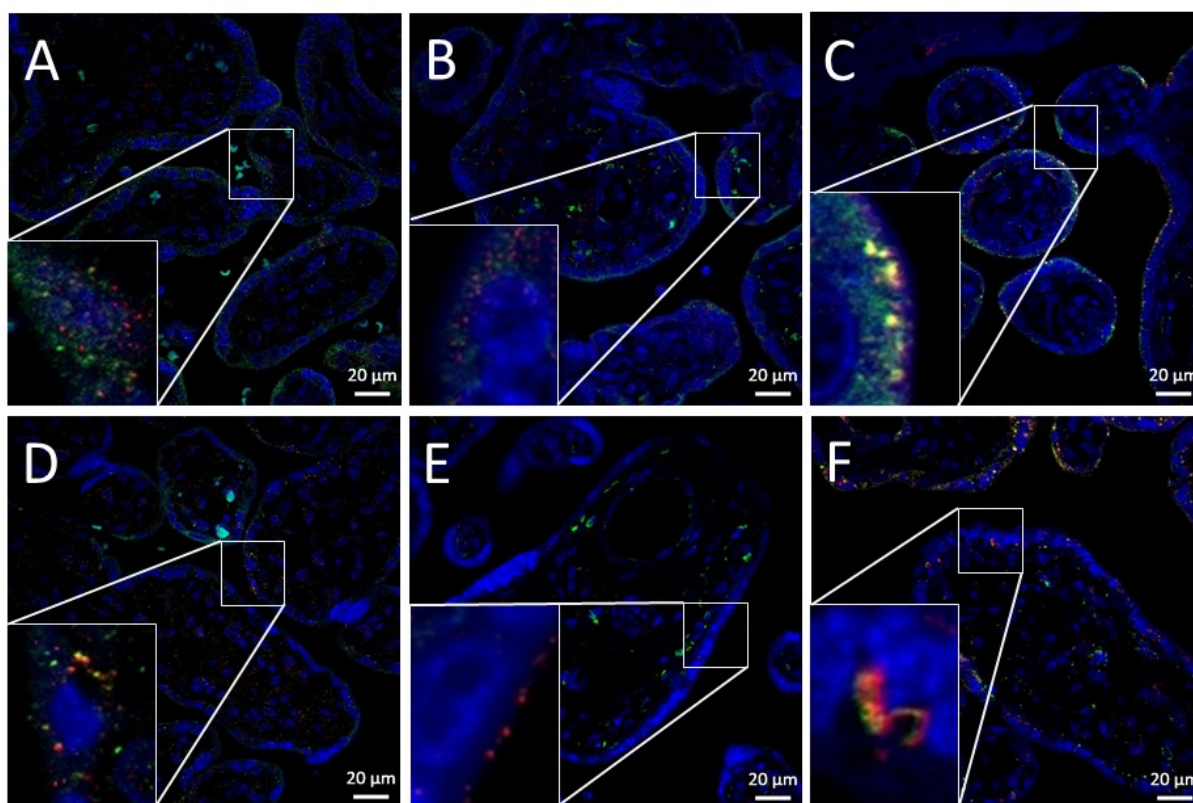


Figure 37. Perfusion with IgG1-anti HER2 antibody leads to a change in HER2, LAMP1 and FcRn localization in the syncytiotrophoblast. Representative pictures of double immunofluorescence staining of HER2, LAMP 1 and FcRn of unperfused Stainability of investigated proteins decreased in perfused tissue in all areas to a varying degree. The distribution of stained proteins was more uniform in unperfused tissue independent of observed placental area. A) HER2 (red) and LAMP 1 (green) are present homogeneous in the syncytium with sporadic co-localizations. B) HER2 (red) and FcRn (green) showed no co-

localization. FcRn showed a trend to be closer in proximity to the apical membrane of the syncytium. C) LAMP 1 (red) and FcRn (green) were frequently co-localized close to the apical membrane of the syncytium. D) HER2 (red) and LAMP 1 (green) occurred more condensed and more frequent co-localized after IgG1-anti HER2 antibody perfusion. E) After IgG1-anti HER2 antibody perfusion HER2 (red) showed a depleted staining. FcRn (green) was not stained in the syncytium but remained well presented in clear localized stromal areas. F) After IgG1-anti HER2 antibody perfusion LAMP 1 (red) and FcRn (green) showed decreased signals but increased in co-localization. The co-localized areas were in proximity to the basolateral membrane of the syncytium.

#### 4.2.5. Syn 1436 a peptide inhibitor for FcRn

##### Peptide based FcRn inhibitor Syn 1436 interferes with total IgG in ELISA approach

Cell culture experiments with hFcRn transfected HMEC1 cells showed an influence of the peptide inhibitor Syn 1436 on the applied total IgG ELISA assay (Figure 38). The experimental matrix is presented in table

Table 12. Sample matrix of the hFcRn HMEC1 experiments

	Negative control	IgG positive	IgG and Syn positive	Syn positive
IgG	-	X	X	-
Syn 1436	-	-	X	X

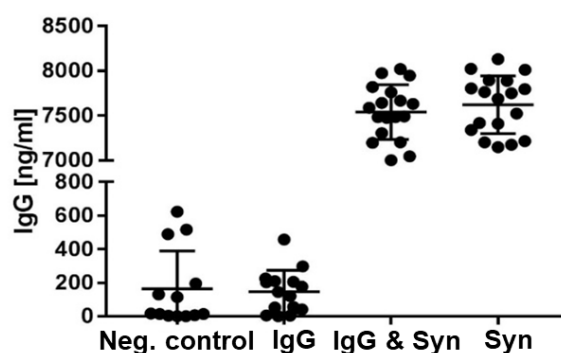


Figure 38. Syn 1436 interferes with total IgG ELISA assay. Quantification results from the HMEC1 cell culture supernatants of the IgG recycling assay after 4h experiments. Samples were analysed with total IgG ELISA. The assay showed Syn 1436 related interference, which made a valid readout impossible. Data is presented by plotting individual data points and mean  $\pm$ SD (N=3).

The purpose of the experiments was to determine IgG recycling capacity mediated by FcRn in the presence and absence of the inhibitor. In the IgG ELISA assay, precipitation was detectable after stopping the enzyme mediated quantification step with a low pH agent when the inhibitor was present. The formation of precipitates was independent of the presence of IgGs and occurred in all samples that contained Syn 1436, which was further reflected in the ELISA readout resulting in unreasonable high signals. Therefore, the assay could not be analysed properly.

The interference of Syn 1436 with a total IgG ELISA assay encouraged to repeat the experiment with targeted quantification approach with IgG1-anti HER2 antibody. The purpose of the experiments was to validate the inhibition potential of Syn 1436 on FcRn mediated IgG1-anti HER2 antibody recycling. The observed precipitation did not occur in the used IgG1-anti HER2 antibody ELISA assay. The inhibition of FcRn with Syn 1436 lead to a reduction in recycling of intracellular IgG1-anti HER2 antibody in a dose dependent manner after 4h of the recycling assay (Figure 39).

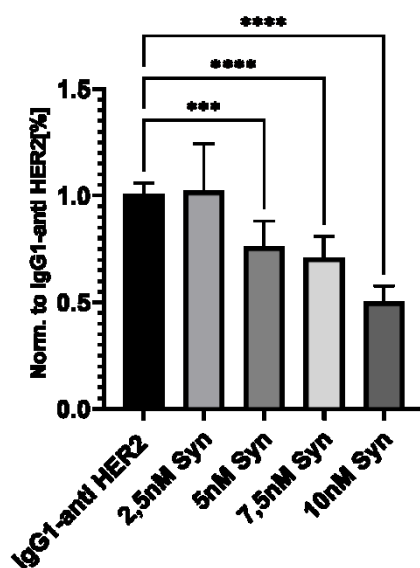


Figure 39. Syn 1436 inhibits IgG1-anti HER2 antibody recycling in a concentration dependent manner in hFcRn overexpressed HMEC1 cells. A significant reduction in IgG1-anti HER2 antibody recycling from HMEC1 cells could be observed in the presence of 5nM ( $p=0.0005$ ), 7.5 nM ( $p<0.0001$ ) and 10 nM ( $p<0.0001$ ) Syn 1436 inhibitor. Data is normalized to IgG1-anti HER2 antibody control concentration and is presented as mean  $\pm$  SD. Data was analysed with One-Way ANOVA and Tukey's multiple comparison. (N=3)

## 5. Discussion

Humans were constantly exposed to natural NPs as they arise by order of millions of metric tons per year (78). In recent decades, additional exposure to engineered NPs has increased. Such exposure may be desirable for pharmaceutical applications (213) or undesirable for environmental pollution or co-exposure from consumer products (44,84) during pregnancy. Regardless of the type and quantity of exposure, a limited amount of data is available about the action of NPs on the human placenta, especially under physiological conditions e.g., in the presence of human plasma or serum (90,91,214). In particular, interactions between plasma proteins and NPs can influence NP biological processing at tissue barriers (215). In the context of this dissertation, an attempt was made to improve the knowledge in this research area using the *ex-vivo* placenta perfusion model.

NP characterization concerning their physical properties is a mandatory requirement for further investigations of such materials. The chosen analytical approaches of dynamic light scattering, NP tracking analysis, transmission electron microscopy and determination of zeta potential are often used to characterize NP properties (216). However, each method applied had its limitations and therefore led to deviations within the results. Remarkable are the size differences between NTA and DLS of 80 nm PS NPs in different media. In more complex media, the polydispersity index (PDI) indicated heterogeneous NP sizes, which limited the interpretation quality of the DLS results. The PDI is a calculated term for the size homogeneity of NPs during DLS measurements. The ability of DLS to measure macromolecules, like proteins, might partially responsible for the detected heterogeneity of the NP samples in the complex perfusion media. The heterogeneity in NP size presents itself as a problem in DLS as the method has better sensitivity but less resolution than NTA, at least with the used instrument. Further, the generated statistical readout of the used instrument took larger NPs or agglomerates of NPs into account to a high degree. This led to an overestimated shift in NP size within the DLS measurements and a large standard deviation.

Nonetheless, the complementary NTA approach confirmed the heterogeneity of the samples. In the macromolecule containing media, more than one fraction was observable. Fractions increased in size with nearly double or triple of original NP size, which could be interpreted as potential NP-di- and trimers. Such di- and trimers were negligible in the NP stock solution diluted in water, indicating a tendency for aggregation of the particles in complex media.

In HSA medium, NTA indicated aggregates of some kind that were below the NP size. These factions may result from HSA protein aggregates or aggregates from the stabilizers in the used pharmaceutical HSA solution formed in the presence of 80 nm PS NPs. The formation of protein aggregates can be induced by NPs but can also be inhibited depending on protein and NP material (217). Furthermore, the average NP size increased in the perfusion medium indicating a formed biocorona around NPs in both DLS and NTA. The increased standard deviation in NTA NP size measurements in plasma and HSA medium can also be interpreted as a less uniform biocorona around PS NPs in these media. Hypothetically, biocoronas could differ drastically between individual particles. Additionally, the increased standard deviation could indicate potential protein aggregation. In contrast, the narrow standard deviation of the PS NP in the IgG medium may indicate an IgG protein monolayer forming with no protein aggregation tendency. Besides, biocoronas around NPs in the plasma medium could contain different plasma proteins on individual NP, resulting in broader size distribution.

Determination of PLGA NP size in complex media was not successful with DLS and NTA because it was not measurable due to a wide variety of changing signals (data not shown). The biodegradability of PLGA (184) could contribute to this analytical problem. Furthermore, the encapsulated dye within PLGA NPs leaked from the NPs in the electron microscope vacuum.

NTA readings showed a higher resolution for NPs in complex media for perfusion, as this approach analysed single NP. DLS measurements in polydisperse samples can be interpreted together with NTA data, but the resolution would be lacking if used alone. However, estimates of biocorona composition and the distinction between monolayers and multilayers of molecules in the biocorona cannot be specifically answered by used approaches.

The presented datasets for the zeta potential are not accurate in terms of absolute numbers for complex media. Information about the absolute permittivity of each used medium was not available. The absolute permittivity is necessary for the equation for the correct calculation of the zeta potential (218). Permittivity was correct and known for measurements of PS NPs in PBS and water without AP. The PS NPs, independent of size, had a negative zeta potential in PBS and water. The zeta potential increased in the protein-containing media, indicating a protein biocorona formation (219). The generated data in the other media can be considered approximations.

AP. affected the zeta potential of 500 nm PS NPs. In water, AP reduced the zeta potential of 500 nm PS NPs indicating interaction of the low molecular weight active ingredient with the PS NPs surface. Presence and absence of AP was the distinguishing factor for differences in the time-resolved concentration of 500 nm PS NPs during perfusion experiments again underpinning AP-NP interplay. The results from the 500 nm PS NP perfusion experiments with AP are in line with published data where AP was used during the experiment (56). A destructive effect of AP on PS NPs or fluorescence quenching effects in a relevant magnitude could be excluded after the validations experiments. Therefore, PS NP placental uptake changes, PS NP sedimentation, or deleterious AP effects on placental tissue are likely. Antipyrine-dependent PS NP aggregation and sedimentation in the reservoir cups of the medium were not investigated. Microscopic examination showed distinct localized fluorescent areas within the syncytium if 500 nm PS NPs were perfused after AP was applied. As the surface charge of the 500 nm PS NP changed, the particles with modified surface properties could have been taken up into the syncytium. The adsorption of pharmaceuticals on PS NPs was observed earlier (220) and showed that it affects pharmaceuticals cytotoxicity in a marine cell line setting (221). The AP molecule (222) and the PS molecule contain phenyl groups, resulting in potential  $\pi$ - $\pi$  stacking interactions of the drug and the PS NPs. Whether a modification of PS NPs or a change in the apical placental membrane was the driving force could not be clarified.

However, this finding should be confirmed by more specific approaches for potential uptake changes. Inductively coupled plasma mass spectrometry or energy-dispersive X-ray spectroscopy with slightly modified PS NPs would be potential candidates for the future detection of a change in NP uptake into the tissue. Human data for unintended interactions between drugs and nanomaterials connected with pregnancy are not available to the author's knowledge. Therefore, future studies on unintended NP drug interactions would be appropriate.

Nevertheless, the results underline the importance of cross-validating NP properties in the presence of experimental additives such as AP. Consequently, to avoid AP interactions, the experiments with 80 nm PS NPs, PLGA NPs and IgG were performed before the AP clearance experiment phase was appended in the respective perfusion. A different approach would be to wash out the AP from the placental tissue. Such an approach was not followed in these studies in order to avoid an artificial prolongation of the experimental time. An

experimental time extension would lead to more stress for the placental tissue, leading to an increased fail rate of experiments.

*Ex vivo* perfusion data with non-functionalized PLGA NPs confirmed *in vitro* results based on a BeWo cell line model (90). The time-resolved concentration data during perfusion indicated a high placental uptake of PLGA NPs in addition to immediate but limited transfer. This can be explained by the nearly identical PLGA NP concentrations observed in maternal and foetal veins after 15 minutes. The PLGA NPs placental perfusion results are consistent with reported results in a static vascular smooth muscle cell model for non-functionalized PLGA NPs (223). The NP uptake equilibrium occurred after 4h in the reported model and comparable with the determined 3h observed by perfusion experiments. Exocytosis of PLGA NPs that were taken up depended on the extracellular PLGA NP concentration. The exocytosis had a significant time delay in the reported concentration data, which was in contrast to the perfusion results where exocytosis was indicated faster after 4h. A reason for the deviation in exocytosis could be differences between the dynamic perfusion model and the reported static cell culture model. Differences between the placenta and other cells could as well influence the biodegradation of PLGA and the exocytosis of likely leaked Texas red dye. Additionally, the observed volume shift in perfusion medium from fetal to maternal side could contribute to the observed PLGA NP increase in the maternal circulation. The author would like to add that the biodegradability of PLGA led to several challenges, as demonstrated by the depletion of PLGA NPs within hours in perfusion samples.

Nevertheless, cautious use of approved and future PLGA-based nano drugs (85) during pregnancy is indicated to avoid unintended foetal exposure. Since PLGA is used in various hybrid NPs, e.g., PLGA-lipid NPs, investigations should be intensified with commercially available and near-market PLGA-containing NP drugs (85). A first proposed future approach would be to optimize the sample preparation and storage of PLGA NPs after tissue interaction to counteract biodegradation.

PS NPs cross the placenta depending on size and surface modifications (56,97). The control medium used in this study was in approximation to these published results, and led to similar findings in the transfer of unmodified 80 nm PS NPs. Within this study, an average foetal to maternal (F/M) ratio of 0.41 was observed with the control medium, which was nearly identical to the plotted average F/M ratio around 0.4-0.43 in literature (56,97) The absolute

concentrations in transported PS NPs showed deviations, which could result from differences in applied BSA concentrations. BSA concentration differed by 3 g/l between the published medium and the used medium in this study (56). Nevertheless, results with control medium highlighted the robustness of the perfusion model for PS NP transfer studies and the robustness of the underlying baseline NP transfer process.

The change from control medium to human plasma containing medium significantly increased the placental transfer of 80 nm PS NPs. The relevance of plasma proteins was proven in BeWo cells before (95) and could be confirmed in the perfusion model. A more detailed analysis of potentially in the transfer-involved proteins on 80 nm PS NPs was done by isolating and investigating the proteins via proteomics.

NP isolation protocol out of perfusion medium was validated for plausibility via western blot. The comparing experiment via western blot indicated that no relevant co-isolation of lipoproteins occurred with the used method. The lipoproteins were considered as biological reference nanoparticles. In particular, Apo proteins were in the 10 fold concentrated plasma barely detectable if PS NPs were missing. In the presence of 80 nm PS NPs, the recovery of these proteins was increased, indicating PS NP relevance and successful isolation and low relevance of unintentional isolated Apo proteins.

Proteomics analysis of NPs perfused with plasma medium revealed albumin as the most abundant protein in biocoronas of plasma PS NP samples and foetal PS NP samples after perfusion. This observation was not surprising as albumin is the protein with the highest plasma abundancy. Further, albumin was supplemented to the plasma medium as albumin was shown to be of relevance for molecular transport across the placenta (73,224). Further albumin was supplemented to enhance colloid osmotic pressure and to contain endothelial integrity (225). Of note, albumin showed the highest relative concentration difference between foetal and maternal isolated NP biocorona composition. That was surprising as the medium had the same starting composition in foetal and maternal circulation. A relevance of albumin for PS NP transport across the placenta could be hypothesized from published data from experiments with BeWo cells as in a native page a size band in the range of albumin was increased on transferred PS NP (95). Interestingly, a recent study showed similar albumin depending observations at an artificial blood-brain barrier system (106). In the study, increased albumin content was found on NPs after it crossed the barrier. Further, free albumin

and NP crosslinked with albumin showed a transport enhancing effect in a human intestinal epithelial model system (226). In addition, bovine albumin was shown to mediate PS NPs binding to cells. The increased binding depended on NPs surface charge, which influenced albumin protein folding (108). In contrast, literature reports that transport of radioiodine labelled album across the human placenta is very limited during the last month of gestation (227).

Next to albumin, IgG-1 heavy chain C region and the immunoglobulin lambda light chain 2 constant were promising candidates for responsible for the enhanced transfer of PS NPs. IgGs crosses the placenta and could therefore alter PS NPs properties to facilitate transfer. Other interesting significant enriched, but not further investigated protein candidates, in the foetal PS NP biocorona were apolipoproteins A1, E, and (a). Apolipoprotein E was shown to influence solid-lipid NP transport across cellular barriers (228). Because of these findings, the HSA and IgG medium for more detailed 80 nm PS NP perfusion experiments were formulated.

As a result of these specific media changes plasma and albumin containing medium increased the placental transfer. Next to enhanced transfer, a reduction in overall PS NP loss occurred during the experiments. The validation experiments to exclude effects of the stabilizers caprylic acid and N-acetyltryptophanate confirmed that the protein albumin is responsible for the transfer enhancing effects on 80 nm PS NPs. Medium containing solely IgGs did not have these effects on 80 nm PS NPs transfer and recovery. These observations indicate an active transfer mechanism that additionally increases placental transfer depending on HSA.

The neonatal Fc receptor could be relevant in the observed transfer of 80 nm PS NPs as it binds to albumin and IgG in a pH-dependent manner (226). This receptor is expressed in the human placental tissue and is held responsible for placental IgG transfer and recycling (229–231).

Nevertheless, the lack of a specific inhibitor for the albumin-binding site of FcRn led to the usage of Chloroquine during the study. Chloroquine was used to reduce IgG transfer across endothelial cells significant by interfering with endosome acidification (185), an essential aspect in FcRn mediated processes (39).

The perfusion experiments with chloroquine partially supported the involvement of FcRn in albumin mediated PS NP transport. The data was not significant but showed a trend in FcRn

transfected cells that overexpression leads to increased PS NP concentration in the foetal circulation over time. Nevertheless, in the presence of chloroquine, the PS NP concentration decreased insignificantly less in the maternal circulation, which could contribute to the observed trend in foetal circulation.

The generated BeWo cell culture data showed a clear relevance of albumin on PS NP recycling in the transwell system. The usage of chloroquine did not result in a significant decrease but showed a trend that reducing intracellular acidification could influence PS NP recycling. The results may be clearer with a specific FcRn-albumin binding inhibitor, which was not available during this thesis. Transfer of 80 nm PS NPs was not significantly linked to the albumin concentration in the less complex model, which does not contain a basement membrane, placental stroma or fetal endothelium. In addition, the introduction of chloroquine had no effect on PS NP transfer. Nevertheless, an FcRn linkable trend resulting in PS NP recycling and transfer between transfected and not transfected cells was observable in the presence of albumin. This observation counteracts the estimation that FcRn facilitates PS NP transfer, which was indicated by perfusion. Further, Chloroquine did not impact the PS NP transfer in the transwell model.

The contribution of FcRn on albumin mediated PS NP transfer remains unclear and would be a worthwhile topic for subsequent research by using specific inhibitors. However, the investigation of nanomaterial and size dependent effects on albumin unfolding and potential changes in FcRn albumin binding could contribute to the generation of NPs with the purpose of placental transfer for *in utero* drug delivery to the foetus.

Next to these observations, the media composition influenced the foetal vascular backpressure in the perfusion system. The HSA medium containing the pharmaceutical HSA solution, including stabilizers, reduced vascular backpressure significantly. An explanation could be the tryptophan derivate N-acetyltryptophanate, one of the stabilizers in HSA solution, which may affect placental vasculature via the indoleamine 2,3-dioxygenase-1 (IDO1) pathway, leading to a relaxation of the vasculature (232). The even more pronounced vascular relaxation effect in the plasma medium may result from the same IDO1 pathway stimulus with additional plasma-derived vasoactive factors.

Further, proteomics data demonstrated a tissue exposure depending change in the protein biocorona composition on PS NPs isolated from maternal circulation compared or plasma

medium. Such a change was expected as the biocorona composition was proven to be already dynamic in static systems without tissues or cells (104). In more complex models such as animal models, the change in biocorona composition is even more pronounced (233). The biocorona composition after tissue interaction was further dependent on whether the PS NPs passed the placenta or not. A similar transfer dependent change in the protein biocorona with a potential estimation of the transfer route was reported recently (234).

Next to the information gathered on PS NP, transfer enhancing biocorona proteins additional information was present in maternally isolated NP. Maternally isolated PS NP had the qualitative most diverse biocorona. In the dataset, the indication of bidirectional 80 nm PS NP transport can be found due to the presence of proteins from foetal circulation. Isolated PS NPs from the maternal circuit contained foetal haemoglobin  $\gamma$ -2 in the biocorona. The observation is analogous to a previous reported bidirectional PS NP transfer using the placental perfusion model (97). However, leakage of tissue within the perfusion experiments cannot be ruled out. Minor leakage of foetal medium to the maternal circulation could not be detected even using strong QC checkpoints.

Additionally, proteomics data from maternally isolated PS NP indicated that the change in the biocorona protein composition on maternally isolated PS NPs involves several different pathways. The probability pathway analysis with the three reported databases showed tremendous differences in the readout. This variation in outcome was astonishing as all three databases are frequently cited but did not result in a clear consensus. Probability analysis in DAVID showed a trend towards signal transduction and regulation, where the STRING results favoured vesicle-mediated transport processes and Reactome trended towards cellular stress responses to external stimuli. The String data indicated clear clusters of proteins with distinct functions like keratins and a prominent cluster of interacting proteins for vesicular transport with an influence of protein miss-folding response proteins. The primary readout in Reactome indicating a cellular reaction to an external stimulus seems legit as PS NP exposure is an external stimulus. The further indicated immune response, vesicular transport, protein metabolism and programmed cell death are tempting probability-based estimations.

Nevertheless, the deviations in these used scientific bioinformatic databases encouraged the author to utilise an alternative approach for data interpretation. In this approach, the biocorona composition is addressed like a photograph of a crime scene giving retrospective insight into

the PS NP's whereabouts (235). Such an approach was recently published for gold NPs at an intestinal cancer cell model (234). The enrichment of intracellular proteins in the biocorona of isolated maternal NPs after perfusion indicates uptake, internal cellular handling and exocytotic processes. Proposed processing with subsequent exocytosis but not transcytosis of 80 nm PS NPs at the placental barrier is shown in Figure 40. The potential pathways were manually linked to known pathways of the KEGG database. The suggested processing pathway map contains additional information on proteins involved in stress granule formation, the exocyst complex, ante- and retrograde vesicle transport from the Golgi apparatus and the protein folding TRIC complex.

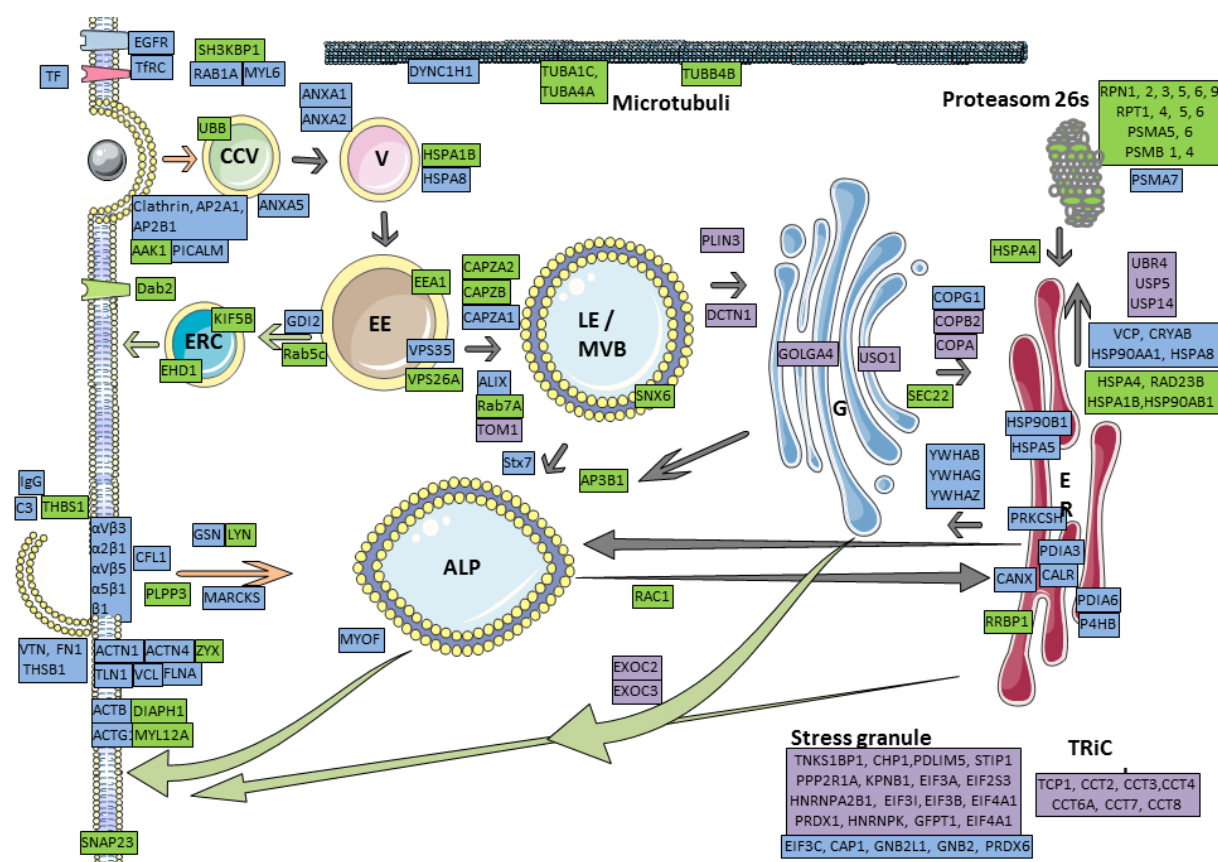


Figure 40. Postulated uptake, intracellular processing and exocytosis routes indicated by significant enriched proteins of the on isolated NPs of the maternal circuit. Processing pathway map of PS NP in the syncytiotrophoblast based on the KEGG pathways database, and additional primary literature sources (193–202). Green and blue gene names within the map are described in this function the KEGG pathways database. Purple gen names within the map are additional suggestions by the author base on literature (193–202).

Regarding detected proteins, clathrin-mediated endocytosis, IgG-mediated phagocytosis, and integrin-mediated phagocytosis could be possible routes of PS NPs uptake into the placenta. Subsequent processing in early endosomes could lead to the first separation in intracellular PS NP handling. On the one hand, endosomal recycling of PS NP was indicated by several proteins. These proteins were early endosome antigen 1 (EEA1), ras-related protein RAB-5C (RAB5C) (236), EH domain-containing protein 1 (EHD1) (237) and kinesin-1 heavy chain (KIF5B) (238). Their presence implied a fast secretion of some PS NPs.

On the other hand, endosomal maturation from early to late endosomes was indicated by target of myb protein 1 (TOM1) and ras-related protein RAB-7A (RAB7A) (238). In the late endosome, the subsequent separation into different pathways was potentially mediated by miss folded proteins. Depending on the degree of protein miss folding due to the protein NP interaction, the PS NPs either ended in lysosomes or the trans-Golgi network (239). In lysosomes, the track of the PS could not be further followed. Likely, PS NPs remained in the lysosomes for a prolonged time, indicated by the generated TEM pictures. Subsequently, the lysosomal content could also be secreted to some degree (240). Alternatively, PS NPs were processed by the trans-Golgi network via the retromer complex (239). That was indicated by three different routes for the PS NPs. The first route led back to lysosomes, where the track of the PS NPs was lost. The second route would shuttle the PS NPs back to the apical membrane via the exocyst pathway (195,196) and snap 23. The third route transported the PS NPs into the endoplasmic reticulum via the coatamer 1 complex (241). In the endoplasmic reticulum, the misfolded proteins were refolded, e.g. by the chaperonin-containing T-complex (TRiC) (242) and transferred back with their PS NPs to the Golgi via 14-3-3 proteins (202). Many contributing proteins in the protein biocorona can be attributed to the endoplasmic reticulum in the specific function in reacting to protein unfolding. That proteins can be unfolded at NP surfaces is not a new concept and was summarized before (243). If misfolded proteins were tagged for degradation, they would be processed via the proteasome 26s complex (244).

The further faith of a PS NPs engaged with the proteasome would depend on whether the proteasome could degrade the misfolded proteins. Nevertheless, if PS NPs would reach the proteasome, their track would be lost there.

Further, misfolded proteins could lead to stress granules formation, the protective response of specific RNA binding proteins. Stress granule formation was shown before in the presence of different NPs (245).

The proof of all these concepts would exceed the frame of the thesis by far. Therefore, future research will be needed to investigate each step of the processing cascade. The first step towards this direction would be the usage of intracellularly better traceable PS NPs. Further steps could include cell culture experiments with pathway knockouts to confirm the involvement of the suggested pathways.

### **IgG1-anti HER2 antibody**

Another aspect of this thesis was to investigate a potential IgG1-anti HER2 antibody transfer across the placenta. Within this study, HER2 was predominantly detected in human-term placenta's syncytiotrophoblast as reported before (246,247). Additionally, HER2 localization in the foetal endothelium was observed, similar to reported observations in the human protein atlas database (247). The binding of IgG1-anti HER2 antibody to placental HER2 was indirectly shown by the observed reduction in HER2 staining in placental tissue, which was exposed to IgG1-anti HER2 antibody during perfusion. That was expectable as the staining antibody and IgG1-anti HER2 antibody bind to the same region, the subunit IV of the HER2 receptor (248). The overlap in the antigen region led to a steric inhibition of the staining antibody as the IgG1-anti HER2 antibody obscured the epitope. The used IgG1-anti HER2 antibody was a humanized IgG kappa 1, which should be transferred across the placenta via the FcRn receptor (249). By using ELISA, no pharmaceutical active IgG1-anti HER2 antibody was observable in the foetal circulation.

Therefore, control experiments with polyclonal human IgGs were performed. These experiments demonstrated a transfer of IgGs in the used perfusion setting, which correlates with reports of others (63,250). Nevertheless, the detected concentration of transferred IgGs reached in this study 31% of the reported value of Mathiesen et al. (63) and 15% of the value reported by Malek et al. (250). These deviations may result from a difference in the media composition, the analytical approaches, placental tissue handling before perfusion and the perfusion setup itself. Nevertheless, all studies showed placental transfer of IgGs.

In the study, the mean observed IgG transfer across the placenta was 4.4 mg, which were around 0.15% of offered IgG during perfusion. A similar uptake process between

physiological IgG and therapeutic IgG1-anti HER2 antibody was estimated. The estimate based on the loss of 3 mg of IgG1-anti HER2 antibody in the maternal circulation during perfusion. As the IgG1-anti HER2 antibody was not detected in foetal circulation it was estimated that the IgG bound to HER2 in the placenta. The concentration of HER2 was shown to be around 100 fmol of receptor per mg of isolated total protein from the placenta (171). Therefore, the loss of 3 mg of therapeutic IgG cannot be explained by binding to its epitope in the placenta, as a loss in the  $\mu\text{g}$  range would be feasible but not in the mg range.

The approach of tracking the IgG1-anti HER2 antibody in placental tissue was not possible in the chosen setting. Alternatively, HER2 was tracked in the placental tissue after the perfusion experiments using an antibody that is directed to a different subdomain of the HER2 receptor as it was performed with Pertuzumab by Ram et al. (251). The observed distribution of FcRn and LAMP 1 in unperfused tissue in the syncytiotrophoblast is close to published colocalization data of IgGs and FcRn in the placenta (252). The observed localization of FcRn can be placed between the FcRn expression findings of Latvala et al. (253) in the second-trimester placenta and Simister et al. (254) in term placenta. Technological differences between immunohistochemistry and immunofluorescence performed with a confocal laser scanning microscope may explain these localization deviations between this study and the literature.

Further, the colocalization experiments showed the proximity of HER2, FcRn and LAMP1 in the placenta after 6h perfusion experiments with IgG1-anti HER2 antibody. This proximity may be seen as the formation of a HER2- IgG1-anti HER2 antibody -FcRn complex in the placental tissue. These findings indicate a sorting of the potential complex into lysosomes for degradation (Figure 41). The degradation of FcRn in the tissue would subsequently explain the gathered perfusion results in two ways. First, the IgG1-anti HER2 antibody, taken up by the placenta, could not be recycled efficiently into the maternal circulation. The blocking and degradation of FcRn would explain that loss of IgG1-anti HER2 antibody during the experiments without being detected in the foetal circulation. Second, FcRn degradation would lead to a reduced transfer of IgG1-anti HER2 antibody across the syncytiotrophoblast and maybe other tissue compartments (57). A subsequent limited IgG1-anti HER2 antibody transfer across the tissue would explain the ELISA results that were not able to detect antibody in the foetal circulation. If the antibody enters the foetal placental vasculature, it would likely bind to HER2 expressed by the foetal endothelium. Therefore, the IgG1-anti

HER2 antibody concentrations is be below the detection limit of the used ELISA assays as foetal endothelium showed unsaturated HER2 after perfusion.

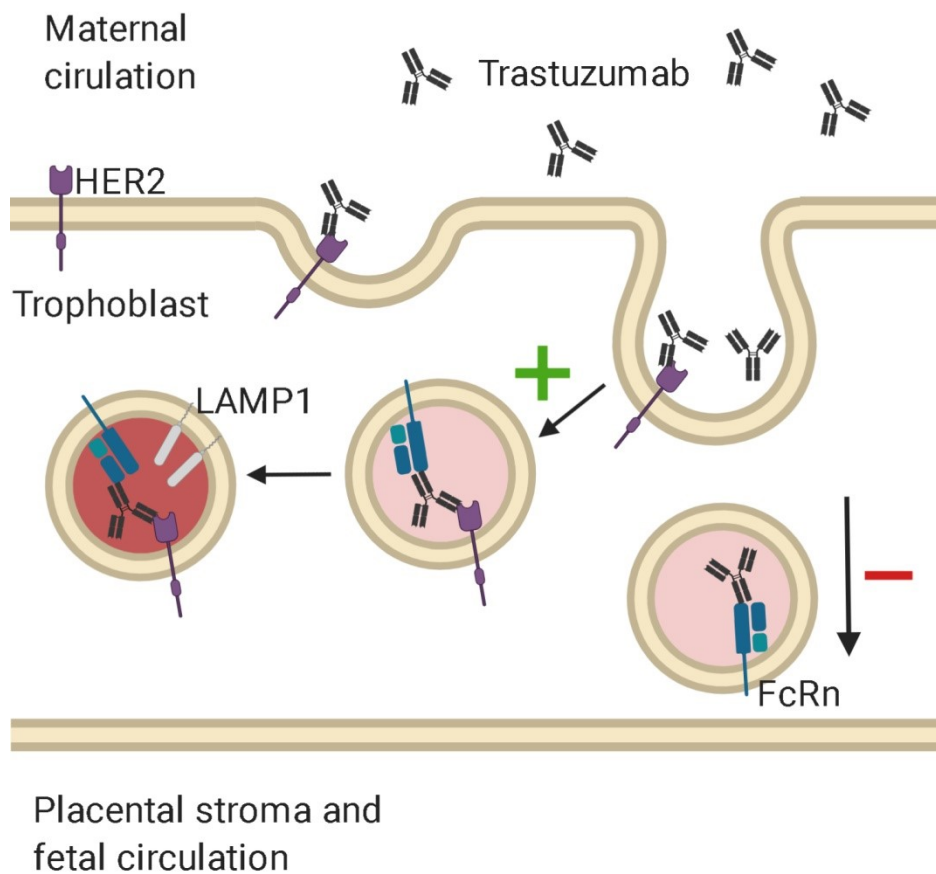


Figure 41. Proposed interplay of IgG1-anti HER2 antibody, HER2 receptor and FcRn in the human placenta. The IgG1-anti HER2 antibody binds to placental HER2 but is still taken up through macropinocytosis or other uptake mechanisms as an antibody-HER2 complex into the syncytiotrophoblast. There, binding to FcRn would occur in early endosomes. Even if this antibody-HER2-FcRn complex would be shuttled to the apical side of the syncytium, the IgG could not be released from the HER2 receptor as this binding is not pH sensitive and HER2 would stay linked in the membrane. The data suggested a degradation of the antibody-HER2-FcRn complex in lysosomes, indicated by the green plus. Such FcRn degradation would decrease the transfer rate of IgG across the placenta, indicated by the red minus. Created with BioRender.com.

The observations during this thesis indicate a participation of the placenta on the reported adverse events on human foetuses after IgG1-anti HER2 antibody administration during pregnancy. The saturation of HER2 by IgG1-anti HER2 antibody was proven in the study. That indicates a potential link between HER2 and foetal water homeostasis. A recent study showed a link between a HER2 targeted therapy combined with radiotherapy in HER2+ breast cancer patients with the upregulation of aquaporin 4 (255). The dysregulation of aquaporin in the placenta could explain the clinical presentation of oligo- or anhydramnios after IgG1-anti HER2 antibody exposure during pregnancy. Especially, aquaporin 4 is worthwhile for further investigations as it was down-regulated in the syncytium of healthy term placentas compared to first trimester placentas (256).

A valid question is if a prolongation of the experimental time would lead to different results. Extension of experimental placental perfusion time lacks literature data, and further validation would be needed. It is also likely that the tissue will act less physiologically during the prolonged experimental time. This estimation is based on experiences made during this study. Several experiments had to be terminated because the placenta showed a decrease in viability markers. The observations included media volume loss or elevated vascular backpressure, which led to exclude these not valid experiments. Overall, these observations indicated increasing tissue damage with an extension of perfusion time during IgG1-anti HER2 antibody perfusions.

Nonetheless, the study design and placental perfusion cannot rule out a potential delayed transfer of IgG1-anti HER2 antibody in the range of days or weeks. Such a delayed direct transfer could impact the foetus directly in a negative way.

### **IgG2-anti-RANKL antibody**

For IgG2-anti-RANKL antibody transfer, the detected specific peptide sequence confirmed its passage across the placenta. The concentration of 0.1 µg/ml of IgG2-anti-RANKL antibody was below the limit of detection in the foetal circulation. The deviations in foetal/maternal ratio between the 27 µg/ml and 6 µg/ml experiments with the antibody result from the unknown uptake of that specific IgG 2 into the placenta. In the case of a directed and limited transfer like for IgGs, the maternal offered concentration would drastically affect the calculated F/M ratio. Nevertheless, the observed F/M ratios within the experiments are in line with reported placental IgG2 transfer (142,250) regarding their magnitude order. Additionally,

increased relative IgG transfer was reported at low IgG concentrations (142), impacting the F/M ratio further.

The presence of RANKL in the term placenta was proven by this study. A faint expression of RANKL in the syncytium was shown before in the first-trimester placenta (257) The localization of RANKL was comparable with findings in term placenta by this study. Additionally, a distinct localization of RANKL in the term placental stroma was observed which has not been described yet. The pattern of RANKL staining indicated a single or few cell expression site of the protein in the placenta. These RANKL expression sites were CD163 negative, indicating to exclude Hofbauer cells as source of expression (212).

Nevertheless, the small number of expression sites within the tissue may play a minor role for mother and foetus. Still, placental derived RANKL may play a critical role in the maternal placental microenvironment's immunological regulation to sustain the pregnancy (257,258). Or, RANKL may have a local regulating function in placental angiogenesis (259,260).

The observed expression and secretion of RANKL combined with the presence of IgG2-anti-RANKL antibody may lead to the formation of immune complexes. An indication, therefore, is the insufficient binding of RANKL by the antibody in the foetal circulation. The placental passage of the antibody was proven via the detected specific peptide. Nevertheless, the therapeutically function of the antibody could not be confirmed after the antibody crossed the placenta. Therefore, the formation of IgG2-anti-RANKL antibody and RANKL immune complexes was indicated. Such complexes could be sorted into degradation pathways. Consequently, the degradation of the IgG2-anti-RANKL antibody during the experiment could contribute to the F/M ratio deviation between the different experimental setups.

Nevertheless, the transfer of immune complexes across the placenta was reported before (8,59). Therefore, the detection of the antibody specific peptide in the foetal circulation was not contradicted.

In future studies, a selective quantitative approach of analytics could help gain insight into immunocomplex degradation and transport across the placenta in a quantitative manner. However, animal models demonstrated an effect on offspring if the same IgG2-anti-RANKL antibody in this study or other anti-RANKL antibodies were applied during gestation (161–163). In the study of Bussiere et al., pharmacologically active IgG2-anti-RANKL antibody was detected in cynomolgus monkey foetuses when the mothers were treated with similar

concentrations as they were used in the 27 µg/ml experiments (163). Therefore, it can be assumed that a transfer of pharmacologically active IgG2-anti-RANKL antibody across the human placenta may occur *in vivo* as well.

## 6. Conclusion

The data gathered during this thesis showed the potential of PLGA NP to cross placental tissue. Future work should address the PLGA NP directly by adding targeting molecules to aim for placental tissue in a more complex model directly.

Further, an influence of the small molecule drug antipyrine and plasma proteins on the interaction of PS NP with the placenta could be shown. Albumin was the identified plasma protein that increased the placental transfer of 80 nm PS NP. A biological processing suggestion of PS NP at the syncytium was phrased, involving several pathways. Cross-validation of the antipyrine results with other NP materials, predominantly lipophilic ones, is indicated to clarify a potential pattern of the observation. In general, the field of unintended drug and chemical uptake and NP will likely be a future research field as NP pollution increases. This may be more relevant for other organ systems than the placenta, like the gastrointestinal tract.

Regarding the biocorona findings, a plethora of subsequent experiments is recommended to investigate the indicated pathways. The first steps could be cellular knockouts and specific inhibitors for the different pathway branches. Perfusion of PS NP with an Apo E enriched medium should be performed with subsequent proteomics to verify if PS NP transfer could be enhanced with other proteins. Further, other NP materials in a size of 70-100 nm should be perfused with the plasma medium. The size is essential as extracellular vesicles have similar sizes, which could be a reason for the observations, as a cellular crossing of extracellular vesicles across barriers could be similar.

The investigations of therapeutic IgG1-anti HER2 revealed an interaction of the antibody with placental expressed HER2. Further, during the experiments, the IgG1 could not cross the placenta. The next indicated steps will be to investigate a crosslink of HER2 in the placenta and water transport, e.g. by the expression of aquaporin's if HER2 is blocked or knocked out. This suggestion is based on the clinical presentation of poly and anhydramnios in fetuses exposed to Trastuzumab in utero. The lack of amniotic fluid could be based on adverse events on the foetal kidney but also an impaired placental water transport.

In contrast to the IgG1, the investigated IgG2-anti-RANKL was detectable after perfusion in foetal circulation on peptide level. If the IgG2 was functional after placental passage could not be clarified as the placenta released RANKL into the foetal circulation. Future work should

address the expression site, as the secretion of RANKL by term placenta is a novel observation. A highly specialised and alternative differentiated kind of Hofbauer cell is indicated as an expression site since specific macrophages express RANKL in other tissues. Additionally, the biological function of RANKL in the term placenta and the organs surrounding it is worthwhile investigating.

## 7. References

1. Gruber MM, Hirschmugl B, Berger N, Holter M, Radulović S, Leitinger G, et al. Plasma proteins facilitates placental transfer of polystyrene particles. *J Nanobiotechnology*. 2020 Dec 9;18(1):128.
2. Burton GJ, Fowden AL. The placenta: a multifaceted, transient organ. *Philos Trans R Soc B Biol Sci*. 2015;370(1663):20140066–20140066.
3. Benirschke K, Burton GJ, Baergen RN. *Pathology of the Human Placenta*. Berlin, Heidelberg: Springer Berlin Heidelberg; 2012. XVIII, 941.
4. Brownbill P, Mahendran D, Owen D, Swanson P, Thornburg KL, Nelson DM, et al. Denudations as paracellular routes for alpha-fetoprotein and creatinine across the human syncytiotrophoblast. *Am J Physiol Regul Integr Comp Physiol*. 2000 Mar;278(3):R677-83.
5. Kertschanska S, Kosanke G, Kaufmann P. Pressure dependence of so-called transtrophoblastic channels during fetal perfusion of human placental villi. *Microsc Res Tech*. 1997;38(1–2):52–62.
6. Huppertz B. The anatomy of the normal placenta. *J Clin Pathol*. 2008;61(12):1296–302.
7. Heinrich D, Metz J, Raviola E, Forssmann WG. Ultrastructure of perfusion-fixed fetal capillaries in the human placenta. *Cell Tissue Res*. 1976 Sep 14;172(2):157–69.
8. Malek A, Sager R, Lang AB, Schneider H. Protein Transport Across the In Vitro Perfused Human Placenta. *Am J Reprod Immunol*. 1997 Oct;38(4):263–71.
9. Muoth C, Aengenheister L, Kucki M, Wick P, Buerki-Thurnherr T. Nanoparticle transport across the placental barrier: pushing the field forward! *Nanomedicine*. 2016 Apr;11(8):941–57.
10. Valero L, Alhareth K, Gil S, Simasotchi C, Roques C, Scherman D, et al. Assessment of dually labelled PEGylated liposomes transplacental passage and placental penetration using a combination of two ex-vivo human models: the dually perfused placenta and the suspended villous explants. *Int J Pharm*. 2017 Nov 5;532(2):729–37.

11. Harris LK. Could peptide-decorated nanoparticles provide an improved approach for treating pregnancy complications? *Nanomedicine*. 2016;11:2235–8.
12. Pant S, London MB, Blumenfeld M, Farrar W, Shapiro CL. Treatment of Breast Cancer With Trastuzumab During Pregnancy. *J Clin Oncol*. 2008;26(9):1566–7.
13. Hoelting L, Scheinhardt B, Bondarenko O, Schildknecht S, Kapitza M, Tanavde V, et al. A 3-dimensional human embryonic stem cell (hESC)-derived model to detect developmental neurotoxicity of nanoparticles. *Arch Toxicol*. 2013;87(4):721–33.
14. Mozafari M, Khoradmehr A, Danafar A, Miresmaeili M, Kalantar SM. Toxic effects of maternal exposure to silver nanoparticles on mice fetal development during pregnancy. *Birth Defects Res*. 2020 Jan 16;112(1):81–92.
15. Wang Z, Zhang C, Huang F, Liu X, Wang Z, Yan B. Breakthrough of ZrO<sub>2</sub> nanoparticles into fetal brains depends on developmental stage of maternal placental barrier and fetal blood-brain-barrier. *J Hazard Mater*. 2021 Jan;402(April 2020):123563.
16. Luo J, Hao S, Zhao L, Shi F, Ye G, He C, et al. Oral exposure of pregnant rats to copper nanoparticles caused nutritional imbalance and liver dysfunction in fetus. *Ecotoxicol Environ Saf*. 2020 Dec;206(August):111206.
17. Huang J-P, Hsieh PCH, Chen C-Y, Wang T-Y, Chen P-C, Liu C-C, et al. Nanoparticles can cross mouse placenta and induce trophoblast apoptosis. *Placenta*. 2015 Dec;36(12):1433–41.
18. Wu Y, Chen L, Chen F, Zou H, Wang Z. A key moment for TiO<sub>2</sub>: Prenatal exposure to TiO<sub>2</sub> nanoparticles may inhibit the development of offspring. *Ecotoxicol Environ Saf*. 2020 Oct;202(March):110911.
19. Guillard A, Gaultier E, Cartier C, Devoille L, Noireaux J, Chevalier L, et al. Basal Ti level in the human placenta and meconium and evidence of a materno-foetal transfer of food-grade TiO<sub>2</sub> nanoparticles in an ex vivo placental perfusion model. *Part Fibre Toxicol*. 2020 Dec 7;17(1):51.
20. Pegoraro V, Urbinati D, Visser GHA, Di Renzo GC, Zipursky A, Stotler BA, et al. Hemolytic disease of the fetus and newborn due to Rh(D) incompatibility: A preventable disease that still produces significant morbidity and mortality in children. Oei JL, editor. *PLoS One*. 2020 Jul 20;15(7):e0235807.

21. Yameen B, Choi W Il, Vilos C, Swami A, Shi J, Farokhzad OC. Insight into nanoparticle cellular uptake and intracellular targeting. *J Control Release*. 2014 Sep;190(5):485–99.
22. Champion JA, Mitragotri S. Role of target geometry in phagocytosis. *Proc Natl Acad Sci*. 2006 Mar 28;103(13):4930–4.
23. Banerjee A, Berezhkovskii A, Nossal R. Kinetics of cellular uptake of viruses and nanoparticles via clathrin-mediated endocytosis. *Phys Biol*. 2016 Feb 12;13(1):016005.
24. Garaiova Z, Strand SP, Reitan NK, Lélou S, Størset SØ, Berg K, et al. Cellular uptake of DNA–chitosan nanoparticles: The role of clathrin- and caveolae-mediated pathways. *Int J Biol Macromol*. 2012 Dec;51(5):1043–51.
25. Wang Z, Tiruppathi C, Minshall RD, Malik AB. Size and Dynamics of Caveolae Studied Using Nanoparticles in Living Endothelial Cells. *ACS Nano*. 2009 Dec 22;3(12):4110–6.
26. Jin J, Shen Y, Zhang B, Deng R, Huang D, Lu T, et al. In situ exploration of characteristics of macropinocytosis and size range of internalized substances in cells by 3D-structured illumination microscopy. *Int J Nanomedicine*. 2018 Sep;Volume 13:5321–33.
27. Kato T, Jin CS, Ujiie H, Lee D, Fujino K, Wada H, et al. Nanoparticle targeted folate receptor 1-enhanced photodynamic therapy for lung cancer. *Lung Cancer*. 2017 Nov;113(September):59–68.
28. Soe ZC, Kwon JB, Thapa RK, Ou W, Nguyen HT, Gautam M, et al. Transferrin-Conjugated Polymeric Nanoparticle for Receptor-Mediated Delivery of Doxorubicin in Doxorubicin-Resistant Breast Cancer Cells. *Pharmaceutics*. 2019 Feb 1;11(2):63.
29. Tsai W-H, Yu K-H, Huang Y-C, Lee C-I. EGFR-targeted photodynamic therapy by curcumin-encapsulated chitosan/TPP nanoparticles. *Int J Nanomedicine*. 2018 Feb;Volume 13:903–16.
30. Luo D, Wang X, Zeng S, Ramamurthy G, Burda C, Basilion JP. Prostate-specific membrane antigen targeted gold nanoparticles for prostate cancer radiotherapy: does size matter for targeted particles? *Chem Sci*. 2019;10(35):8119–28.
31. Wang Z, Duan X, Lv Y, Zhao Y. Low density lipoprotein receptor (LDLR)-targeted lipid nanoparticles for the delivery of sorafenib and Dihydroartemisinin in liver

- cancers. *Life Sci.* 2019 Dec;239(October):117013.
32. Martins JP, D'Auria R, Liu D, Fontana F, Ferreira MPA, Correia A, et al. Engineered Multifunctional Albumin-Decorated Porous Silicon Nanoparticles for FcRn Translocation of Insulin. *Small.* 2018 Jul;14(27):e1800462.
  33. King A, Ndifon C, Lui S, Widdows K, Kotamraju VR, Agemy L, et al. Tumor-homing peptides as tools for targeted delivery of payloads to the placenta. *Sci Adv.* 2016 May 6;2(5):1–16.
  34. Reinholz J, Diesler C, Schöttler S, Kokkinopoulou M, Ritz S, Landfester K, et al. Protein machineries defining pathways of nanocarrier exocytosis and transcytosis. *Acta Biomater.* 2018 Apr;71:432–43.
  35. Cao Y, Long J, Liu L, He T, Jiang L, Zhao C, et al. A review of endoplasmic reticulum (ER) stress and nanoparticle (NP) exposure. *Life Sci.* 2017 Oct;186(July):33–42.
  36. Zhang L, Xu Y, Cao W, Xie S, Wen L, Chen G. Understanding the translocation mechanism of PLGA nanoparticles across round window membrane into the inner ear: a guideline for inner ear drug delivery based on nanomedicine. *Int J Nanomedicine.* 2018 Jan;Volume 13:479–92.
  37. Liu C-G, Han Y-H, Kankala RK, Wang S-B, Chen A-Z. Subcellular Performance of Nanoparticles in Cancer Therapy. *Int J Nanomedicine.* 2020 Feb;Volume 15:675–704.
  38. Zhang J, Zhang X, Liu G, Chang D, Liang X, Zhu X, et al. Intracellular Trafficking Network of Protein Nanocapsules: Endocytosis, Exocytosis and Autophagy. *Theranostics.* 2016;6(12):2099–113.
  39. Pyzik M, Sand KMK, Hubbard JJ, Andersen JT, Sandlie I, Blumberg RS. The neonatal Fc Receptor (FcRn): A misnomer? *Front Immunol.* 2019;10(JULY).
  40. Hutson JR, Garcia-Bournissen F, Davis A, Koren G. The human placental perfusion model: a systematic review and development of a model to predict in vivo transfer of therapeutic drugs. *Clin Pharmacol Ther.* 2011 Jul;90(1):67–76.
  41. Wick P, Malek A, Manser P, Meili D, Maeder-Althaus X, Diener L, et al. Barrier capacity of human placenta for nanosized materials. *Environ Health Perspect.* 2010 Mar;118(3):432–6.
  42. Ala-Kokko TI, Myllynen P, Vähäkangas K. Ex vivo perfusion of the human placental

- cotyledon: implications for anesthetic pharmacology. *Int J Obstet Anesth.* 2000 Jan;9(1):26–38.
43. Pentšuk N, Van Der Laan JW, Pentšuk N, Van Der Laan JW. An interspecies comparison of placental antibody transfer: New insights into developmental toxicity testing of monoclonal antibodies. *Birth Defects Res Part B - Dev Reprod Toxicol.* 2009;86(4):1–17.
  44. Aengenheister L, Dugershaw BB, Manser P, Wichser A, Schoenenberger R, Wick P, et al. Investigating the accumulation and translocation of titanium dioxide nanoparticles with different surface modifications in static and dynamic human placental transfer models. *Eur J Pharm Biopharm.* 2019 Sep;142:488–97.
  45. Panigel M. Placental perfusion experiments. *Am J Obstet Gynecol.* 1962 Dec;84(11):1664–83.
  46. Schneider H, Panigel M, Dancis J. Transfer across the perfused human placenta of antipyrine, sodium and leucine. *Am J Obstet Gynecol.* 1972;114(6):822–8.
  47. Urbaniak SJ, Duncan JI, Armstrong-Fisher SS, Abramovich DR, Page KR. Transfer of anti-D antibodies across the isolated perfused human placental lobule and inhibition by high-dose intravenous immunoglobulin: a possible mechanism of action. *Br J Haematol.* 1997 Jan 29;96(1):186–93.
  48. Buerki-Thurnherr T, von Mandach U, Wick P. Knocking at the door of the unborn child: engineered nanoparticles at the human placental barrier. *Swiss Med Wkly.* 2012 Jan;142(April):w13559.
  49. Mathiesen L, Mose T, Mørck TJ, Nielsen JKS, Nielsen LK, Maroun LL, et al. Quality assessment of a placental perfusion protocol. *Reprod Toxicol.* 2010 Aug;30(1):138–46.
  50. Nye GA, Ingram E, Johnstone ED, Jensen OE, Schneider H, Lewis RM, et al. Human placental oxygenation in late gestation: experimental and theoretical approaches. *J Physiol.* 2018 Dec;596(23):5523–34.
  51. Poulsen MS, Mose T, Maroun LL, Mathiesen L, Knudsen LE, Rytting E. Kinetics of silica nanoparticles in the human placenta. *Nanotoxicology.* 2015 May 25;9(sup1):79–86.
  52. Ghaghada KB, Starosolski ZA, Bhayana S, Stupin I, Patel C V., Bhavane RC, et al. Pre-clinical evaluation of a nanoparticle-based blood-pool contrast agent for MR

- imaging of the placenta. *Placenta*. 2017 Sep;57:60–70.
53. Bajoria R, Contractor SF. Effect of surface charge of small unilamellar liposomes on uptake and transfer of carboxyfluorescein across the perfused human term placenta. *Pediatr Res*. 1997 Oct;42(4):520–7.
  54. Myllynen PK, Loughran MJ, Howard CV, Sormunen R, Walsh AA, Vähäkangas KH. Kinetics of gold nanoparticles in the human placenta. *Reprod Toxicol*. 2008 Oct;26(2):130–7.
  55. Vidmar J, Loeschner K, Correia M, Larsen EH, Manser P, Wichser A, et al. Translocation of silver nanoparticles in the ex vivo human placenta perfusion model characterized by single particle ICP-MS. *Nanoscale*. 2018;10(25):11980–91.
  56. Wick P, Malek A, Manser P, Meili D, Maeder-Althaus X, Diener L, et al. Barrier capacity of human placenta for nanosized materials. *Environ Health Perspect*. 2010 Mar;118(3):432–6.
  57. Roy S, Nanovskaya T, Patrikeeva S, Cochran E, Parge V, Guess J, et al. M281, an anti-FcRn antibody, inhibits IgG transfer in a human ex vivo placental perfusion model. *Am J Obstet Gynecol*. 2019 May;220(5):498.e1–498.e9.
  58. Stapleton NM, Brinkhaus M, Armour KL, Bentlage AEH, de Taeye SW, Temming AR, et al. Reduced FcRn-mediated transcytosis of IgG2 due to a missing Glycine in its lower hinge. *Sci Rep*. 2019 Dec 14;9(1):7363.
  59. May K, Grube M, Malhotra I, Long CA, Singh S, Mandaliya K, et al. Antibody-dependent transplacental transfer of malaria blood-stage antigen using a human ex vivo placental perfusion model. *PLoS One*. 2009;4(11).
  60. Vaccaro C, Bawdon R, Wanjie S, Ober RJ, Ward ES. Divergent activities of an engineered antibody in murine and human systems have implications for therapeutic antibodies. *Proc Natl Acad Sci*. 2006 Dec 5;103(49):18709–14.
  61. Lubega J. A kinetic study of human IgG binding to placental Fcγ-receptor. *Mol Immunol*. 1990 Jan;27(1):45–55.
  62. Porter C, Armstrong-Fisher S, Kopotsha T, Smith B, Baker T, Kevorkian L, et al. Certolizumab pegol does not bind the neonatal Fc receptor (FcRn): Consequences for FcRn-mediated in vitro transcytosis and ex vivo human placental transfer. *J Reprod Immunol*. 2016;116:7–12.

63. Mathiesen L, Nielsen LK, Andersen JT, Grevys A, Sandlie I, Michaelsen TE, et al. Maternofetal transplacental transport of recombinant IgG antibodies lacking effector functions. *Blood*. 2013 Aug 15;122(7):1174–81.
64. Leach L, Eaton BM, Firth JA, Contractor SF. Uptake and intracellular routing of peroxidase-conjugated immunoglobulin-G by the perfused human placenta. Vol. 261, *Cell and Tissue Research*. 1990. p. 383–8.
65. Stapleton NM, Armstrong-Fisher SS, Andersen JT, van der Schoot CE, Porter C, Page KR, et al. Human IgG lacking effector functions demonstrate lower FcRn-binding and reduced transplacental transport. *Mol Immunol*. 2018 Mar;95(January):1–9.
66. Morgan CL, Cannell GR, Addison RS, Minchinton RM. The effect of intravenous immunoglobulin on placental transfer of a platelet-specific antibody: anti-P1A1. *Transfus Med*. 1991 Dec;1(4):209–16.
67. Nekhayeva IA, Nanovskaya TN, Pentel PR, Keyler DE, Hankins GD V, Ahmed MS. Effects of nicotine-specific antibodies, Nic311 and Nic-IgG, on the transfer of nicotine across the human placenta. *Biochem Pharmacol*. 2005;70(11):1664–72.
68. Conings S, Amant F, Annaert P, Van Calsteren K. Integration and validation of the ex vivo human placenta perfusion model. *J Pharmacol Toxicol Methods*. 2017 Nov;88(Pt 1):25–31.
69. Gomez-Garcia MJ, Doiron AL, Steele RRM, Labouta HI, Vafadar B, Shepherd RD, et al. Nanoparticle localization in blood vessels: dependence on fluid shear stress, flow disturbances, and flow-induced changes in endothelial physiology. *Nanoscale*. 2018;10(32):15249–61.
70. Falanga AP, Pitingolo G, Celentano M, Cosentino A, Melone P, Vecchione R, et al. Shuttle-mediated nanoparticle transport across an in vitro brain endothelium under flow conditions. *Biotechnol Bioeng*. 2017;114(5):1087–95.
71. Perazzolo S, Lewis RM, Sengers BG. Modelling the effect of intervillous flow on solute transfer based on 3D imaging of the human placental microstructure. *Placenta*. 2017;60:21–7.
72. Perazzolo S, Hirschmugl B, Wadsack C, Desoye G, Lewis RM, Sengers BG. The influence of placental metabolism on fatty acid transfer to the fetus. *J Lipid Res*. 2017 Feb 2;58(2):443–54.

73. Mathiesen L, Rytting E, Mose T, Knudsen LE. Transport of benzo[alpha]pyrene in the dually perfused human placenta perfusion model: effect of albumin in the perfusion medium. *Basic Clin Pharmacol Toxicol*. 2009 Sep;105(3):181–7.
74. Nanovskaya T, Patrikeeva S, Zhan Y, Fokina V, Hankins GDV, Ahmed MS. Transplacental transfer of vancomycin and telavancin. *Am J Obstet Gynecol*. 2012 Oct;207(4):331.e1-331.e6.
75. Schalkwijk S, Greupink R, Colbers AP, Wouterse AC, Verweij VGM, van Drongelen J, et al. Placental transfer of the HIV integrase inhibitor dolutegravir in an ex vivo human cotyledon perfusion model. *J Antimicrob Chemother*. 2016;71(2):480–3.
76. Nanovskaya TN, Nekhayeva I, Hankins GD V, Ahmed MS. Effect of human serum albumin on transplacental transfer of glyburide. *Biochem Pharmacol*. 2006 Aug 28;72(5):632–9.
77. Commission E. European Commission, Types and uses of nanomaterials, including safety aspects. Brussels, (2012). 2012. p. 1–111.
78. Hochella MF, Spencer MG, Jones KL. Nanotechnology: nature’s gift or scientists’ brainchild? *Environ Sci Nano*. 2015;2(2):114–9.
79. Huang P, Wang X, Liang X, Yang J, Zhang C, Kong D, et al. Nano-, micro-, and macroscale drug delivery systems for cancer immunotherapy. *Acta Biomater*. 2019 Feb;85:1–26.
80. Nabil G, Bhise K, Sau S, Atef M, El-Banna HA, Iyer AK. Nano-engineered delivery systems for cancer imaging and therapy: Recent advances, future direction and patent evaluation. *Drug Discov Today*. 2019 Feb;24(2):462–91.
81. Giese B, Klaessig F, Park B, Kaegi R, Steinfeldt M, Wigger H, et al. Risks, Release and Concentrations of Engineered Nanomaterial in the Environment. *Sci Rep*. 2018 Dec 25;8(1):1565.
82. Amereh F, Babaei M, Eslami A, Fazelpour S, Rafiee M. The emerging risk of exposure to nano(micro)plastics on endocrine disturbance and reproductive toxicity: From a hypothetical scenario to a global public health challenge. *Environ Pollut*. 2020 Jun;261:114158.
83. Bongaerts E, Nawrot TS, Van Pee T, Ameloot M, Bové H. Translocation of (ultra)fine particles and nanoparticles across the placenta; a systematic review on the evidence of

- in vitro, ex vivo, and in vivo studies. *Part Fibre Toxicol.* 2020 Dec 2;17(1):56.
84. Hesler M, Aengenheister L, Ellinger B, Drexel R, Straskraba S, Jost C, et al. Multi-endpoint toxicological assessment of polystyrene nano- and microparticles in different biological models in vitro. *Toxicol Vitro.* 2019 Dec;61(July):104610.
  85. Ghitman J, Biru EI, Stan R, Iovu H. Review of hybrid PLGA nanoparticles: Future of smart drug delivery and theranostics medicine. *Mater Des.* 2020 Aug;193:108805.
  86. Ho BT, Roberts TK, Lucas S. An overview on biodegradation of polystyrene and modified polystyrene: the microbial approach. *Crit Rev Biotechnol.* 2018 Feb 17;38(2):308–20.
  87. Xu Y, Kim C-S, Saylor DM, Koo D. Polymer degradation and drug delivery in PLGA-based drug-polymer applications: A review of experiments and theories. *J Biomed Mater Res Part B Appl Biomater.* 2017 Aug;105(6):1692–716.
  88. Kwon BG, Koizumi K, Chung S-Y, Kodera Y, Kim J-O, Saido K. Global styrene oligomers monitoring as new chemical contamination from polystyrene plastic marine pollution. *J Hazard Mater.* 2015 Dec;300:359–67.
  89. Schwabl P, Köppel S, Königshofer P, Bucsecs T, Trauner M, Reiberger T, et al. Detection of Various Microplastics in Human Stool. *Ann Intern Med.* 2019 Oct 1;171(7):453.
  90. Albekairi NA, Al-Enazy S, Ali S, Rytting E. Transport of digoxin-loaded polymeric nanoparticles across BeWo cells, an in vitro model of human placental trophoblast. *Ther Deliv.* 2015 Dec;6(12):1325–34.
  91. Ali H, Kalashnikova I, White MA, Sherman M, Rytting E. Preparation, characterization, and transport of dexamethasone-loaded polymeric nanoparticles across a human placental in vitro model. *Int J Pharm.* 2013 Sep 15;454(1):149–57.
  92. Li H, van Ravenzwaay B, Rietjens IMCM, Lousse J. Assessment of an in vitro transport model using BeWo b30 cells to predict placental transfer of compounds. *Arch Toxicol.* 2013 Sep 21;87(9):1661–9.
  93. Waring RH, Harris RM, Mitchell SC. Plastic contamination of the food chain: A threat to human health? *Maturitas.* 2018 Sep;115(June):64–8.
  94. Kik K, Bukowska B, Sicińska P. Polystyrene nanoparticles: Sources, occurrence in the

- environment, distribution in tissues, accumulation and toxicity to various organisms. *Environ Pollut.* 2020 Jul;262:114297.
95. Kloet SK, Walczak AP, Louisse J, van den Berg HHJ, Bouwmeester H, Tromp P, et al. Translocation of positively and negatively charged polystyrene nanoparticles in an in vitro placental model. *Toxicol Vitro.* 2015 Oct 1;29(7):1701–10.
  96. Grafmueller S, Manser P, Diener L, Maurizi L, Diener P-A, Hofmann H, et al. Transfer studies of polystyrene nanoparticles in the ex vivo human placenta perfusion model: key sources of artifacts. *Sci Technol Adv Mater.* 2015 Aug 1;16(4):044602.
  97. Grafmueller S, Manser P, Diener L, Diener P-A, Maeder-Althaus X, Maurizi L, et al. Bidirectional Transfer Study of Polystyrene Nanoparticles across the Placental Barrier in an ex Vivo Human Placental Perfusion Model. *Environ Health Perspect.* 2015;(May).
  98. Cartwright L, Poulsen MSS, Nielsen HMM, Pojana G, Knudsen LE, Saunders M, et al. In vitro placental model optimization for nanoparticle transport studies. *Int J Nanomedicine.* 2012 Jan;7:497–510.
  99. Monopoli MP, Åberg C, Salvati A, Dawson KA. Biomolecular coronas provide the biological identity of nanosized materials. *Nat Nanotechnol.* 2012 Dec 5;7(12):779–86.
  100. Müller J, Prozeller D, Ghazaryan A, Kokkinopoulou M, Mailänder V, Morsbach S, et al. Beyond the protein corona – lipids matter for biological response of nanocarriers. *Acta Biomater.* 2018;71:420–31.
  101. Abarca-Cabrera L, Fraga-García P, Berensmeier S. Bio-nano interactions: binding proteins, polysaccharides, lipids and nucleic acids onto magnetic nanoparticles. *Biomater Res.* 2021 Dec 21;25(1):12.
  102. Lundqvist M, Stigler J, Elia G, Lynch I, Cedervall T, Dawson KA. Nanoparticle size and surface properties determine the protein corona with possible implications for biological impacts. *Proc Natl Acad Sci.* 2008 Sep 23;105(38):14265–70.
  103. Mirshafiee V, Kim R, Mahmoudi M, Kraft ML. The importance of selecting a proper biological milieu for protein corona analysis in vitro: Human plasma versus human serum. *Int J Biochem Cell Biol.* 2016;75:188–95.
  104. Tenzer S, Docter D, Kuharev J, Musyanovych A, Fetz V, Hecht R, et al. Rapid formation of plasma protein corona critically affects nanoparticle pathophysiology. *Nat*

- Nanotechnol. 2013 Oct 22;8(10):772–81.
105. Palchetti S, Pozzi D, Capriotti AL, Barbera G La, Chiozzi RZ, Digiacomo L, et al. Influence of dynamic flow environment on nanoparticle-protein corona: From protein patterns to uptake in cancer cells. *Colloids Surfaces B Biointerfaces*. 2017 May;153:263–71.
  106. Cox A, Andreozzi P, Dal Magro R, Fiordaliso F, Corbelli A, Talamini L, et al. Evolution of Nanoparticle Protein Corona across the Blood–Brain Barrier. *ACS Nano*. 2018 Jul 24;12(7):7292–300.
  107. Solorio-Rodríguez A, Escamilla-Rivera V, Uribe-Ramírez M, Chagolla A, Winkler R, Garcia-Cuellar C, et al. A comparison of human and mouse protein corona profiles of functionalized SiO<sub>2</sub> nanocarriers. *Nanoscale*. 2017;
  108. Fleischer CC, Payne CK. Secondary Structure of Corona Proteins Determines the Cell Surface Receptors Used by Nanoparticles. *J Phys Chem B*. 2014 Dec 11;118(49):14017–26.
  109. Ge C, Du J, Zhao L, Wang L, Liu Y, Li D, et al. Binding of blood proteins to carbon nanotubes reduces cytotoxicity. *Proc Natl Acad Sci*. 2011 Oct 11;108(41):16968–73.
  110. Deng ZJ, Liang M, Monteiro M, Toth I, Minchin RF. Nanoparticle-induced unfolding of fibrinogen promotes Mac-1 receptor activation and inflammation. *Nat Nanotechnol*. 2011 Jan 19;6(1):39–44.
  111. Jayaram DT, Runa S, Kemp ML, Payne CK. Nanoparticle-induced oxidation of corona proteins initiates an oxidative stress response in cells. *Nanoscale*. 2017;9(22):7595–601.
  112. Salvati A, Pitek AS, Monopoli MP, Prapainop K, Bombelli FB, Hristov DR, et al. Transferrin-functionalized nanoparticles lose their targeting capabilities when a biomolecule corona adsorbs on the surface. *Nat Nanotechnol*. 2013 Feb 20;8(2):137–43.
  113. Sharifi S, Caracciolo G, Mahmoudi M. Biomolecular Corona Affects Controlled Release of Drug Payloads from Nanocarriers. *Trends Pharmacol Sci*. 2020 Sep;41(9):641–52.
  114. Malek a, Sager R, Kuhn P, Nicolaidis KH, Schneider H. Evolution of maternofetal transport of immunoglobulins during human pregnancy. *Am J Reprod Immunol*.

- 1996;36(5):248–55.
115. Ciobanu AM, Dumitru AE, Gica N, Botezatu R, Peltecu G, Panaitescu AM. Benefits and Risks of IgG Transplacental Transfer. *Diagnostics*. 2020 Aug 12;10(8):583.
  116. Jones C, Pollock L, Barnett SM, Battersby A, Kampmann B. Specific antibodies against vaccine-preventable infections: a mother–infant cohort study. *BMJ Open*. 2013 Apr 11;3(4):e002473.
  117. Galluzzo M, D’Adamio S, Bianchi L, Talamonti M. Psoriasis in pregnancy: case series and literature review of data concerning exposure during pregnancy to ustekinumab. *J Dermatolog Treat*. 2019 Jan 2;30(1):40–4.
  118. Luu M, Benzenine E, Doret M, Michiels C, Barkun A, Degand T, et al. Continuous Anti-TNF $\alpha$  Use Throughout Pregnancy: Possible Complications For the Mother But Not for the Fetus. A Retrospective Cohort on the French National Health Insurance Database (EVASION). *Am J Gastroenterol*. 2018 Nov;113(11):1669–77.
  119. McBain RD, Crowther CA, Middleton P. Anti-D administration in pregnancy for preventing Rhesus alloimmunisation. *Cochrane Database Syst Rev*. 2015 Sep 3;2015(9).
  120. Shepard HM, Phillips GL, Thanos CD, Feldmann M. Developments in therapy with monoclonal antibodies and related proteins. *Clin Med (Northfield Il)*. 2017 Jun;17(3):220–32.
  121. Nelson EL. HER2/neu: an increasingly important therapeutic target. Part 2: Distribution of HER2/neu overexpression and gene amplification by organ, tumor site and histology. *Clin Investig (Lond)*. 2014 Aug;4(8):705–28.
  122. Watson WJ. Herceptin (trastuzumab) therapy during pregnancy: Association with reversible anhydramnios. *Obstet Gynecol*. 2005;105(3):642–3.
  123. DeSesso JM, Williams AL, Ahuja A, Bowman CJ, Hurtt ME. The placenta, transfer of immunoglobulins, and safety assessment of biopharmaceuticals in pregnancy. *Crit Rev Toxicol*. 2012 Mar;42(3):185–210.
  124. Bowman CJ, Breslin WJ, Connor A V., Martin PL, Moffat GJ, Sivaraman L, et al. Placental transfer of Fc-containing biopharmaceuticals across species, an industry survey analysis. *Birth Defects Res Part B - Dev Reprod Toxicol*. 2013;98(6):459–85.

125. Anderson NL, Anderson NG. The Human Plasma Proteome. *Mol Cell Proteomics*. 2002 Nov;1(11):845–67.
126. Vidarsson G, Dekkers G, Rispens T. IgG subclasses and allotypes: From structure to effector functions. *Front Immunol*. 2014;5(OCT):1–17.
127. Lobner E, Traxlmayr MW, Obinger C, Hasenhindl C. Engineered IgG1-Fc - one fragment to bind them all. *Immunol Rev*. 2016;270(1):113–31.
128. de Taeye SW, Rispens T, Vidarsson G. The Ligands for Human IgG and Their Effector Functions. *Antibodies*. 2019 Apr 25;8(2):30.
129. Brambell FWR. The Transmission of Immunity From Mother to Young and the Catabolism of Immunoglobulins. *Lancet*. 1966 Nov;288(7473):1087–93.
130. Simister NE, Rees AR. Isolation and characterization of an Fc receptor from neonatal rat small intestine. *Eur J Immunol*. 1985;15(7):733–8.
131. Simister NE, Story CM, Chen H-L, Hunt JS. An IgG-transporting Fc receptor expressed in the syncytiotrophoblast of human placenta. *Eur J Immunol*. 1996 Jul;26(7):1527–31.
132. West AP, Bjorkman PJ. Crystal Structure and Immunoglobulin G Binding Properties of the Human Major Histocompatibility Complex-Related Fc Receptor  $\uparrow$  ,  $\ddagger$ . *Biochemistry*. 2000;39(32):9698–708.
133. Suzuki T, Ishii-Watabe A, Tada M, Kobayashi T, Kanayasu-Toyoda T, Kawanishi T, et al. Importance of neonatal FcR in regulating the serum half-life of therapeutic proteins containing the Fc domain of human IgG1: a comparative study of the affinity of monoclonal antibodies and Fc-fusion proteins to human neonatal FcR. *J Immunol*. 2010;184(4):1968–76.
134. Dickinson BL, Claypool SM, D'Angelo JA, Aiken ML, Venu N, Yen EH, et al. Ca<sup>2+</sup>-dependent calmodulin binding to FcRn affects immunoglobulin G transport in the transcytotic pathway. *Mol Biol Cell*. 2008 Jan;19(1):414–23.
135. Chaudhury C, Mehnaz S, Robinson JM, Hayton WL, Pearl DK, Roopenian DC, et al. The Major Histocompatibility Complex-related Fc Receptor for IgG (FcRn) Binds Albumin and Prolongs Its Lifespan. *J Exp Med*. 2003 Feb 3;197(3):315–22.
136. Abdiche YN, Yeung YA, Chaparro-Riggers J, Barman I, Strop P, Chin SM, et al. The

- neonatal Fc receptor (FcRn) binds independently to both sites of the IgG homodimer with identical affinity. *MAbs*. 2015;7(2):331–43.
137. Chaudhury C, Brooks CL, Carter DC, Robinson JM, Anderson CL. Albumin Binding to FcRn: Distinct from the FcRn–IgG Interaction †. *Biochemistry*. 2006 Apr;45(15):4983–90.
  138. Kim J, Bronson CL, Hayton WL, Radmacher MD, Roopenian DC, Robinson JM, et al. Albumin turnover: FcRn-mediated recycling saves as much albumin from degradation as the liver produces. *Am J Physiol Liver Physiol*. 2006 Feb;290(2):G352–60.
  139. Andersen JT, Daba MB, Berntzen G, Michaelsen TE, Sandlie I. Cross-species binding analyses of mouse and human neonatal Fc receptor show dramatic differences in immunoglobulin G and albumin binding. *J Biol Chem*. 2010;285(7):4826–36.
  140. Neuber T, Frese K, Jaehrling J, Jäger S, Daubert D, Felderer K, et al. Characterization and screening of IgG binding to the neonatal Fc receptor. *MAbs*. 2014;6(4):928–42.
  141. Miller RK, Mace K, Polliotti B, DeRita R, Hall W, Treacy G. Marginal transfer of ReoPro<sup>TM</sup> (Abciximab) compared with immunoglobulin G (F105), inulin and water in the perfused human placenta in vitro. *Placenta*. 2003;24(7):727–38.
  142. Einarsdottir HK, Stapleton NM, Scherjon S, Andersen JT, Rispens T, Van Der Schoot CE, et al. On the perplexingly low rate of transport of IgG2 across the human placenta. *PLoS One*. 2014;9(9):1–9.
  143. Jennewein MF, Goldfarb I, Dolatshahi S, Cosgrove C, Noelette FJ, Krykbaeva M, et al. Fc Glycan-Mediated Regulation of Placental Antibody Transfer. *Cell*. 2019 Jun;178(1):202-215.e14.
  144. Borghi S, Bournazos S, Thulin NK, Li C, Gajewski A, Sherwood RW, et al. FcRn, but not FcγRs, drives maternal-fetal transplacental transport of human IgG antibodies. *Proc Natl Acad Sci U S A*. 2020 Jun 9;117(23):12943–51.
  145. Patel DD, Bussel JB. Neonatal Fc receptor in human immunity: Function and role in therapeutic intervention. *J Allergy Clin Immunol*. 2020 Sep;146(3):467–78.
  146. Grilo AL, Mantalaris A. The Increasingly Human and Profitable Monoclonal Antibody Market. *Trends Biotechnol*. 2019 Jan;37(1):9–16.
  147. Sun LK, Curtis P, Rakowicz-Szulczynska E, Ghrayeb J, Chang N, Morrison SL, et al.

- Chimeric antibody with human constant regions and mouse variable regions directed against carcinoma-associated antigen 17-1A. *Proc Natl Acad Sci.* 1987 Jan 1;84(1):214–8.
148. Safdari Y, Farajnia S, Asgharzadeh M, Khalili M. Antibody humanization methods – a review and update. *Biotechnol Genet Eng Rev.* 2013 Oct;29(2):175–86.
  149. Weiner LM. Fully Human Therapeutic Monoclonal Antibodies. *J Immunother.* 2006 Jan;29(1):1–9.
  150. Nelson AL, Dhimolea E, Reichert JM. Development trends for human monoclonal antibody therapeutics. *Nat Rev Drug Discov.* 2010 Oct 3;9(10):767–74.
  151. Sanz-Salvador L, García-Pérez MÁ, Tarín JJ, Cano A. ENDOCRINOLOGY IN PREGNANCY: Bone metabolic changes during pregnancy: a period of vulnerability to osteoporosis and fracture. *Eur J Endocrinol.* 2015 Feb;172(2):R53–65.
  152. Andersson TM-L, Johansson AL V, Hsieh C-C, Cnattingius S, Lambe M. Increasing incidence of pregnancy-associated breast cancer in Sweden. *Obstet Gynecol.* 2009;114(3):568–72.
  153. Tuna F, Akleyek C, Özdemir H, Demirbağ Kabayel D. Risk factors, fractures, and management of pregnancy-associated osteoporosis: a retrospective study of 14 Turkish patients. *Gynecol Endocrinol.* 2019 Aug 6;0(0):1–5.
  154. Eibye S, Kjær SK, Mellekjær L. Incidence of Pregnancy-Associated Cancer in Denmark, 1977–2006. *Obstet Gynecol.* 2013;122(3):608–17.
  155. Lee GE, Rosenberg SM, Mayer EL, Borges V, Meyer ME, Schapira L, et al. Contemporary management of breast cancer during pregnancy and subsequent lactation in a multicenter cohort of young women with breast cancer. *Breast J.* 2019;25(6):1104–10.
  156. Weilbaecher KN, Guise TA, McCauley LK. Cancer to bone: a fatal attraction. *Nat Rev Cancer.* 2011 Jun 19;11(6):411–25.
  157. Rao S, Cronin SJF, Sigl V, Penninger JM. RANKL and RANK: From Mammalian Physiology to Cancer Treatment. *Trends Cell Biol.* 2018 Mar;28(3):213–23.
  158. Bekker PJ, Holloway DL, Rasmussen AS, Murphy R, Martin SW, Leese PT, et al. A Single-Dose Placebo-Controlled Study of AMG 162, a Fully Human Monoclonal

- Antibody to RANKL, in Postmenopausal Women. *J Bone Miner Res.* 2004 Mar 1;19(7):1059–66.
159. Miyamoto T, Miyakoshi K, Sato Y, Kasuga Y, Ikenoue S, Miyamoto K, et al. Changes in bone metabolic profile associated with pregnancy or lactation. *Sci Rep.* 2019 Dec 13;9(1):6787.
  160. Sanchez A. Two cases of pregnancy- and lactation- associated osteoporosis successfully treated with denosumab. *Clin Cases Miner Bone Metab.* 2016;13(3):244–6.
  161. Okamoto N, Sakai N, Karakawa A, Kouyama N, Sato Y, Inagaki K, et al. Biological effects of anti-RANKL antibody administration in pregnant mice and their newborns. *Biochem Biophys Res Commun.* 2017 Sep;491(3):614–21.
  162. Boyce RW, Varela A, Chouinard L, Bussiere JL, Chellman GJ, Ominsky MS, et al. Infant cynomolgus monkeys exposed to denosumab in utero exhibit an osteoclast-poor osteopetrotic-like skeletal phenotype at birth and in the early postnatal period. *Bone.* 2014 Jul;64:314–25.
  163. Bussiere JL, Pyrah I, Boyce R, Branstetter D, Loomis M, Andrews-Cleavenger D, et al. Reproductive toxicity of denosumab in cynomolgus monkeys. *Reprod Toxicol.* 2013 Dec;42:27–40.
  164. Stensheim H, Møller B, Van Dijk T, Fosså SD. Cause-specific survival for women diagnosed with cancer during pregnancy or lactation: A registry-based cohort study. *J Clin Oncol.* 2009;27(1):45–51.
  165. Lee YY, Roberts CL, Dobbins T, Stavrou E, Black K, Morris J, et al. Incidence and outcomes of pregnancy-associated cancer in Australia, 1994-2008: A population-based linkage study. *BJOG An Int J Obstet Gynaecol.* 2012;119(13):1572–82.
  166. Amant F, von Minckwitz G, Han SN, Bontenbal M, Ring AE, Giermek J, et al. Prognosis of Women With Primary Breast Cancer Diagnosed During Pregnancy: Results From an International Collaborative Study. *J Clin Oncol.* 2013;31(20):2532–9.
  167. Loibl S, Schmidt A, Gentilini O, Kaufman B, Kuhl C, Denkert C, et al. Breast Cancer Diagnosed During Pregnancy. Adapting Recent Advances in Breast Cancer Care for Pregnant Patients. *JAMA Oncol.* 2015 Nov 1;1(8):1145.
  168. Waks AG, Winer EP. Breast Cancer Treatment. *JAMA.* 2019 Jan 22;321(3):288.

169. Genin A-S, Lesieur B, Gligorov J, Antoine M, Selleret L, Rouzier R. Pregnancy-associated breast cancers: Do they differ from other breast cancers in young women? *The Breast*. 2012 Aug;21(4):550–5.
170. Casalini P, Iorio M V., Galmozzi E, Ménard S. Role of HER receptors family in development and differentiation. *J Cell Physiol*. 2004 Sep;200(3):343–50.
171. Mielke S, Meden H, Marx D, Wuttke W, Kuhn W. In vivo effects of estrogens on oerbB-2 oncoprotein levels in chorionic villous tissue and maternal serum. *Gynecol Endocrinol*. 1997 Jan 7;11(4):237–41.
172. Press MF, Cordon-Cardo C, Slamon DJ. Expression of the HER-2/neu proto-oncogene in normal human adult and fetal tissues. *Oncogene*. 1990 Jul;5(7):953–62.
173. Potter CR, Daele S, Vijver MJ, Pauwels C, Maertens G, Boever J, et al. The expression of the neu oncogene product in breast lesions and in normal fetal and adult human tissues. *Histopathology*. 1989 Oct;15(4):351–62.
174. Perry CM, Wiseman LR. Trastuzumab. *BioDrugs*. 1999 Aug;12(2):129–35.
175. Witzel ID, Müller V, Harps E, Janicke F, DeWit M, Muller V, et al. Trastuzumab in pregnancy associated with poor fetal outcome. *Ann Oncol*. 2007;19(1):191–2.
176. Zagouri F, Sergentanis TN, Chrysikos D, Papadimitriou CA, Dimopoulos M-A, Bartsch R. Trastuzumab administration during pregnancy: a systematic review and meta-analysis. *Breast Cancer Res Treat*. 2013 Jan 15;137(2):349–57.
177. Lambertini M, Martel S, Campbell C, Guillaume S, Hilbers FS, Schuehly U, et al. Pregnancies during and after trastuzumab and/or lapatinib in patients with human epidermal growth factor receptor 2-positive early breast cancer: Analysis from the NeoALTTO (BIG 1-06) and ALTTO (BIG 2-06) trials. *Cancer*. 2019 Jan 15;125(2):307–16.
178. Bader AA, Schlembach D, Tamussino KF, Pristaux G, Petru E. Anhydramnios associated with administration of trastuzumab and paclitaxel for metastatic breast cancer during pregnancy. *Lancet Oncol*. 2007;8(1):79–81.
179. Goller SS, Markert UR, Fröhlich K. Trastuzumab in the Treatment of Pregnant Breast Cancer Patients – an Overview of the Literature. *Geburtshilfe Frauenheilkd*. 2019 Jun 14;79(06):618–25.

180. Van Calsteren K, Verbesselt R, Devlieger R, De Catte L, Chai D, Van Bree R, et al. Transplacental Transfer of Paclitaxel, Docetaxel, Carboplatin, and Trastuzumab in a Baboon Model. *Int J Gynecol Cancer*. 2010;20(9):1459–64.
181. Schneider H, Mohlen K, Dancis J, Möhlen KH. Transfer of amino acids across the in vitro perfused human placenta. *Pediatr Res*. 1979;13(4 Pt 1):236–40.
182. Hirschmugl B, Brandl W, Csapo B, van Poppel M, Köfeler H, Desoye G, et al. Evidence of Human Milk Oligosaccharides in Cord Blood and Maternal-to-Fetal Transport across the Placenta. *Nutrients*. 2019 Nov 4;11(11):2640.
183. Mose T, Mathiesen L, Karttunen V, Nielsen JKS, Sieppi E, Kumm M, et al. Meta-analysis of data from human ex vivo placental perfusion studies on genotoxic and immunotoxic agents within the integrated European project NewGeneris. *Placenta*. 2012;33(5):433–9.
184. Weissenböck A, Wirth M, Gabor F. WGA-grafted PLGA-nanospheres: Preparation and association with Caco-2 single cells. *J Control Release*. 2004;99(3):383–92.
185. Antohe F, Rădulescu L, Gafencu A, Ghe V, Simionescu M. Expression of functionally active FcRn and the differentiated bidirectional transport of IgG in human placental endothelial cells. *Hum Immunol*. 2001;62(2):93–105.
186. Sohn W, Simiens MA, Jaeger K, Hutton S, Jang G. The pharmacokinetics and pharmacodynamics of denosumab in patients with advanced solid tumours and bone metastases: a systematic review. *Br J Clin Pharmacol*. 2014 Sep;78(3):477–87.
187. Sutjandra L, Rodriguez RD, Doshi S, Ma M, Peterson MC, Jang GR, et al. Population Pharmacokinetic Meta-Analysis of Denosumab in Healthy Subjects and Postmenopausal Women with Osteopenia or Osteoporosis. *Clin Pharmacokinet*. 2011 Dec;50(12):793–807.
188. Sohn W, Lee E, Kankam MK, Egbuna O, Moffat G, Bussiere J, et al. An open-label study in healthy men to evaluate the risk of seminal fluid transmission of denosumab to pregnant partners. *Br J Clin Pharmacol*. 2016 Feb;81(2):362–9.
189. International Conference on Harmonisation of Technical Requirements for Registration of Pharmaceuticals for Human use. VALIDATION OF ANALYTICAL PROCEDURES: TEXT AND METHODOLOGY Q2(R1). Vol. 1994. The International Council for Harmonisation of Technical Requirements for

- Pharmaceuticals for Human Use (ICH); 2005.
190. Docter D, Distler U, Storck W, Kuharev J, Wünsch D, Hahlbrock A, et al. Quantitative profiling of the protein coronas that form around nanoparticles. *Nat Protoc.* 2014 Sep;9(9):2030–44.
  191. Cox J, Hein MY, Lubner CA, Paron I, Nagaraj N, Mann M. Accurate proteome-wide label-free quantification by delayed normalization and maximal peptide ratio extraction, termed MaxLFQ. *Mol Cell Proteomics.* 2014 Sep;13(9):2513–26.
  192. Vizcaíno JA, Csordas A, Del-Toro N, Dianes JA, Griss J, Lavidas I, et al. 2016 update of the PRIDE database and its related tools. *Nucleic Acids Res.* 2016 Jan 4;44(D1):D447-56.
  193. Jain S, Wheeler JR, Walters RW, Agrawal A, Barsic A, Parker R. ATPase-Modulated Stress Granules Contain a Diverse Proteome and Substructure. *Cell.* 2016 Jan;164(3):487–98.
  194. Markmiller S, Soltanieh S, Server KL, Mak R, Jin W, Fang MY, et al. Context-Dependent and Disease-Specific Diversity in Protein Interactions within Stress Granules. *Cell.* 2018 Jan;172(3):590-604.e13.
  195. Wu B, Guo W. The Exocyst at a Glance. *J Cell Sci.* 2015 Aug 15;128(16):2957–64.
  196. Gonzalez IM, Ackerman WE, Vandre DD, Robinson JM. Exocyst complex protein expression in the human placenta. *Placenta.* 2014 Jul;35(7):442–9.
  197. Kanehisa M, Sato Y, Furumichi M, Morishima K, Tanabe M. New approach for understanding genome variations in KEGG. *Nucleic Acids Res.* 2019 Jan 8;47(D1):D590–5.
  198. Kanehisa M, Furumichi M, Tanabe M, Sato Y, Morishima K. KEGG: new perspectives on genomes, pathways, diseases and drugs. *Nucleic Acids Res.* 2017 Jan 4;45(D1):D353–61.
  199. Watson P, Stephens DJ. ER-to-Golgi transport: Form and formation of vesicular and tubular carriers. *Biochim Biophys Acta - Mol Cell Res.* 2005 Jul;1744(3):304–15.
  200. Gomez-Navarro N, Miller E. Protein sorting at the ER–Golgi interface. *J Cell Biol.* 2016 Dec 19;215(6):769–78.
  201. Collins GA, Goldberg AL. The Logic of the 26S Proteasome. *Cell.* 2017;169(5):792–

806.

202. O'Kelly I, Butler MH, Zilberberg N, Goldstein SAN. Forward Transport: 14-3-3 Binding Overcomes Retention in Endoplasmic Reticulum by Dibasic Signals. *Cell*. 2002 Nov;111(4):577–88.
203. Chambers MC, Maclean B, Burke R, Amodei D, Ruderman DL, Neumann S, et al. A cross-platform toolkit for mass spectrometry and proteomics. *Nat Biotechnol*. 2012 Oct 10;30(10):918–20.
204. MacLean B, Tomazela DM, Shulman N, Chambers M, Finney GL, Frewen B, et al. Skyline: an open source document editor for creating and analyzing targeted proteomics experiments. *Bioinformatics*. 2010 Apr 1;26(7):966–8.
205. Ellinger I, Reischer H, Lehner C, Leitner K, Hunziker W, Fuchs R. Overexpression of the human neonatal Fc-receptor  $\alpha$ -chain in trophoblast-derived BeWo cells increase cellular retention of  $\alpha$ 2-microglobulin. *Placenta*. 2005;26(2–3):171–82.
206. Hunziker W, Mellman I. Expression of macrophage-lymphocyte Fc receptors in Madin-Darby canine kidney cells: polarity and transcytosis differ for isoforms with or without coated pit localization domains. *J Cell Biol*. 1989 Dec;109(6 Pt 2):3291–302.
207. Mathiesen L, Mørck TA, Zuri G, Andersen MH, Pehrson C, Frederiksen M, et al. Modelling of human transplacental transport as performed in Copenhagen, Denmark. *Basic Clin Pharmacol Toxicol*. 2014;115(1):93–100.
208. Mezo AR, McDonnell K a, Hehir C a T, Low SC, Palombella VJ, Stattel JM, et al. Reduction of IgG in nonhuman primates by a peptide antagonist of the neonatal Fc receptor FcRn. *Proc Natl Acad Sci U S A*. 2008;105(7):2337–42.
209. Weflen AW, Baier N, Tang Q-J, Van den Hof M, Blumberg RS, Lencer WI, et al. Multivalent immune complexes divert FcRn to lysosomes by exclusion from recycling sorting tubules. Gruenberg JE, editor. *Mol Biol Cell*. 2013 Aug;24(15):2398–405.
210. Grevys A, Nilsen J, Sand KMK, Daba MB, Øynebråten I, Bern M, et al. A human endothelial cell-based recycling assay for screening of FcRn targeted molecules. *Nat Commun*. 2018 Dec 12;9(1):621.
211. Ellinger I, Schwab M, Stefanescu A, Hunziker W, Fuchs R. IgG transport across trophoblast-derived BeWo cells: a model system to study IgG transport in the placenta. *Eur J Immunol*. 1999 Mar;29(3):733–44.

212. Tang Z, Tadesse S, Norwitz E, Mor G, Abrahams VM, Guller S. Isolation of Hofbauer cells from human term placentas with high yield and purity. *Am J Reprod Immunol*. 2011 Oct;66(4):336–48.
213. Zhang B, Liang R, Zheng M, Cai L, Fan X. Surface-Functionalized Nanoparticles as Efficient Tools in Targeted Therapy of Pregnancy Complications. *Int J Mol Sci*. 2019 Jul 25;20(15):3642.
214. Cowie H, Magdolenova Z, Saunders M, Drlickova M, Correia Carreira S, Halamoda Kenzaoui B, et al. Suitability of human and mammalian cells of different origin for the assessment of genotoxicity of metal and polymeric engineered nanoparticles. *Nanotoxicology*. 2015 May;9 Suppl 1(S1):57–65.
215. Cai R, Chen C. The Crown and the Scepter: Roles of the Protein Corona in Nanomedicine. *Adv Mater*. 2018 Dec 27;1805740(11):1805740.
216. Fedotov PS, Vanifatova NG, Shkinev VM, Spivakov BY. Fractionation and characterization of nano- and microparticles in liquid media. *Anal Bioanal Chem*. 2011 Jun 12;400(6):1787–804.
217. Khan R, Ahmad E, Zaman M, Qadeer A, Rabbani G. Nanoparticles in relation to peptide and protein aggregation. *Int J Nanomedicine*. 2014 Feb;9(1):899.
218. Bhattacharjee S. DLS and zeta potential - What they are and what they are not? *J Control Release*. 2016;235:337–51.
219. Monopoli MP, Walczyk D, Campbell A, Elia G, Lynch I, Baldelli Bombelli F, et al. Physical–Chemical Aspects of Protein Corona: Relevance to in Vitro and in Vivo Biological Impacts of Nanoparticles. *J Am Chem Soc*. 2011 Mar 2;133(8):2525–34.
220. Zhang H, Wang J, Zhou B, Zhou Y, Dai Z, Zhou Q, et al. Enhanced adsorption of oxytetracycline to weathered microplastic polystyrene: Kinetics, isotherms and influencing factors. *Environ Pollut*. 2018 Dec;243:1550–7.
221. Almeida M, Martins MA, Soares AMV, Cuesta A, Oliveira M. Polystyrene nanoplastics alter the cytotoxicity of human pharmaceuticals on marine fish cell lines. *Environ Toxicol Pharmacol*. 2019 Jul;69:57–65.
222. Bashkatova NV, Korotkova EI, Karbainov YA, Yagovkin AY, Bakibaev AA. Electrochemical, quantum-chemical and antioxidant properties of antipyrine and its derivatives. *J Pharm Biomed Anal*. 2005 Apr;37(5):1143–7.

223. Panyam J, Labhasetwar V. Dynamics of endocytosis and exocytosis of poly(D,L-lactide-co-glycolide) nanoparticles in vascular smooth muscle cells. *Pharm Res.* 2003 Feb;20(2):212–20.
224. Dancis J, Jansen V, Levitz M. Placental transfer of steroids: effect of binding to serum albumin and to placenta. *Am J Physiol.* 1980 Mar;238(3):E208-13.
225. Aldecoa C, Llau J V., Nuvials X, Artigas A. Role of albumin in the preservation of endothelial glycocalyx integrity and the microcirculation: a review. *Ann Intensive Care.* 2020 Dec 22;10(1):85.
226. Hashem L, Swedrowska M, Vllasaliu D. Intestinal uptake and transport of albumin nanoparticles: Potential for oral delivery. *Nanomedicine.* 2018 Jun;13(11):1255–65.
227. Gitlin D, Kumate J, Urrusti J, Morales C. The Selectivity of the Human Placenta in the Transfer of Plasma Proteins from Mother to Fetus. *J Clin Invest.* 1964 Oct;43(2):1938–51.
228. Dal Magro R, Ornaghi F, Cambianica I, Beretta S, Re F, Musicanti C, et al. ApoE-modified solid lipid nanoparticles: A feasible strategy to cross the blood-brain barrier. *J Control Release.* 2017;249:103–10.
229. Firan M, Bawdon R, Radu C, Ober RJ, Eaken D, Antohe F, et al. The MHC class I-related receptor, FcRn, plays an essential role in the maternofetal transfer of gamma-globulin in humans. *Int Immunol.* 2001;13(8):993–1002.
230. He W, Ladinsky MS, Huey-Tubman KE, Jensen GJ, Mcintosh R, Björkman PJ, et al. FcRn-mediated antibody transport across epithelial cells revealed by electron tomography. *Nature.* 2009 Sep;455(7212):542–6.
231. Knudsen Sand KM, Bern M, Nilsen J, Noordzij HT, Sandlie I, Andersen JT. Unraveling the interaction between FcRn and albumin: Opportunities for design of albumin-based therapeutics. *Front Immunol.* 2015;6(JAN):1–21.
232. Zardoya-Laguardia P, Blaschitz A, Hirschmugl B, Lang I, Herzog SA, Nikitina L, et al. Endothelial indoleamine 2,3-dioxygenase-1 regulates the placental vascular tone and is deficient in intrauterine growth restriction and pre-eclampsia. *Sci Rep.* 2018 Dec 3;8(1):5488.
233. Hadjidemetriou M, Al-Ahmady Z, Kostarelou K. Time-evolution of in vivo protein corona onto blood-circulating PEGylated liposomal doxorubicin (DOXIL)

- nanoparticles. *Nanoscale*. 2016;8(13):6948–57.
234. Qin M, Zhang J, Li M, Yang D, Liu D, Song S, et al. Proteomic analysis of intracellular protein corona of nanoparticles elucidates nano-trafficking network and nano-bio interactions. *Theranostics*. 2020;10(3):1213–29.
235. Lundqvist M, Stigler J, Cedervall T, Berggård T, Flanagan MB, Lynch I, et al. The evolution of the protein corona around nanoparticles: a test study. *ACS Nano*. 2011 Sep 27;5(9):7503–9.
236. Stenmark H, Aasland R, Toh B-H, D'Arrigo A. Endosomal Localization of the Autoantigen EEA1 Is Mediated by a Zinc-binding FYVE Finger. *J Biol Chem*. 1996 Sep 27;271(39):24048–54.
237. Naslavsky N, Caplan S. EHD proteins: key conductors of endocytic transport. *Trends Cell Biol*. 2011 Feb;21(2):122–31.
238. Huotari J, Helenius A. Endosome maturation. *EMBO J*. 2011 Aug 31;30(17):3481–500.
239. Seaman MNJ. Enhanced SnapShot: Endosome-to-Golgi Retrieval. *Cell*. 2009 Dec;139(6):1198-1198.e1.
240. van der Sluijs P, Zibouche M, van Kerkhof P. Late Steps in Secretory Lysosome Exocytosis in Cytotoxic Lymphocytes. *Front Immunol*. 2013 Dec 5;4(34):24315–21.
241. Arakel EC, Schwappach B. Correction: Formation of COPI-coated vesicles at a glance [J. Cell Sci, 131, (jcs209890)] doi:10.1242/jcs.209890. *J Cell Sci*. 2018;131(7).
242. Lopez T, Dalton K, Frydman J. The Mechanism and Function of Group II Chaperonins. *J Mol Biol*. 2015 Sep;427(18):2919–30.
243. Saptarshi SR, Duschl A, Lopata AL. Interaction of nanoparticles with proteins: relation to bio-reactivity of the nanoparticle. *J Nanobiotechnology*. 2013;11(1):26.
244. Collins GA, Goldberg AL. The Logic of the 26S Proteasome. *Cell*. 2017 May;169(5):792–806.
245. Romashchenko A V., Kan T-W, Petrovski D V., Gerlinskaya LA, Moshkin MP, Moshkin YM. Nanoparticles Associate with Intrinsically Disordered RNA-Binding Proteins. *ACS Nano*. 2017 Feb 28;11(2):1328–39.
246. Mühlhauser J, Crescimanno C, Kaufmann P, Höfler H, Zaccheo D, Castellucci M.

- Differentiation and proliferation patterns in human trophoblast revealed by c-erbB-2 oncogene product and EGF-R. *J Histochem Cytochem.* 1993;41(2):165–73.
247. Uhlen M, Fagerberg L, Hallstrom BM, Lindskog C, Oksvold P, Mardinoglu A, et al. Tissue-based map of the human proteome. *Science (80- )*. 2015;347(6220):1260419–1260419.
248. Cho H-S, Mason K, Ramyar KX, Stanley AM, Gabelli SB, Denney DW, et al. Structure of the extracellular region of HER2 alone and in complex with the Herceptin Fab. *Nature.* 2003 Feb 13;421(6924):756–60.
249. Ellinger I, Rothe A, Grill M, Fuchs R. Apical to basolateral transcytosis and apical recycling of immunoglobulin G in trophoblast-derived BeWo cells: effects of low temperature, nocodazole, and cytochalasin D. *Exp Cell Res.* 2001;269:322–31.
250. Malek A, Sager R, Zakher A, Schneider H. Transport of immunoglobulin G and its subclasses across the in vitro perfused human placenta. *Am J Obstet Gynecol.* 1995;173(3 Part 1):760–7.
251. Ram S, Kim D, Ober RJ, Ward ES. The level of HER2 expression is a predictor of antibody-HER2 trafficking behavior in cancer cells. *MAbs.* 2014;6(5):1211–1219.
252. Kristoffersen EK, Matre R. Co-localization of the neonatal Fc gamma receptor and IgG in human placental term syncytiotrophoblasts. *Eur J Immunol.* 1996;26(7):1668–71.
253. Latvala S, Jacobsen B, Otteneder MB, Herrmann A, Kronenberg S. Distribution of FcRn Across Species and Tissues. *J Histochem Cytochem.* 2017;002215541770509.
254. Simister NE, Story CM, Chen HL, Hunt JS. An IgG - transporting Fc receptor expressed in the syncytiotrophoblast of human placenta. *Eur J Immunol.* 1996;26(7):1527–31.
255. Stumpf PK, Cittelly DM, Robin TP, Carlson JA, Stuhr KA, Contreras-Zarate MJ, et al. Combination of Trastuzumab Emtansine and Stereotactic Radiosurgery Results in High Rates of Clinically Significant Radionecrosis and Dysregulation of Aquaporin-4. *Clin Cancer Res.* 2019 Jul 1;25(13):3946–53.
256. De Falco M, Cobellis L, Torella M, Acone G, Varano L, Sellitti A, et al. Down-regulation of aquaporin 4 in human placenta throughout pregnancy. *In Vivo (Brooklyn).* 2007;21(5):813–8.

257. Meng Y-H, Zhou W-J, Jin L-P, Liu L-B, Chang K-K, Mei J, et al. RANKL-mediated harmonious dialogue between fetus and mother guarantees smooth gestation by inducing decidual M2 macrophage polarization. *Cell Death Dis.* 2017 Oct 12;8(10):e3105–e3105.
258. Chang R-Q, Shao J, Meng Y-H, Wang J, Li D-J, Li M-Q. Decidual RANKL/RANK interaction promotes the residence and polarization of TGF- $\beta$ 1-producing regulatory  $\gamma\delta$  T cells. *Cell Death Dis.* 2019 Feb 8;10(2):113.
259. Min J-K, Kim Y-MY-M, Kim Y-MY-M, Kim E-C, Gho YS, Kang I-J, et al. Vascular Endothelial Growth Factor Up-regulates Expression of Receptor Activator of NF- $\kappa$ B (RANK) in Endothelial Cells. *J Biol Chem.* 2003 Oct 10;278(41):39548–57.
260. McGonigle JS, Giachelli CM, Scatena M. Osteoprotegerin and RANKL differentially regulate angiogenesis and endothelial cell function. *Angiogenesis.* 2009 Mar 23;12(1):35–46.

## 8. Appendix

Table 13: Significant enriched biocorona proteins on 80 nm PS NP isolated from foetal circulation after 6h perfusion and plasma incubated particles before perfusion. Data was compared to the biocorona protein composition on 80 nm PS NP from maternal circulation after 6h perfusion. Statistical analysis was done with multiple t-test (N=4).

<b>Foetal 6h</b>	<b>Plasma 0h</b>
Actin, cytoplasmic 2	14-3-3 protein eta
Afamin	Afamin
Alpha-2-antiplasmin	Alpha-1-antitrypsin
Apolipoprotein A-I	Alpha-1B-glycoprotein
Apolipoprotein E	Alpha-2-antiplasmin
Apolipoprotein(a)	Alpha-2-HS-glycoprotein
ATP synthase subunit alpha, mitochondrial	Apolipoprotein A-I
Band 3 anion transport protein	Apolipoprotein A-II
Complement factor H	Apolipoprotein A-IV
Desmoglein-1	Apolipoprotein B-100
Fibrinogen alpha chain	Apolipoprotein C-III
Fibrinogen beta chain	Apolipoprotein E
Flotillin-1	Beta-2-glycoprotein 1
Haptoglobin	C4b-binding protein alpha chain
Hemoglobin subunit gamma-2	Clusterin
Hemopexin	Complement C3
Histidine-rich glycoprotein	Complement C4-B
Hornerin	Complement component C6
Ig gamma-1 chain C region	Complement component C9

Ig lambda-2 chain C regions	Complement factor H
Integrin alpha-6	Fibrinogen alpha chain
Integrin alpha-Iib	Fibrinogen beta chain
Keratin, type I cytoskeletal 10	Fibrinogen gamma chain
Keratin, type I cytoskeletal 14	Fibronectin
Keratin, type I cytoskeletal 16	Filamin-A
Keratin, type I cytoskeletal 9	Haptoglobin
Keratin, type II cytoskeletal 1	Hemopexin
Keratin, type II cytoskeletal 2 epidermal	Ig alpha-1 chain C region
Keratin, type II cytoskeletal 6C	Ig gamma-1 chain C region
Keratinocyte proline-rich protein	Ig gamma-2 chain C region
Neutrophil defensin 3	Ig gamma-3 chain C region
Properdin	Ig kappa chain C region
Serum albumin	Ig lambda-2 chain C regions
Serum amyloid A-1 protein	Ig mu chain C region
Spectrin alpha chain, erythrocytic 1	Integrin alpha-Iib
Spectrin beta chain, erythrocytic	Integrin beta-3
Thrombospondin-1	Inter-alpha-trypsin inhibitor heavy chain H2
Vitamin K-dependent protein S	Inter-alpha-trypsin inhibitor heavy chain H4
Vitronectin	Keratin, type I cytoskeletal 10
	Keratin, type I cytoskeletal 14
	Keratin, type I cytoskeletal 16
	Keratin, type I cytoskeletal 9
	Keratin, type II cytoskeletal 1
	Keratin, type II cytoskeletal 2 epidermal
	Keratin, type II cytoskeletal 5

	Keratin, type II cytoskeletal 6C
	Kininogen-1
	Multimerin-1
	Plasminogen
	Platelet factor 4
	Sarcoplasmic/endoplasmic reticulum calcium ATPase 3
	Serotransferrin
	Serum albumin
	Serum amyloid A-1 protein
	Spectrin alpha chain, erythrocytic 1
	Transthyretin
	Vinculin
	Vitamin D-binding protein
	Vitamin K-dependent protein S
	Vitronectin
	von Willebrand factor

## Materials and instruments

The subsequent tables summarize used antibodies, databases, instruments with respective software, analytical software packages and reagents for generated and analysed data sets. The degree of detail of the materials and methods described here has been shortened for readability in the materials and method section.

Table 14: Placental perfusion equipment

Material/Instrument	Supplier
ABL 800 blood gas analyser	Radiometer, Copenhagen, DK
Gas exchange oxygenators	Living Systems Instruments, St. Albans, USA
Cartridge for self-made oxygenators	Kurt Ansperger Konstruktion Entwicklung und Bau von Prototypen, Graz, AUT
Gas exchange membranes for self-made oxygenators	3M, Wuppertal, GER
Glass condensor	Bartelt GmbH, Graz, AUT
Mikro-Cath <sup>TM</sup> pressure catheter	Millar, Houston, USA
Perfusion chamber	Kurt Ansperger Konstruktion Entwicklung und Bau von Prototypen, Graz, AUT
Perfusion pump peristaltic	Codan, Salzburg, AUT
Placenta perfusion data logger software	BEKO, Nöhagen, AUT
Roller pump, REGLO Digital MS-2/12	Cole-Parmer GmbH, Wertheim, GER
Silicon tubing	Roth, Karlsruhe, GER
Tygon tubing	Saint-Gobain, Courbevoie, France
Water bath	Lauda Dr. R. Wobser GmbH & Co. KG, Lauda-Königshofen, GER

Table 15: Reagents and nanoparticles for the *ex-vivo* placental perfusion experiments

Chemical	Supplier
80 nm polystyrene particles (PFP-00558)	Kisker, Steinfurt, GER

500 nm polystyrene particles (PFP-0558)	Kisker, Steinfurt, GER
100 nm Poly (lactic-co-glycolic acid) particles with Texas red	University Vienna, Department of pharmaceutical technology and Biopharmacy, Vienna, AUT
Albunorm 20%, pharmaceutical solution	HSA Octapharma, Vienna, AUT
Albiomin 200 g/l, pharmaceutical solution	HSA Biotest, Vienna, AUT
Amoxicillin	Sigma-Aldrich, Steinheim, GER
Antipyrine	Sigma-Aldrich, Steinheim, GER
Argatroban	Mitsubishi Tanabe Pharma, Vienna, AUT
BSA, lyophilized powder, $\geq 96\%$	Sigma-Aldrich, Steinheim, GER
CaCl <sub>2</sub>	Merck, Darmstadt, GER
Dextran 40FP	SERVA Electrophoresis, Heidelberg, GER
D-glucose	Merck, Darmstadt, GER
DMEM without phenol red, low glucose	Gibco, Carlsbad, CA, USA
HSA, lyophilized powder, $\geq 96\%$	Sigma-Aldrich, Steinheim, GER
KCl	Merck, Darmstadt, GER
MgSO <sub>4</sub> · 7H <sub>2</sub> O	Merck, Darmstadt, GER
NaCl	Merck, Darmstadt, GER
NaHCO <sub>3</sub>	Merck, Darmstadt, GER
NaH <sub>2</sub> PO <sub>4</sub> · 2H <sub>2</sub> O	Merck, Darmstadt, GER
Chloroquine diphosphate salt	Merck-Millipore, Vienna, AUT

Table 16: Analytics of nanoparticles

Material/Instrument	Supplier
Nanosight NS 300	Malvern Instruments, Malvern, UK

Zetasizer Nano ZS	Malvern Instruments, Malvern, UK
FluoStar Optima fluorescence plate reader	BMG Labtech, Ortenberg, GER
Spectra Max 250 UV plate reader	Molecular Devices, San José, USA
Single use semi micro-cuvettes (Polystyrene)	Roth, Karlsruhe, GER
Disposable folded capillary cell	Malvern Instruments, Malvern, UK

Table 17: Antipyrine sample preparation for HPLC, reagents and suppliers

Material/Instrument	Supplier
Acetonitrile	Honeywell, Seelte, GER
KH <sub>2</sub> PO <sub>4</sub>	Merck, Darmstadt, GER
Methanol	Sigma-Aldrich, Steinheim, GER
auto sampler 3950	Knauer, Berlin, GER
degasser 5050	Knauer, Berlin, GER
pump 1050	Knauer, Berlin, GER
UV detector 2500	Knauer, Berlin, GER
150x2.1 5µ column	Thermo Fisher Scientific, Vienna, AUT
1260 Infinity II HPLC system	Agilent Technologies, Vienna, AUT
quaternary HPLC pump G7111B	Agilent Technologies, Vienna, AUT
photodiode array detector G7117C	Agilent Technologies, Vienna, AUT
auto sampler G7129A	Agilent Technologies, Vienna, AUT
ClarityChrom version 3.0.5.505	Knauer, Berlin, GER
OpenLAB CDS ChemStation Edition Rev. C.01.08	Agilent Technologies, Vienna, AUT

Table 18: List of materials for sample preparation and proteomic analysis

<b>Chemical</b>	<b>Supplier</b>
2.2.2-Trifluoroethanol	Thermo Fisher Scientific, Vienna, AUT
Tris-HCl	Thermo Fisher Scientific, Vienna, AUT
tris(2-carboxyethyl) phosphine (TCEP)	Thermo Fisher Scientific, Vienna, AUT
Chloroacetamide	Thermo Fisher Scientific, Vienna, AUT
Ammonium bicarbonate	Thermo Fisher Scientific, Vienna, AUT
rLysC	Promega, Walldorf, GER
Modified trypsin	Promega, Walldorf, GER
Formic acid	Thermo Fisher Scientific, Vienna, AUT
heptafluorobutyric acid	Thermo Fisher Scientific, Vienna, AUT
<sup>13</sup> C <sup>15</sup> N labelled, delta mass+16 Da, peptide standard (R.LEPEDFAVFYCQYGGSSPR.T)	Thermo Fisher Scientific, Vienna, AUT
Aurora Series Emitter nanocolumn with CSI fitting (C18, 1.6 µm, 120 Å, 250 x 0.075 mm)	IonOpticks, Melbourne, AUS
NAb Protein G Spin Columns 1ml	Thermo Fisher Scientific, Vienna, AUT
Anotop 25, 20 nm syringe filters	Whatman, Dassel, GER
maXis-II ETD QTOF	Brucker, Vienna, AUT
nano-HPLC, Dionex Ultimate 3000	Dionex, Vienna, AUT
C18, 5 µm, 100 Å. 5 x 0.3 mm	Thermo Fisher Scientific, Vienna, AUT
Acclaim PepMap RSLC nanocolumn C18. 2 µm. 100 Å. 500 x 0.075 mm	Thermo Fisher Scientific, Vienna, AUT
MaxQuant	Max Planck Institute of Biochemistry, Martinsried, GER
Perseus	Max Planck Institute of Biochemistry, Martinsried, GER
Skyline (version 4.1.0.11796)	University of Washington, Seattle, USA
Proteinscape 4.0.	Bruker, Billerica, USA
Proteome Discoverer 1.4.	Thermo Fisher Scientific, Vienna, Austria

SwissProt	UniProt consortium, international
Data analysis software	Bruker, Billerica, USA
Mascot 2.4.1	MatrixScience, London, UK

Table 19: Material and instrument for TEM

<b>Material</b>	<b>Supplier</b>
EM 900 transmission electron microscope	Zeiss, Jena, GER
FEI Tecnai 20	Thermo Fisher Scientific, Vienna, AUT
Formaldehyde	Merck, Darmstadt, GER
Glutardialdehyde	Merck, Darmstadt, GER
Sodium cacodylate buffer	Electron Microscopy Services, Hatfield, USA
Osmium tetroxide	Electron Microscopy Services, Hatfield, USA
TAAB embedding resin	TAAB, Aldermaston, UK
Ethanol	Merck, Darmstadt, GER
Propylene oxide	Sigma-Aldrich, Steinheim, GER
UC 6 ultramicrotome	Leica, Vienna, AUT

Table 20: Materials for Western Blots

<b>Material</b>	<b>Supplier</b>
4–20% precast polyacrylamide gel, 10-well, 50 µl	Biorad, Hercules, CA, USA
TGX System	Biorad, Hercules, CA, USA
TransBlot Turbo system	Biorad, Hercules, CA, USA
Non-fat dry milk powder	Biorad, Hercules, CA, USA
TBE Buffer	In-house Pharmacy, University Hospital Graz, AT
Page Ruler Plus Prestained Protein Marker	Invitrogen, Carlsbad, CA, USA

10x Tris-Glycine SDS Running Buffer	Biorad, Hercules, CA, USA
TransBlot Turbe Mini Nitrocellulose Membranes	Biorad, Hercules, CA, USA
West Pico/Femto ECL Reagent	Pierce, Waltham, MA, USA
Tween 100	Sigma-Aldrich, Steinheim, GER
4x Laemmli Buffer	Sigma-Aldrich, Steinheim, GER
Apo A1, mouse monoclonal antibody (sc-58230)	Santa Cruz Biotechnologies, TX, USA
Apo B, mouse monoclonal antibody (ab39560)	Abcam, Cambridge, UK
Apo M, mouse monoclonal antibody (ab57471)	Abcam, Cambridge, UK
Goat anti mouse antibody	Biorad, Hercules, CA, USA
Fusion FX	Vilber, Colléiqn, FR

Table 21: Tissue staining antibodies

Antibody	Supplier
Anti-RANKL, #ab9957	Abcam, Cambridge, UK
Anti-CD163, #MA1-82342	Thermo Fisher Scientific, Vienna, AUT
Anti-RANKL (Denosumab), #Xgeva, 120 mg	Amgen, Vienna, AUT
Human normal immunoglobulin (IVIg), #Privigen 100mg/ml	CLS Behring, Marburg, GER
Anti-HER2 (Trastuzumab), #Trastuzumab	Roche, Vienna, AUT
Anti-HER2 (single staining), # PA5-14635 (1:100)	Thermo Scientific, Vienna, AUT
Anti-HER2 (costaining), # MABE320 (1:50)	Merck-Millipore, Vienna, AUT
Anti-FcRn, # HPA012122 (1:100)	Sigma-Aldrich, Steinheim, GER
Anti-LAMP1 (co to FcRn), # HPA014750 (1:100)	Sigma-Aldrich, Steinheim, GER
Anti-LAMP1 (co to HER2), # AMAB91170 (1:50)	Sigma-Aldrich, Steinheim, GER

Dylight 633 goat anti mouse IgG, #35512	Thermo Scientific, Vienna, AUT
Goat anti-Rabbit IgG Secondary Antibody, DyLight 488, #35552	Thermo Scientific, Vienna, AUT
Negative Control Rabbit Immunglobulin Fraction, # X0936	Dako, Santa Clara, USA
Negative Control (mouse IgG1), # X0931	Dako, Santa Clara, USA

Table 22: Materials and instrumentation for immunohistochemistry microscopy

Material/Instrument	Supplier
Aquatex mounting medium	Merck-Millipore, Vienna, AUT
Olympus BX53 Microscope	Olympus Austria GmbH, Vienna, AUT
UPplaneFL 20x/0.5 infinite 0.17FN26 objective	Olympus Austria GmbH, Vienna, AUT
Axiocam MRc 5 camera	Zeiss, Jena, GER
Axiovision V 4.8.2.0	Zeiss, Jena, GER
Lab Vision™ Hydrogen Peroxide Block	Thermo Fisher Scientific, Vienna, AUT
Ultra V Block	Thermo Fisher Scientific, Vienna, AUT
Mayer's Haematoxylin	Gatt-Koller, Absam, AUT
Lab Vision™ HRP-Polymer/AEC-Chromogen	Thermo Fisher Scientific, Vienna, AUT

Table 23: Materials and instrumentation for fluorescence microscopy

Material/Instrument	Supplier
ProLong gold antifade reagent	Thermo Fisher Scientific, Vienna, AUT
Olympus BX53 Microscope	Olympus Austria GmbH, Vienna, AUT
UPplaneFL 20x/0.5 infinite 0.17FN26 objective	Olympus Austria GmbH, Vienna, AUT
Axiocam MRc 5 camera	Zeiss, Jena, GER

Axiovision V 4.8.2.0	Zeiss, Jena, GER
antibody diluent containing background reducing components	Dako, Vienna, AUT
Primary antibody enhancer	Thermo Fisher Scientific, Vienna, AUT
LSM510 Meta	Zeiss, Jena, GER

Table 24: Tissue sample handling materials

Chemical	Supplier
Formaldehyde solution 4% buffered acc. to Lillie	Donau Chem, Vienna, AUT
PBS	Merck, Darmstadt, GER
Xylene	Roth, Karlsruhe, GER
Ethanol	Merck, Darmstadt, GER

Table 25: Cell culture material and instrumentation

Material/Instrument	Supplier
Blasticidin, #21001	Thermo Fisher Scientific, Vienna, AUT
L-Glutamine, # 35050-061	Thermo Fisher Scientific, Vienna, AUT
G418, # A1720-1G	Merck-Millipore, Vienna, AUT
Human epidermal growth factor, # C-39220	PromoCell, Heidelberg, GER
Hydrocortisone, # C-39220	PromoCell, Heidelberg, GER
MCDB 131 medium, # 10372019	ThermoScientific, Vienna, AUT
Chloroquine diphosphate salt	Merck-Millipore, Vienna, AUT
Foetal Bovine Serum Defined, Hyclone, # 30070.03	GE Healthcare Life Sciences, Vienna, AUT
EVOM2, Epithelial Voltometer	World Precision Instruments, Sarasota, USA
Nunc Nunclone 75 cm <sup>2</sup> , cultivation flasks	Thermo Fisher Scientific, Vienna, AUT

TrypEL Express	Thermo Fisher Scientific, Vienna, AUT
Hanks buffered salt solution (HBSS) 1x	Thermo Fisher Scientific, Vienna, AUT
Stericup Quick Release-GP Sterile Vacuum Filtration System	Merck-Millipore, Vienna, AUT
12 well Transwell®, 12mm Inserts, 3µm pore size, polycarbonate membrane	Corning Incorporated, Kennenbunk, USA
Bovine Serum Albumin	Sigma, Steinheim, DE
Penicillin-Streptomycin # 15140-122	Thermo Fisher Scientific, Vienna, AUT
Penicillin-Streptomycin-Neomycin # 15640-055	Thermo Fisher Scientific, Vienna, AUT

Table 26: ELISA and additional material

Material	Supplier
Total IgG ELISA, # ab100547	Abcam, Cambridge, UK
Trastuzumab ELISA, #SHIKARI® Q-TRAS	Matriks Biotek, Ankara, TUR
RANKL ELISA	Biomedica, Vienna, AUT
SpectroStar nano	BMG Labtech, Ortenberg, GER
recombinant RANKL, #GF091	Sigma-Aldrich, Vienna, AUT
Denosumab ELISA, # SHIKARI® Q-DEN	Matriks Biotek, Ankara, TUR

Table 27: List of additionally used software

Software	Supplier
GraphPad Prism 8.4.0	GraphPad Software, San Diego, USA
String: functional protein association network Version 11	String consortium
Reactome pathway Database version 3.6 database v70	Reactome Project consortium
SAS software version 9.4	SAS Institute. Inc., Cary, USA
Kyoto Encyclopedia of Genes and Genomes (KEGG)	KEGG consortium